The contribution of Sting and Nlrp3 activation to anti-tumour immunity in microsatellite instable colorectal cancer

By

Courtney Victoria Mowat

A thesis submitted in partial fulfillment of the requirements for the degree of

Master of Science

In

Cancer Sciences

Department of Oncology

University of Alberta

ABSTRACT

The constant exposure of the intestine to antigens forces the mucosal immune system to be tolerant to avoid a constitutively inflamed state. Unfortunately, immune tolerance can allow colorectal cancers (CRCs) to escape detection. The majority of CRCs are chromosomally instable (CIN) and display the features of an immune ignorant tumour, including the exclusion of cytotoxic T cells (CD8+). Nonetheless, approximately 15% of all CRCs are microsatellite instable (MSI) and have high infiltrating CD8+ T cells and a more favourable prognosis as a result. A prevailing hypothesis to explain MSI CRC's enhanced immunogenicity stems from hypermutability driving the accumulation of tumour associated antigens that stimulate an adaptive immune response. Although this is agreed to be a contributing factor, it is likely not the only influence because not all hypermutable tumours have enhanced anti-tumour immunity. One alternative explanation is that different defective DNA repair pathways may influence the growth of specific intestinal bacteria, driving immunogenicity. A major way intestinal epithelial cells communicate with microbes is through pattern recognition receptors (PRRs), including NLRP3 and STING, which have higher expression in MSI compared to other CRCs. We suspect that the activity of such receptors is aiding in MSI CRC's better prognosis, either by recruiting cytotoxic immune cells, or by inducing programed tumour cell death. We sought to determine if MSI CRCs have altered bacteria recognition when compared to CRCs with other types of genetic instability, and if this could impact the anti-tumour immune response. We discovered that cooperation between NLRP3 and STING signaling aids in MSI CRC's enhanced prognosis, thereby identifying new possible therapeutic targets to enhance anti-tumour immunity and immunotherapy responsiveness in the more aggressive CIN CRCs.

PREFACE

This thesis is an original work by Courtney Victoria Mowat and no part of this thesis has been previously published. The project of which this thesis is a part, received research ethics approval from the Cross Cancer Institute Animal Care Committee, Project Title “Impact of genomic instability in colorectal cancer on the mucosal immune system”, Protocol No. AC15219, July 1, 2015.

DEDICATION

The works of this thesis are dedicated to my grandfather, Mr. Thomas Mowat, who survived non-Hodgkin's lymphoma in the 1970s thanks to treatment at the Cross Cancer Institute. He lived until the age of 80, when he passed away from pancreatic cancer as the work included in this thesis was being conducted. If it were not for the advances made in cancer research and treatment, even at that time, I would have never met my grandfather and all the memories of him helping my dad coach my basketball teams would have never been made.

ACKNOWLEDGEMENTS

I would like to express my gratitude to my supervisor, Dr. Kristi Baker, for providing me the opportunity to develop my research skills and help her establish her research lab. Thank you for being a hands-on mentor and allowing me to try new techniques that excelled my research and developed my skillset as a scientist. I will forever be indebted to you for any success I have in my research career.

Thank you to Baker lab graduate students Allison McNamara, Isaac Menghisteab, and Shayla Mosley for your feedback and suggestions during lab meetings to enhance my research, as well as for assisting with the *in vivo* mouse experiments. Also, thanks to all the undergraduate students that came into our lab, especially Jianyin Liu, Louise Ibalio, and Katie Du, for teaching me how to be a successful mentor and helping conduct experiments and optimize their conditions. I would also like to thank Joanne Smith for her friendship and helping me through my coursework by being a second pair of eyes for my papers and giving feedback on my presentations.

I would also like to thank my supervisory committee members for their feedback during the course of my Masters: Dr. Michael Weinfeld and Dr. Edan Foley. Also, thank you to Dr. Karen Madsen for being the external examiner for my thesis defense. Additionally, I would like to thank Tingting Ju and Jinghong Kang from the Ben Willing group for performing and analyzing the 16s rRNA DNA sequencing.

Of course, research is not possible without financial support, which is why I am grateful for Dr. Baker's funding from NSERC and CIHR that helped pay for my stipend, along with the

two Queen Elizabeth II scholarships, the Sarah and Nancy South Memorial Graduate Scholarship, and the friends of the Faculty of Graduate Studies and Research Scholarship I received. I would also like to thank BioCanRx and the Cancer Research Institute of Northern Alberta/Alberta Cancer Foundation for affording me the opportunity to travel to the Summit for Cancer Immunotherapy in Gatineau, QC and Banff, AB and for traveling to the Canadian Cancer Research Conference in Vancouver, BC.

Finally, I wish to thank my family for their support throughout my studies and affording me the opportunity to receive my education, and my boyfriend, Joshua Laplante, for his support and encouragement through stressful times.

TABLE OF CONTENTS

LIST OF TABLES

LIST OF FIGURES

LIST OF RECURRING ABBREVIATIONS

AIM2: absent in melanoma 2

AMP: adenosine monophosphate

AOM/DSS: azoxymethane/dextran sodium sulfate

ASC: apoptosis-associated spec-like protein

ATP: adenosine triphosphate

CARD: caspase activationa and recruitment domain

cGAMP: cyclic GMP-AMP

cGAS: cyclic GMP-AMP synthase

CIN: chromosomal instable

CRC: colorectal cancer

CRISPR: clustered regularly interspersed short palindromic repeats

DC: dendritic cell

dsDNA: double-stranded DNA

ELISA: enzyme linked immunosorbent assay

ER: endoplasmic reticulum

ETBF: enterotoxic Bacteroides fragilis

Foxp3: forkhead box protein p3

GMP: guanosine monophosphate

gRNA: CRISPR guide RNA

GSDM: gasdermin

GTP: guanosine triphosphate

IDO: indoleamine 2,3-dioxygenase

IEC: intestinal epithelial cell

IFN: interferon

IFNa: interferon alpha

IFNb: interferon beta

IFNg: interferon gamma

IHC: immunohistochemistry

IL-R: interleukin 1 receptor

IL18: interleukin 18

IL1b: interleukin 1 beta

IRF: interferon regulatory factor

LAG3: lymphocyte activating 3

LAL: Limulus amebocyte lysate

LRR: leucine rich repeat

MLH1: mutL homolog 1

MMR: mismatch repair

MSI: microsatellite instable

mtDNA: mitochondrial DNA

NLRP3: nod-like Receptor family pyrin domain containing 3

OTU: operational taxonomic unit

OVA: ovalbumin

p: phospho

Panx1: pannexin-1

Pole: polymerase epsilon

PRR: pattern recognition receptor

Pyd: pyrin domain

qPCR: quantitative polymerase chain reaction

rRNA: ribosomal RNA

S100: sting agonist S100

STING: stimulator of interferon genes

TAA: tumour associated antigen

TCGA: The Cancer Genome Atlas

TCR: T cell receptor

TIM3: T-cell immunoglobulin and mucin-domain containing-3

TLR: toll-like receptor

Treg: regulatory T cell

GLOSSARY OF TERMS

Subcutaneous tumour: tumours grown underneath the skin on the flank of a mouse regardless of their tissue of origin (ex. CRCs grown on the rear flank of mice)

Orthotopic tumour: tumours grown in the tumour cells' tissue of origin (ex. CRCs grown in the colon of mice)

Z-score: a measure of the relative expression of a transcript in a tumour sample compared to the average expression in normal samples divided by the standard deviation of the expression of that transcript in a reference sample

Effector T cells: T cells that have an active rather than suppressive response when they bind their cognate antigen

Syngeneic: genetically similar to the point that no immune rejection should occur (ex. MC38 cell line injected into C57BL/6 mice)

Murine: mouse

Axenic: a model lacking microorganisms, except the organism of interest (ex. a germ-free mouse inoculated with one microbial species

CHAPTER 1: INTRODUCTION

Colorectal cancer

Colorectal cancer (CRC) is a major health concern in Canada, being the second most common and deadly cancer in Canadian men, and the third most common and deadly in cancer in Canadian women.[1] Only 30% of CRCs arise in the rectum, while most originate in the large intestine.[2] Since 1988 there has been a decline in CRC incidence of 11.3% and 14.5% in males and females above the age of 50 in North America respectively, while the rates in those under 50 have not improved.[2] As of 2017, if CRC is diagnosed at stage I, there is a 92% 5 year survival rate, but the 5 year survival rate for metastatic CRC is only 11%.[2] Unfortunately, almost 50% of CRCs are diagnosed once the disease has already reached stage III or IV,[2] which is why significant effort is being invested into developing better screening tools for CRCs in addition to developing therapies that can target advanced cancers.

Chromosomal instability

The majority of CRCs are chromosomally instable (CIN)[3] and, as the name suggests, these cancers have recurring missegregation of chromosomes during cell division resulting in genetic instability.[4] CIN CRCs arise from a well characterized mechanism: the Vogelstein adenoma-carcinoma sequence of mutations.[5] This process is initiated by the inactivation of the *APC* tumour suppressor gene that results in dysregulated β-Catenin, and therefore rapid

proliferation of normal intestinal cells into an adenoma.[6] This rapid proliferation results in the activation of oncogenes, especially *KRAS*,[7] that further exacerbate proliferation rates, and ultimately results in the inactivation of the suppressor, *TP53*, driving the full transformation of the adenoma into an adenocarcinoma.[8] These cancers occur most often in the distal colon, and are characterized as having poor immune infiltration, high invasiveness, and a higher incidence of metastatic disease.[9] Although CIN CRCs respond well to 5-flurouracil chemotherapy treatment compared to less common types of CRC,[10] these patients have a much worse prognosis.[11]

Microsatellite instability

A small proportion of CRCs, constituting approximately 15% of all cases,[12] are microsatellite instable (MSI) and have a favourable prognosis compared to CIN CRCs.[13] These cancers are considered hypermutable due to possessing a dysfunctional DNA mismatch repair (MMR) response, mainly from having an inactive mutL homolog 1 (*MLH1)* gene.[9] The DNA MMR system is highly conserved and is responsible for detecting and repairing mismatched base pairs during DNA replication or following either physical or chemical DNA damage.[14] Often these mismatches occur at long stretches of repetitive DNA sequences known as microsatellites.[15] The MSH2/MSH6 heterodimer binds the mismatched region, and subsequently the MLH1/PMS2 heterodimer excises the DNA at the mismatched site and then synthesizes the correct DNA.[14] Because of its repetitive nature, base mismatches are most common at microsatellite regions in the DNA such that loss of MMR predominantly affects these sites,

leading to expansion or contraction of the microsatellites that generate instability. MSI is most common in early stage CRCs with only 4% of metastatic CRCs displaying MSI.[16] MSI CRCs arise most often in the proximal colon, and are characterized as having poor differentiation, being diploid, having a higher infiltration of cytotoxic (CD8+) T-cells, and being less invasive compared to CIN CRCs. Combined, these features contribute to a better prognosis for patients with MSI CRCs.[8]

Intestinal immunity

The intestine has a specialized immune system because constant exposure of the gut to microbial and food derived antigens requires the system to be tolerant to avoid a constitutive inflammatory state. At the same time, the intestinal immune system must limit bacterial breach of the epithelial barrier and rapidly kill any cells that do invade so they do not reach the body's interior.[17] There are several mechanisms that exist in the intestinal immune environment to maintain a homeostatic state while also preventing infection. Goblet cells are a specialized epithelial cell that secrete mucin glycoproteins that form a mucus layer along the intestine.[18] This mucus layer is up to 700μm thick in the colon and forms two layers: the outer layer is loose and non-sterile, while the inner layer is thick and therefore resistant to microbial penetration.[19] Intestinal epithelial cells (IECs) release antimicrobial proteins, known as defensins, into the mucus layer that can kill bacteria, fungi, or viruses that make it into the mucus layer.[17] To monitor mucosal bacteria, dendritic cells (DCs) of the lamina propria extend dendrites between epithelial cells to sample bacteria in contact with the apical epithelial surface.[17] DCs are a key

bridge between innate and adaptive immunity. One of their main functions in the intestine is to induce the differentiation of naïve B cells into plasma cells that produce IgA that is shuttled through IECs and released in the lumen. This secretory IgA binds and neutralizes microbes to prevent them from associating with the IEC surface.[20] To prevent a systemic immune response, bacteria-exposed lamina propria DCs do not migrate further than the mesenteric lymph nodes where they present antigens to naïve T cells.[17] If bacteria manage to translocate through the epithelial barrier, the lamina propria macrophages immediately phagocytose them but, unlike macrophages in non-mucosal tissues, tolerant intestinal macrophages do not induce a potent inflammatory response upon bacterial recognition.[17] Further contributing to intestinal homeostasis, the T cells of the lamina propria are mostly regulatory T cells (Tregs) that function to limit inflammation in the intestine by producing IL10 and preventing cytotoxic responses.[21] Further confining adaptive immune responses to the intestine, locally activated B and T cells will circulate through the lymphatic system but only home back to the intestine, thereby distributing the local response all along the intestinal tissue but limiting its systemic spread.[17] All of these mechanisms aim to localize the necessary immune response to the intestine while also minimizing constitutive inflammation there. Unfortunately having these mechanisms of tolerance in the intestine also creates an immune environment more conducive to cancer growth.

Genetic instability and anti-CRC immunity

It is important to understand how different forms of genetic instability impact the tumour microenvironment not only for staging the disease, but also for deciding on a treatment regimen. For instance, MSI CRCs show sensitivity to oxaliplatin,[16] but not to 5-fluorouracil chemotherapy, while CIN CRCs have an inverse response.[9] CIN CRCs display the features of an immune ignorant tumour, including the exclusion of CD8+ T cells which are the main effectors of immune mediated tumour cell killing.[22] Contrary to CIN CRCs, MSI CRCs display anti-tumour immunity, including the presence of intratumoural CD8+ T cells thought to be driving the better prognosis of patients with MSI CRCs.[23] The reason MSI CRCs have enhanced infiltration by CD8+ T cells is debated. A prevailing hypothesis stems from the hypermutability of MSI CRC where defective MMR in cancer cells results in the accumulation of mutations within protein coding regions of genes. This effectively generates an abundance of aberrant proteins that can be recognized by the immune system as tumour associated antigens (TAAs), stimulating an adaptive immune response.[24] Although this is agreed to be a contributing factor to the anti-tumour immunity of MSI CRC, it is likely not the only mechanism.

The genetic instability that is inherent in MSI CRC results in a paradox where the high mutation rate promotes rapid adaptation that would enhance the cancer's ability to thrive in a dynamic tumour microenvironment[25] but also results in the production of aberrant proteins that can be used to mount an adaptive immune response against the tumour.[15] TAAs are the consequence of non-synonymous mutations that arise during tumour evolution.[23] Whole exome sequencing of CRCs found 1304 somatic mutations on average in each MSI tumour

compared to an average of just 198 in each CIN CRC. This illustrates that genetic instability through MSI results in the accumulation of an immense number of TAAs compared to genetic instability arising from CIN.[26] Nevertheless, the production of TAAs cannot entirely explain MSI CRC's increased CD8+ T-cell infiltration because 20% of CIN CRCs have immune infiltration similar to MSI CRC despite having low TAA loads.[26] Furthermore, when the DNA synthesis gene polymerase epsilon (*POLE*) is mutated in CRC, these cancers accumulate many point mutations resulting in even more TAAs per tumour than MSI.[27] Patients with these cancers, however, have a worse overall survival compared to either MSI or CIN CRCs, indicating that TAA load is not sufficient for immune mediated killing.[27,28] Additionally, it is not solely the MSI status driving anti-tumour immunity in CRC since there is ample evidence that the microenvironment of a tumour contributes to its progression.[29] MSI is also common in cancers of other mucosal sites, such as the endometrium, but the MSI status does not confer any benefit to survival in these cancers.[30] Since MSI CRCs bear an entirely different gene signature than MSI endometrial cancers, the evidence suggests that evolution of these cancers is more strongly influenced by their microenvironment rather than their shared MSI status.[31] Taken together it appears that MSI CRC's improved prognosis is likely determined by MSI specific TAAs as well as the context of the specialized intestinal immune microenvironment. The specific mechanisms that govern this, however, have yet to be determined.

CRC immune escape mechanisms

For cancers to progress they must evade immune detection and the already tolerant immune landscape of the intestine diminishes the hurdles preventing CRC development.[32] Within a tumour there is significant cell death that provides a source of tumour antigens. These can be taken up by DCs that present them on MHC class I and II molecules to antigen specific T-cells that should then be capable of killing tumour cells.[33,34] Despite many cancers producing abundant TAAs, the immune system fails to eliminate tumour progression using mechanisms that have only partially been explained.[35] Tumours escape immune detection by modulating the immune environment through such mechanisms as recruiting myeloid derived suppressor cells, regulatory T cells (Tregs), and M2 macrophages, while simultaneously decreasing the presentation of antigens on MHC class I.[26] Tumour cells can directly inhibit immune reactivity through the release of anti-inflammatory molecules, such as IL-10 and TGFb,[36] which serve to inhibit effector T cell function.[37] Although MSI CRCs are infiltrated with CD8+ T cells, these cells can be anergic through the expression of high levels of suppressive co-receptors such as PD-1, which explains why these T cells are not successfully eliminating the tumour and why PD-1 blockade is successful for MSI CRCs.[26] Additionally, 60% of MSI CRCs have the loss of MHC class I expression, while only 17% of CIN CRCs do, meaning that although there are tumour specific T cells in the environment, many of the tumour cells are no longer recognized and killed by the CD8+ T cells.[26,38] This serves as a mechanism for the MSI CRCs to evade immune detection despite their high TAA load.[39] Furthermore, when T cells are constantly exposed to a persistent antigen and to inflammation, such as in the case of cancer or a chronic infection, the T cells can acquire an exhausted phenotype that prevents tumour cell killing.[40] One of the ways that immune cells signal to one another is through interferons such as Type I IFN that induces STAT3

transcription of the cytotoxic effector molecule granzyme b in T cells. However, IFNAR1 is often downregulated on the cytotoxic T cells of CRC patients, leading to hindered T cell effector function.[41]

In addition to directly altering the immune environment, cancers modulate cell signaling pathways that indirectly serve to hinder anti-tumour immunity. For instance, the metabolism of tumours creates a hostile environment for effector T cells.[26] The process of aerobic glycolysis that tumours use to produce ATP, nucleotides, and amino acids, results in an acidic environment that hinders T cell survival.[26] Moreover, effector T cells require a lot of energy to exert their effect and, due to high consumption of glucose and nutrients by tumour cells, there is limited glucose or nutrients left for proper T cell proliferation and function.[37] In an attempt to increase oxygen and nutrient supply, tumours upregulate angiogenic factors, such as VEGF, causing the vasculature to be disorganized. This can prevent T-cell transendothelial migration and therefore infiltration into the tumour bed.[42,43] This disorganized vasculature also results in spontaneous hypoxic regions arising within the tumour that are not conducive to T cell survival or infiltration.[37] Additionally, angiogenic factors secreted by tumours upregulate endothelial FASL expression, resulting in the apoptosis of effector T and NK cells trying to infiltrate the tumour.[37,44] With knowledge of how CRC evades immune detection, components of the process can be therapeutically targeted to regain the functionality of the patient's anti-tumour immune response.

Immunotherapy in CRC

In recent years there has been a shift away from cancer treatments directly targeting the tumour, to ones that instead activate the patient's immune system to attack cancerous cells. Immunotherapy has seen great success in certain cancers, most notably in the treatment of melanoma[45,46], but these therapies have yet to show a clinical benefit in the majority of CRCs.[47] Standard treatment for CRC is with surgery or segmental resection of the colon in conjunction with chemotherapy.[48] This allows some patients to enter remission for months, or even years, but 30-50% of these patients experience recurrence and this often occurs as metastatic disease.[49] Unfortunately, most CRC patients are only eligible for chemotherapy since immunotherapy has only been shown to be effective in MSI CRCs.[50]

Immunotherapies are expensive[51] and have many serious associated complications, namely cytokine release syndrome.[52] Since most tumours are unlikely to respond, it is important to establish biomarkers that distinguish responders from non-responders.[14] Two signals are required to activate T cell killing: the first is the T cell receptor (TCR) binding to its cognate antigen on an antigen presenting cell, and the second is a co-stimulatory signal.[53] In contrast, T cell activity can be prevented by a co-inhibitory signal that does not depend on the TCR receptor binding its antigen.[54] The two best described co-inhibitory signals are B7 binding to the CTLA-4 receptor,[55,56] and PD-L1 binding to the PD-1 receptor. [57] Several tumours escape immune detection by upregulating inhibitory ligands on their surface, such as PD-L1, which causes tumour infiltrating CD8+ T cells to enter an unresponsive state called anergy.[58–60]

Because MSI CRCs have an active anti-tumour immune response, this results in the production of IFNγ that can cause the tumour cells to upregulate immune checkpoint ligands on their surface.[61] A monoclonal antibody for either PD-1 or its ligand, PD-L1, blocks the exhaustion of CD8+ T cells, allowing infiltrated immune cells to engage in tumour killing.[47] The Food and Drug Administration has approved PD-1 blockade as a second line treatment in patients with MSI CRC, as these patients have a 40% response rate, compared to 0% in the CIN CRC patients.[15] Beyond PD-1 blockade, other checkpoint inhibitors that are highly expressed in CRC tumours are being investigated as clinical targets although none has proven to be as effective at limiting T cell activation as PD-1 blockade.[62] MSI CRCs have high levels of lymphocyte activating 3 (LAG3) and T cell immunoglobulin and mucin-domain containing-3 (TIM3) that cause CD8+ T cell exhaustion by synergizing with PD-1.[62] There are also immune checkpoint blockades being developed for CRC that do not act to prevent T cell exhaustion but rather focus on alternate mechanisms of T cell activation such as inhibiting the indolamine 2,3-dioxygenase (IDO) enzyme which blocks catalysis of tryptophan, preventing immune tolerance to TAAs.[63] To increase CRC survival, immunotherapies are going to have to be able to target CIN CRCs. If we can understand why the majority of CRCs are refractory to immunotherapy intervention, then we can work to remove these blockades to enhance sensitivity to treatment.[64] Since the microbiota are an integral component of the immune microenvironment of CRC, their role in both immune evasion and anti-tumour immunity cannot be overlooked as a possible therapeutic target.

Intestinal microbiota

The microenvironment of the colon is essential to the progression of CRC due to both the mucosal immune system and the presence of specialized microbes.[65] Diverse microbial populations are in direct contact with CRCs and have been linked to CRC development and progression.[66,67] Changes in the colon microbiota could either exacerbate tumourigenesis or aid in its prevention, depending on whether the microbes present drive a pro-tumourigenic inflammatory immune landscape or strengthen tumour-preventing epithelial barrier integrity. Diet has also been identified as a major modulator of CRC risk, particularly Western diets that favor the intake of alcohol, salt, high-fructose corn syrup, and fatty meats. This has been shown to foster an inflammatory environment that can result in decreased intestinal microbial diversity associated with the onset of several diseases.[68,69]

One of the best studied microbes encouraging CRC development is *Fusobacterium nucleatum*, whose presence is associated with lower T cell infiltration and more metastatic disease and, therefore, a worse prognosis.[70] There are studies that show enriched dietary fibre from whole grains is associated with lower *F. nucleatum* abundance in CRC. Patients with a high fiber consumption have a better disease outcome, at least in part because of an expansion of *Bifidobacteria*[71] that can outcompete *F. nucleatum* for the intestinal niche.[69] Other well studied pathogenic bacteria that enhance CRC progression are enterotoxic *Bacteroides Fragilis* (ETBF) and *pks+ Escherichia coli.*[72] ETBF produce a fragilin toxin that compromises epithelial tight junction integrity[70] while the pks pathogenicity island in *pks+ E. coli* produces colibactin, a molecule that induces DNA damage.[73,74]

Although much effort has been expended to identify bacteria that serve as markers for severe CRC disease, there are also microbes recognized for enhancing cancer survival. Oral administration of *Bifidobacterium* reduces tumour burden to the same degree as anti-PD-L1 by enhancing dendritic cell (DC) antigen presentation to CD8+ T-cells, while the combination of *Bifidobacterium* and anti-PD-L1 further ameliorated anti-tumour effects.[75] Additionally, when fecal microbiota were transplanted from anti-PD-1 responders into tumour bearing mice, the anti-tumour effect of anti-PD1 was enhanced, while transplanting fecal microbiota from non-responders failed to improve response to anti-PD1.[76] When the fecal microbiota of non-responders was supplemented with the *Akkermansia muciniphila* microbe, the tumour bearing mice responded to anti-PD1 therapy via a mechanism attributed to the recruitment of helper T cells to the tumour.[76]

The microbiome is integral in shaping the mucosal immune system in the intestine as evidenced by the fact that the structures of the gut associated lymphoid tissues (lymphoid follicles, mesenteric lymph nodes) are significantly smaller in germ-free, compared to conventionally reared, mice.[21] Additionally, the lamina propria contains far fewer plasma cells and Th17 cells in germ-free mice.[21] For these reasons, studying the immune response to axenic inoculations in these germ-free mice is not representative of how the microbe of interest would regulate immunity in a normal intestinal environment. Interestingly, when TAA sequences are aligned with microbial peptides sequences, there are significant homologies, indicating that

anti-tumour immunity may be a result of cross-reactive TCRs recognizing TAAs that mimic microbial antigens.[77] Bacteria can also induce intestinal tolerance. For example, *B. fragilis* produce polysaccharide A that activates toll-like receptor 2 (TLR2) and the subsequent differentiation of CD4+ T cells into FOXP3+ regulatory T cells that can resolve an active immune response.[21] While the primary research focus of immune evasion in CRC has been on the adaptive immune system, the first line of defense when there is a threat is the innate immune system. IECs, and therefore CRC cells, are equipped with pattern recognition receptors (PRRs) to detect conserved structures on intestinal microbiota.[78] Understanding how this innate response confers adaptive anti-tumour immunity in the context of the different subtypes of CRC, may be an avenue for novel therapeutic manipulation.

Pattern recognition receptors

PRRs are germline encoded molecules designed to be the first line of defense against extracellular or intracellular pathogens by recognizing conserved molecular patterns.[79] Since these receptors respond to molecular patterns rather than specific epitopes on a single ligand, they can also respond to molecules released from damaged cells, which are plentiful in the tumour microenvironment.[80] The activation of PRRs initiates a signaling cascade that leads to the production of pro-inflammatory cytokines and activation of an adaptive immune response.[81] It was originally thought that only immune cells, such as macrophages and dendritic cells (DCs), expressed PRRs but mounting research has recently established PRR activity in IECs.[82] Different regions of the intestine and gut associated lymphoid tissues have differential

expression of PRRs and their associated signaling molecules.[82] There are several families of PRRs, including TLRs, interleukin-1 receptors (IL-Rs) and C-type lectin receptors, which are all membrane bound, as well as NOD-like receptors, RIG-I-like receptors and DNA sensors, which are all cytosolic.[83] Although more is understood about the consequence of PRR signaling in immune cells, elucidating their role in the epithelium is important especially since CRC originate from IECs via oncogenic transformation. Cytokines and chemokines released downstream of PRR activation in IECs serve a role in initiating inflammation and recruiting immune cells.[84] Since IECs are the first cellular barrier between the lumen and the immune component of the lamina propria,[85] changes in their PRR status during CRC development can have a profound impact on anti-CRC immunity.

Sting signaling

When intracellular pathogens release DNA in the cytoplasm, it activates PRRs known as cytoplasmic DNA sensors.[86] The presence of DNA in the cytoplasm acts as a danger signal to the cell because the major source of this is typically invading microbes since self DNA should be confined to either the nucleus or mitochondria.[87] However, if the cell is overwhelmed with genotoxic stress, such as in the case of many cancers, micronuclei can form from chromosome missegregation or DNA release from the mitochondria, and activate the cyclic GMP-AMP synthase (cGAS)-stimulator of interferon genes (STING) pathway.[87,88] This drives a type I interferon (IFN) response in a MyD88 independent manner.[86,89] Type I IFNs are required for DCs

to mature and present antigens to CD8+ T cells, which is a necessity for mounting an immune response against the tumour.[33,81]

The cytosolic DNA sensor, cGAS, has a nucleotidyltransferase and two major DNA binding domains, and exists in an autoinhibited state until binding to the sugar backbone of cytosolic DNA induces a conformational change in the active site of the enzyme.[79] When cytoplasmic DNA binds to cGAS, it converts guanosine triphosphate (GTP) and adenosine triphosphate (ATP) into the cyclic GMP-AMP (cGAMP) signaling molecule.[87] Endogenous 2'3'-cGAMP has high affinity for STING and is formed when cGAS creates one phosphodiester bond between the 2'-hydroxyl of Guanosine monophosphate (GMP) and 5'-phosphate of AMP (adenosine monophosphate), and another phosphodiester bond between the 3'-hydroxyl of AMP and 5'-phosphate of GMP.[87] cGAS has an affinity for long dsDNA (>40 base pairs) or short Y-form (unpaired guanosine ends) dsDNA, meaning that both the length and structure influences whether cytosolic DNA activates the cGAS-STING axis.[90] For instance, self-DNA derived from mitochondrial leakage is able to potently activate cGAS, most likely because mitochondrial DNA (mtDNA) is similar in structure to microbial DNA.[90]

Inactive STING exists as a transmembrane homodimer that localizes to the endoplasmic reticulum (ER) (Figure 1-1).[91] The binding of cGAMP to STING induces its translocation to the Golgi apparatus[92] and subsequent oligomerization, initiating the binding and trans-

autophosphorylation of TBK1 clusters.[93] Active TBK1 can phosphorylate the tail of STING,[93] inducing the recruitment and phosphorylation of interferon regulatory factors (IRFs) and NFκBp65 resulting in their translocation to the nucleus for transcription of target genes.[94] Chemokine CCL5 and cytokines IFNα, IFNβ, and pro-IL1β are transcriptionally regulated by IRF3, IRF7, NFκBp50, and NFκBp65, while IFNγ is regulated only by NFκBp50 and NFκBp65.[90] Upon induction of the STING signaling cascade, STING is rapidly degraded to prevent sustained inflammation once the stimulus disappears.[79]

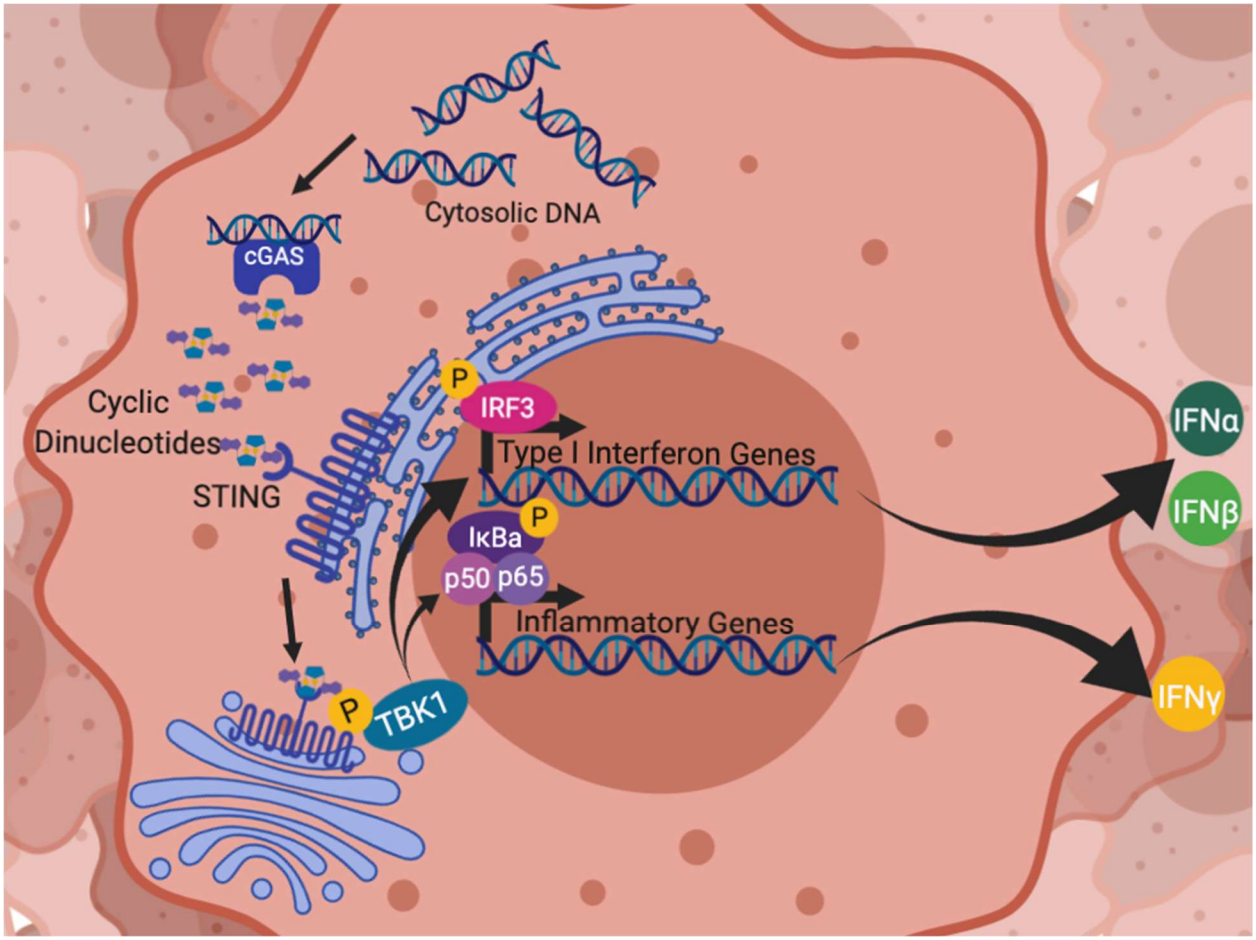

Figure 1-1. STING signaling pathway. Cytosolic DNA is processed by cGAS into cyclic-di-nucleotides that bind to the transmembrane STING receptor in the endoplasmic reticulum resulting in STING's translocation to the Golgi apparatus. STING and TBK1 phosphorylate one another, resulting in the recruitment of interferon regulatory factors (ex. IRF3) that transcribe type I IFNs, as well as NFκB that transcribes multiple inflammatory genes (ex. IFNγ). Figure made in ©BioRender.

Evidence indicates that STING may have a more important role in anti-tumour immunity compared to other PRRs because Sting-deficient mice have defective CD8+ T cell priming[95] while those lacking TLRs, MyD88, or the mitochondrial anti-viral signaling protein do not have this immune defect.[79] Additionally, MyD88 and TRIF are dispensable for the anti-tumour effect of radiation, while Sting is strictly required.[79,87] Evidence from cancer cell lines initially indicated that the majority of cancers, including CRCs,[96] suppress or eliminate *STING* expression.[97] However, analysis of the PanCancer TCGA database reveals that the genes in these pathways are only mutated at low frequencies.[4] The significance of STING downregulation for tumourigenesis is highlighted by the observation that *Sting*$^{-/-}$ mice given azoxymethane/dextran sulfate sodium (AOM/DSS) treatment, a chemically induced model of colitis-associated CRC, have a higher tumour burden compared to their wildtype counterparts.[81] This study has some important limitations though. The work was done in mice with a whole-body knock-out of *Sting* whereas, in the case of human CRC, *STING* gene expression would only be lost in the tumour cells but maintained in the immune cells. This is important because Sting signaling is needed for anti-tumour immunity and its loss in the mouse models is likely to have impacted tumour

development in ways that would not apply to human CRCs. Moreover, most CRCs are not colitis associated and therefore the immune profile of these mice does not represent the majority of human CRCs. Nevertheless, this research demonstrates that Sting can exert anti-tumourigenic effects in some contexts.

Nlrp3 Signaling

Numerous stressors have been identified as activating the nod-like Receptor family pyrin domain containing 3 (NLRP3) inflammasome.[98] Unlike other PRRs, the NLRP3 inflammasome is not thought to directly sense a ligand.[99] Instead, it assembles in response to several cellular insults, namely K+ efflux, resulting from a variety of different signals.[100,101] Bacteria can release pore-forming toxins, ionophores, and ATP, which can all serve to initiate K+ efflux and therefore stimulate NLRP3 inflammasome activity.[102] NLRP3 has three domains: a pyrin (PYD), NACHT, and leucine-rich repeat (LRR) domain.[103] The ATPase activity of the NACHT domain is auto-inhibited by the LRR domain.[103] The NLRP3 protein and the apoptosis-associated spec-like protein (ASC) associate through their pyrin domains (PYD) such that multiple ASCs oligomerize to form a helical filament known as an ASC speck.[103] The caspase activation and recruitment domain (CARD) on ASC associates with the pro-caspase CARD to form the complete, yet inactive, NLRP3 inflammasome.[100] Finally, the pro-caspase auto-cleaves its linker between p20 and p10, resulting in inflammasome activation.[103]

It is hypothesized that activation of the NLRP3 inflammasome requires two events. The first step is activation of another PRR to trigger transcription of NFκBp65 that will then induce transcription of NLRP3 and the inactive pro-form of IL1β.[104] The second step is initiated by either bacterial toxins or extracellular ATP and drives the complexing of NLRP3 with ASC and caspase-1. ATP is released following cell damage from infection or injury in the gut and binds the purinergic P2X7 receptor on the tumour cells.[84] This triggers formation of P2X7 pores in the tumour cell membrane leading to a coordinated Ca^{2+} and Na^{+} influx with a K^{+} efflux that, collectively, activate the NLRP3 inflammasome.[103] This causes caspase-1 to cleave pro-IL1β and pro-IL18 into their mature, active forms.[105] Unlike most cytokines, IL1β and IL18 are not secreted through the ER-Golgi pathway, but they are released either by secretory lysosomes, microvesicles or exosomes.[18]

Alternatively, NLRP3 and ASC can complex with and activate caspase-11 instead of caspase-1 downstream of extracellular P2X7 binding ATP.[106,107] This causes caspase-11 to cleave gasdermin D (GSDMD) and pannexin-1 (PANX1). Cleavage of members of the gasdermin superfamily drives a form of necrotic programmed cell death known as pyroptosis.[108] GSDME is cleaved by caspase-3 subsequent to apoptosis induction, while GSDMD is cleaved downstream of inflammasome activation.[108] During steady state, the necrotic function of the GSDMD N-terminal domain is sequestered by its C-terminal domain, but upon proteolytic cleavage of the GSDMD proteins by caspase-11, the N-terminal domains can localize to the cellular membrane and form membrane-spanning pores and ultimately osmotic cytolysis.[108] The cleaved PANX1

can then mediate the release of ATP through these pores and initiate more pyroptosis in neighbouring cells.[109] Elucidating the differential role of caspase-1 versus caspase-11 in inflammasome activity has recently come under fire, because the caspase-1 knockout mouse model was recently discovered to also be lacking caspase-11 expression.[107] Therefore, the literature is not in agreeance as to whether these caspases serve exclusive purposes in the NLRP3 inflammasome, as stated here, or if they are interchangeable.

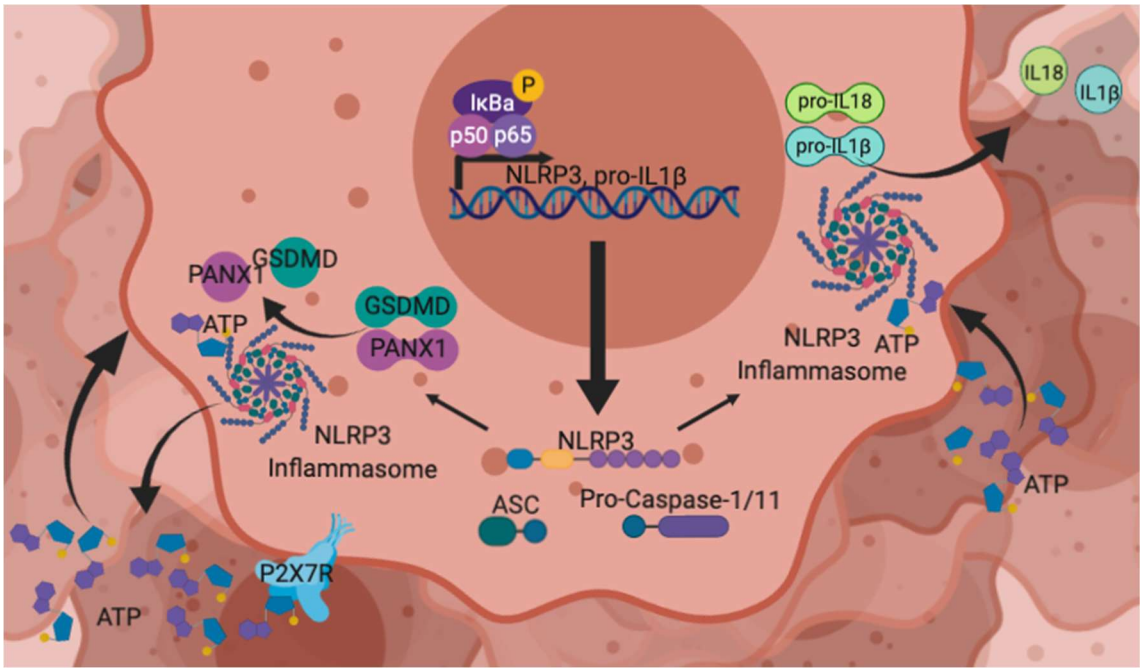

Figure 1-2. NLRP3 signaling pathway. NFκBp50/65 transcribes NLRP3 and pro-IL1β. Changes in potassium efflux triggers the assembly of the NLRP3 inflammasome such that the PYD domains of NLRP3 and ASC bind one another and the CARD domains of ASC and pro-caspase1/11 bind one another. The ASC proteins oligomerize to form the full inflammasome and the **(4)**. ASC and NLRP3 assemble the inflammasome with caspase-1. This activates caspase-1, leading it to cleave pro-IL1β and pro-IL18 into their mature forms **(5)** and resulting in the recruitment of

adaptive immune cells. The release of type I IFNs **(6)** aids in the antigen presentation by the recruited DCs to CD8+ T cells. Figure made in ©BioRender - biorender.com. NFκBp65 driving the transcription of NLRP3 **(4)**. The production of IFNs by STING can drive the production of caspase-11, which can form an inflammasome with NLRP3 and ASC **(5)**. This could initiate pyroptosis via the cleavage of gasdermin D (GSDMD) and the cytosolic portion of pannexin 1 (PANX1). The N-terminal domain of GSDMD creates pores in the cell membrane while the cleaved PANX1 causes ATP to be released from the cell, which can then bind the P2X7 receptor and open the P2X7 pores, resulting in pyroptosis **(6)**. Figure made in ©BioRender.

Clinical and experimental data support the importance of this pathway in cancer development. Survival of patients with local recurrence-free nasopharyngeal carcinoma is associated with high expression of ASC, NLRP3, CASP1, and IL1β, indicating that this pathway may aid in potentiating anti-tumour immunity in cancers of mucosal tissues.[90] When administered AOM/DSS, *Nlrp3*$^{-/-}$ mice display increased tumourigenesis compared to their wildtype counterparts, and this is attributable to downstream production of the Il18 cytokine that promotes enterocyte differentiation as well as epithelial repair.[110,111] Additionally, production of Il18 via activation of the Nlrp3 inflammasome has been found to suppress the growth of metastatic colorectal lesions in the liver.[112] Caspase11$^{-/-}$ mice have an increased susceptibility to colitis associated CRC, including increased angiogenesis and decreased programmed cell death.[113] Of note once again is that these studies were conducted with whole body knock-out mice for *Nlrp3*, leading to the same limitations as for the *Sting*$^{-/-}$ mice.

As with most PRRs, the function of the NLRP3 inflammasome has been almost exclusively elucidated from studies in immune cells. Whether the function of the NLRP3 inflammasome in hematopoietic derived cells is synonymous with its function in IECs remains undetermined.[18] For example, although in immune cells the NLRP3 inflammasome can be activated through a non-canonical pathway that only requires one signal from TLR4, TLR4 expression is lower in IECs compared to epithelial cells elsewhere in the body.[18] Additionally, since IECs are constantly exposed to microbial components, the thresholds to induce PRR activation may be considerably different than those determined in immune cells.[18] The intestinal epithelium does have high levels of GSDMD and P2X7, but the role of P2X7 has so far only been studied in immune cells and whether IECs undergo pyroptosis has yet to be determined.[18,84] Although IECs express limited amounts of IL1β, they are the primary source of IL18 in the intestine[18]. This increases IFNγ production and facilitates activation of intestinal T cells, which have higher expression of the IL18 receptor than systemic T cells.[18] IL18 released from IECs can also drive the production of IFNγ in T cells and natural killer cells expressing IL12 and IL15, thereby skewing the intestinal environment towards a Th1 immune response.[114] Compared to CIN CRCs, IL18 is significantly upregulated in MSI CRCs, alluding to the possibility that the NLRP3 inflammasome could be potentiating the anti-tumour immune phenotype in this CRC subtype.[115]

Rationale

Through mining The Cancer Genome Atlas, we first focused our attention on four innate immune receptors that were significantly upregulated in human MSI CRCs compared to CIN or

POLE mutated CRCs. These included toll-like receptor 3 (*TLR3)*, absent in melanoma 2 (*AIM2)*, *STING*, and *NLRP3*. Through our mouse models of MSI, CIN, and *Pole* mutated CRCs, we showed that *Nlrp3* and *Sting* RNA and protein expression are significantly higher in MSI CRCs that have enhanced infiltration of active CD8+ T cells, as well as a smaller tumour size, both of which are indicative of robust anti-tumour immunity. In seeking to understand why MSI CRCs have enhanced expression of these receptors, we considered that it could be due to numerous microsatellite regions being present in their genes and leading to selective upregulation of their expression in MSI CRC. However frameshift mutations leading to enhanced expression of a gene are relatively rare.[23] Instead, we reasoned that it was more likely that common factors in the tumour microenvironment of MSI CRCs lead to selective upregulation of certain genes. Given the proximity of CRC to the intestinal lumen, we thought it logical that genes involved in coping with intestinal microbiota could be regulated in this manner. While the anti-tumour immunity of MSI CRC had yet to be attributed to any of these genes, we found evidence that both STING and NLRP3 independently promote anti-tumour immunity. In this project, we thus sought to investigate the role of these receptors in regulating the immune response against MSI CRC.

HYPOTHESIS

The overarching hypothesis of this thesis is that microsatellite instable colorectal cancers create a microenvironment that drives the activation of STING and NLRP3 pattern recognition receptors resulting in the initiation of an anti-tumour immune response, and therefore favorable prognosis compared to chromosomally instable colorectal cancers.

Aim 1. Genetic instability from the ablation of *Mlh1* or *Pole* increases the immunogenicity of CRC

We hypothesize that loss of *Pole* or *Mlh1* in CRC cells changes how they interact with the immune system *in vivo* and specifically increase their detection by CD8+ T cells.

Aim 2. MSI CRCs have significantly higher expression of *Sting* and *Nlrp3*

We hypothesize that MSI CRCs have higher infiltrating CD8+ T cells because of the differential expression of pattern recognition receptors compared to CIN CRCs.

Aim 3. Sting and Nlrp3 can be activated in both MSI and CIN CRC cells *in vitro*, and it appears their effects are additive

We hypothesize that Sting and Nlrp3 are working together to enhance anti-tumour immunity and cancer cell death in MSI CRCs.

Aim 4. Orthotopic MSI CRCs have a microbial profile that is disparate from CIN CRC

We hypothesize that increased expression of Nlrp3 and Sting predicts the presence of differential bacterial OTUs in the intestinal microbiota of MSI compared to CIN CRCs.

CHAPTER 2: MATERIALS AND METHODS

Animals

C57BL/6 wildtype mice originally purchased from Charles River were bred and maintained in the Cross Cancer Institute animal housing facility. Mixed groups of male and female mice between the age of 6-20 weeks old were used for experiments. Work done with animals is approved by the University of Alberta Animal Care and Use Committee protocol no. AC15219.

Cell culture

MC38 is a murine cell line derived from a C57BL/6 colon adenocarcinoma possessing an *Apc* mutation and was purchased from Kerafast. Cells were grown in high glucose Dulbecco's modified MEM supplemented with 10% fetal bovine serum, 1% penicillin-streptomycin, and 1% HEPES at 37˚C with 5% CO_2. Cells were transfected with the pSpCas9(BB)-2A-puro (px459) V2.0 plasmid (Addgene) containing CRISPR guide-RNAs (gRNAs) (Table 1) targeting the *Mlh1* or *Pole* genes or no gRNA as a control ("Empty"). Transfections were performed using Lipofectamine™ 2000 (Thermo Fisher Scientific). Transfectants were selected by puromycin (2ug/ml) and knock-outs were confirmed either by sequencing or Western blot (see below). From this transfection, the "Empty" control cells, two independently derived *Mlh1*$^{-/-}$ cell lines, and one confirmed *Pole*$^{-/-}$ cell line were cultured continuously for 6 months to allow full effect of the instability phenotypes. Experiments were done with the 6-month-old cell lines.

CRISPR knock-out sequencing

Genomic DNA was isolated from cell pellets using the Quick Genomic DNA Extraction kit (Truin Science). Primers possessing EcoRI and BamHI cut sites at their ends were used (Table 1) with the Q5®High-Fidelity PCR Kit to amplify the Mlh1 CRISPR target site region. PCR products were purified using a GeneJet Gel Extraction Kit (Thermo Scientific) and then the ends were digested using EcoRI, BamHI and CutSmart® Buffer (New England Biolabs). At this time 5ug of the pUC19 plasmid (Addgene) was also digested with EcoRI and BamHI in CutSmart® Buffer for 1 hour at 37˚C. The digested PCR products were ran on a 1% agarose gel and the desired bands were isolated using the GeneJet Gel Extraction Kit (Thermo Scientific). The digested PCR products and plasmid were ligated together using T4 DNA ligase and buffer (New England Biolabs) with a ratio of 1:3 (vector:insert) at room temperature for 1 hour. The ligated plasmids were then transformed into competent DH5alpha *Escherichia coli* in a 42˚C water bath for 60 seconds. Transformed bacteria were spread onto LB-agar plates with ampicillin and grown overnight at 37˚C. Multiple colonies were picked from each plate then grown in 3 ml LB ampicillin broth at 37˚C overnight. The plasmids were isolated from the bacterial cultures using the MiniPrep Plasmid Purification Kit (Truin Science). The sequencing reaction was done using 3.2mM of the M13 primer (Table 1) along with the BigDye™ Terminator v3.1 Cycle Sequencing kit and 300ng of each plasmid. The sequencing samples were then precipitated using 2.5µl of 125mM EDTA, 25µl of 100% ethanol, and 1µl of GlycoBlue™ (ThermoFisher Scientific). Samples were mixed by inversion then incubated at room temperature for 15 minutes followed by centrifugation at 18,300xg for 10 minutes at 4˚C. Supernatants were removed completely at 4˚C and then 30µl of fresh 70% ethanol was added to each sample, flicked to mix and then

centrifuged at 18,300xg for 5 minutes at 4˚C. The supernatant was aspirated at room temperature and the samples were dried at 95˚C for 1 minutes in the dark with the lids open. Samples were resuspended in 12.5µl of HiDi Formamide (Applied Biosystems) injection buffer. Samples were then heated at 95˚C for 5 minutes in the dark and then chilled for 10 minutes before being spun down and transferred to 310 tubes and loaded onto the sequencer (Applied Biosystems 3100 Genetic Analyzer). At least 4 sequences were ran for each sample. Sequences regions were confirmed by blasting against the *Mus musculus* genome through the NCBI genome browser and then were aligned to one another using the ApE v2.0.53c software. Successful mutants were determined by comparing the sequences to that of the MC38 "Empty" vector control.

Human data

Human RNA sequencing data and DNA sequencing data (Illumina HiSeq RNASeqV2) from The Cancer Genome Atlas (Nature 2012, and PanCancer Atlas) for CRC were downloaded from cBioPortal for Cancer Genomics (https://www.cbioportal.org/)[116,117] and then graphed and statistically analyzed using Prism (GraphPad). The CpG methylation status of the promoter of *MLH1* was analyzed using the UCSC Genome Browser on Human Feb. 2009 (GRCh37/hg19) Assembly with the CpG Islands Tracks (https://genome.ucsc.edu/cgi-bin/hgGateway).[116]

Subcutaneous tumour RNA isolation and reverse transcription

Subcutaneous experiments were set up by injecting $0.5x10^6$ six-month-old MC38 "Empty", *Mlh1*$^{-/-}$ A, *Mlh1*$^{-/-}$ B, and *Pole*$^{-/-}$ cells in 1x PBS into the hind flank of flank of the mice and then allowing the tumours to grow for 2-3 weeks before resection. Resected tumours were dissociated using scissors and then digested in 10ml of pre-warmed enzyme cocktail (RPMI media containing 0.5mg/ml collagenase IV, 10µg/ml DNaseI, 10%FBS, 1% penicillin-streptomycin, 1% HEPES buffer) for 30 minutes at 37˚C in a shaking incubator. Fragments were rigorously pipetted to dissociate and then filtered through a 100µm cell strainer and washed with 2% FBS (in 1x PBS). To separate the epithelial (tumour) from immune cells, the cell pellets were resuspended in 2ml of 40% percoll (GE Healthcare) (diluted with 2% FBS in 1x HBSS) and were overlaid onto 2ml of 80% percoll (diluted with 2% FBS in 1x HBSS). Samples were spun at 493xg (brake off) for 30 minutes at room temperature. The top layer (tumour cells) and the interface (immune cells) were collected into separate tubes and the percoll was washed off using 2% FBS (in 1x PBS). The cell pellets were lysed in TRIzol (Thermo Fisher Scientific), incubated first for 5 minutes at room temperature and then for ≥1 hour at -80˚C. After thawing, chloroform was added and samples were mixed vigorously and incubated for 3 minutes at room temperature before centrifugation at 12,000xg for 15 minutes at 4˚C. While working on ice, the aqueous phase was collected and GlycoBlue™ (Thermo Fisher Scientific) and isopropanol were added and mixed gently. Samples were then incubated at -80˚C for ≥1 hour. Once thawed, the samples were centrifuged at 12,000xg for 20 minutes at 4˚C and then the supernatant was removed and the pellet was washed with cold 75% ethanol and centrifuged at 7,400xg for 15 minutes at 4˚C. The supernatant was removed and the RNA pellet was allowed to air dry for ≥1 hour before being resuspended in nuclease free water and stored at -80˚C.

Equal amounts of RNA from the immune and epithelial cells of each tumour sample were reverse transcribed using the High Capacity Reverse Transcription Kit (Life Technologies) and the cDNA was used for qPCR.

qPCR

For qPCR we mixed our cDNA with EvaGreen 2x qPCR Master-Mix-ROX (ABM) along with the qPCR primers shown in Table 1 and ran the samples on the QuantStudio™ 6 real-time PCR system (Applied Biosystems) in quadruplicate. All samples were normalized to the average Ct of Gapdh (ΔCt) for that sample. To obtain the inverse of ΔCt we calculated $(2^{-\Delta Ct})x10{,}000$[118,119] and averaged this value between the quadruplicates, throwing out technical replicates that were obvious outliers using the Grubb's test for outliers, or that had poor melting temperatures. Results were then graphed and statistically analyzed with Prism (GraphPad). Parametric unpaired t-Tests were performed between all groups.

Immunohistochemistry and microscopy

Subcutaneous tumour samples were fixed in 10% formalin (Fisher Chemical), and then paraffin embedded (FFPE). FFPE blocks were sliced into 7μm thick slices using a microtome and melted onto Superfrost™ Plus glass microscope slides (Fisherbrand™). Once deparaffinized, antigen retrieval was performed in a microwave pressure cooker (Nordic Ware) with antigen retrieval buffer (10mM citrate, 1mM EDTA, 0.05% Tween-20) until the unit pressurized,

followed by an additional 2 minutes. The pressure cooker was slowly cooled to room temperature and the slides were then stained using the DAKO EnVision™ G2 Doublestain System, Rabbit/Mouse (DAB+/Permanent Red). Prior to the dual endogenous enzyme block, the slides were exposed to 3% hydrogen peroxide for 5 minutes to quench endogenous peroxidases. To block before the primary antibody, we used 0.5% fish skin gelatin for 30 minutes at room temperature. Primary antibodies were added at 1:100 for anti-Sting, and 1:50 for anti-CD8a (Table 2) diluted in 1% BSA (in 1x PBS) and the negative control slides for each tumour received 1% BSA (in 1x PBS) rather than a primary antibody. Slides were visualized on the ZEISS Axioscope microscope using the ZEISS ZEN software for imaging. The Sting slides were scored on a scale of 0-4 for intensity by two individuals independently and the CD8 slides were scored by counting total number of stained cells on two 10x images for each tumour sample. Parametric unpaired t-Tests were performed between all groups.

Sting and Nlrp3 co-stimulation and inhibition

Six-month-old MC38 "Empty", *Mlh1*$^{-/-}$ A, *Mlh1*$^{-/-}$ B, and *Pole*$^{-/-}$ cells were seeded into 6-well plates at 2.8x10^5 cells/well one day prior to the stimulation. 2',3'-cGAMP (InVivogen) in Limulus amebocyte lysate (LAL) water was encapsulated in Lipofectamine™ 2000 (Thermo Fisher Scientific) and added to the cells at a final concentration of 9μg/ml, while ATP (Sigma-Aldrich) in nuclease free water was added at a final concentration of 2mM. The vehicle control for the stimulation of Sting was an equal volume of LAL water encapsulated in the same concentration of Lipofectamine™ 2000 as the 2'3'-cGAMP. The vehicle control for the stimulation of Nlrp3 was

nuclease free water at the same volume as ATP. The ATP master mix received 1N NaOH until it was the same pH as the Nlrp3 vehicle control. For the inhibition experiment we added the Sting inhibitor, carbonyl cyanide 3-chlorophenylhydrazone (CCCP) (Abcam) in DMSO, to a final concentration of 25μM. While the Nlrp3 inhibitor, Isoliquiritigenin (Sigma-Aldrich) in DMSO, was added to a final concentration of 10μM. The vehicle control for the inhibition of Sting and Nlrp3 was the addition of DMSO to the same volume as either inhibitor used. Cells were exposed to the combinations of these conditions for 2 hours at 37˚C, 5% CO_2 and then the protein was isolated for Western blotting.

Protein isolation and Western blotting

Following stimulation, adherent cells were washed 1x in cold PBS and then protein was isolated using protein lysis buffer (50mM Tris-HCl, 150mM NaCl, 50mM sodium pyrophosphate, 1mM EDTA, 05% NP40, 1% Triton X-100, 1mM sodium orthovanadate, and 1x protease inhibitor (Sigma-Aldrich). Lysates were rotated for 30 minutes at 4˚C and centrifuged at 18,300xg for 15 minutes. The supernatant was collected for protein quantification via the Pierce™ BCA protein assay kit (Thermo Fisher Scientific). Lysates were normalized to 10μg of protein in equal volume and were suspended in denaturing loading buffer (10% SDS, 25% glycerol, 0.25 M Tris-HCl pH 6.8, bromophenol blue, 5% β-mercaptoethanol). Samples were run on 10% SDS-PAGE gels with the PiNK Plus (FroggaBio) and BLUElf (FroggaBio) prestained protein ladders. Proteins were transferred to 0.22μm nitrocellulose membranes for ≥1.5 hours in 1x transfer buffer (0.25M Tris, 1.91M glycine, 20% methanol) then washed in 1x TBST (10mM tris-HCl pH 8.0, 150mM

NaCl, 0.1% Tween-20) and blocked with 5% powdered skim milk (Carnation) (in 1x TBST) for ≥30 minutes at room temperature. Membranes were washed in 1x TBST prior to incubating with the primary antibody (Table 2) diluted 1:1000 in 5% BSA (1x TBST, 0.02% sodium azide) overnight at 4˚C. The primary antibody was washed off and the membranes were incubated at room temperature with 1:2000 of HRP conjugated secondary antibody in 5% milk (in 1x TBST) for ≥1 hour. Membranes were washed in 1x TBST and visualized using ECL™ Prime Western Blotting Detection Reagent (GE Healthcare Amersham™) and film (Fuji RX) developed in a Kodak developer.

Polε Immunoprecipitation

MC38 Empty and *Pole*$^{-/-}$ cells were grown in 10cm dishes and washed with 1x PBS before isolation with non-denaturing protein lysis buffer (50mM Tris-HCl, 150mM NaCl, 50mM sodium pyrophosphate, 1mM EDTA, 05% NP40, 1% Triton X-100, and 1x protease inhibitor (Sigma-Aldrich) and a cell scraper. Lysates were mixed using end-over-end mixing for 30 minutes at 4˚C and then centrifuged at 21,000xg for 15 minutes at 4˚C. The supernatant was collected for protein quantification via the Pierce™ BCA protein assay kit (Thermo Fisher Scientific) and equal amounts of protein were then precleared with 30ul of a 50% (v/v) slurry of protein G sepharose beads (GE Healthcare Amersham™) in non-denaturing protein lysis buffer. This mixture was incubated with end-over-end mixing for 60 minutes at 4˚C and then the beads were pelleted at 12,000xg for 20 seconds at 4˚C. 2μg/ml of the Polε antibody (Table 2) was added to the supernatant and incubated with end-over-end mixing overnight at 4˚C. 30μl of a 50% (v/v)

slurry of beads was added to the lysates and incubated with end-over-end mixing for 90 minutes at 4˚C. This mixture was then centrifuged at 12,000xg for 20 seconds at 4˚C, the beads were washed in non-denaturing lysis buffer and pelleted again at 12,000xg for 20 seconds at 4˚C. To remove the protein from the beads, 50μl of 2x SDS loading buffer (10% glycerol, 5% β-mercaptoethanol, 4% SDS, 0.1M Tris-HCl pH 6.8, and bromophenol blue in denaturing lysis buffer) was added and the samples were incubated at 100˚C for 5 minutes Samples were centrifuged at 10,000xg for 2 minutes at 4˚C and all of the supernatant for each sample was transferred to a new tube. Samples were separated on an 8% SDS-PAGE gel along with the HiMark™ (Thermo Fisher Scientific) prestained protein ladder. Proteins were transferred to 0.22μm nitrocellulose membranes for ≥4 hours at 70V at 4˚C in 1x high molecular weight transfer buffer (0.25M Tris, 1.91M glycine, 5% methanol, 0.1% SDS) then washed in 1x TBST and blocked with 5% powdered skim milk (in 1x TBST) for ≥30 minutes at room temperature. Membranes were washed in 1x TBST prior to incubating with the Polε primary antibody (Table 2) diluted 1:1000 in 5% BSA (1x TBST, 0.02% sodium azide) overnight at 4˚C. The primary antibody was washed off and the membranes were incubated at room temperature with 1:2000 of HRP conjugated secondary antibody in 5% milk (1x TBST) for ≥1 hour. Membranes were washed in 1x TBST and visualized using ECL™ Prime Western Blotting Detection Reagent (GE Healthcare Amersham™) and film (Fuji RX) developed in a Kodak developer.

Orthotopic tumour model

Fecal samples were collected into sterile tubes from each mouse one day prior to injection of tumour cells and stored at -80˚C. Colon orthotopic experiments were performed by injecting $0.1x10^6$ six-month-old MC38 "Empty", *Mlh1*$^{-/-}$ A, *Mlh1*$^{-/-}$ B, and *Pole*$^{-/-}$ cells in 1x PBS into the descending part of the colon using a flexible needle (Hamilton) inserted through the working channel of a Wolfe endoscope and visualized via the ColoView imaging system (Storz). Orthotopic tumour growth was monitored by endoscope after one week while animal behaviour was monitored daily; the tumours were resected after 2 weeks. Intestines were removed using scissors, while sterile razor blades were used to cut out the part of the colon with the tumour and to collect fecal samples for DNA isolation. The fecal samples were stored at -80˚C. Resected tumours were dissociated using scissors and then digested in 5ml of pre-warmed enzyme cocktail (RPMI media containing 0.5mg/ml collagenase IV, 10μg/ml DNaseI, 10%FBS, 1% penicillin-streptomycin, 1% HEPES buffer) for 30 minutes at 37˚C in a shaking incubator. Fragments were rigorously pipetted to dissociate, filtered through a 100μm cell strainer and washed with 2% FBS (1x PBS). Samples were then stained for flow cytometry.

Flow cytometry

Flow staining was done in 96-well round bottom plates. Cells from each tumour were stained by three separate antibody panels using pooled cells as staining controls. Prior to antibody staining, the cells were treated with the Zombie Aqua viability dye (BioLegend) in 1x PBS in the dark for 30 min. All three panels were then stained with 1:200 of the CD8, CD4, CD3, and CD45 flow cytometry antibodies (Table 2) for 30 min. at 4˚C. For intracellular staining we

used the forkhead box protein p3 (Foxp3)/Transcription Factor Staining Buffer Set (eBioscience) and fixed/permeabilized the cells overnight. After washing, we added 1:100 of either the phospho-Sting, Nlrp3, or phospho-Tbk1 primary antibodies in 1x permeabilization buffer to one panel each for 30 minutes at 4˚C in the dark. After washing, we added the Alexa^{488} conjugated rabbit secondary antibody (Jackson ImmunoResearch) at 1:500 in 1x permeabilization buffer for 30 minutes at 4˚C, and then cells were washed and suspended in FACS buffer (2% FBS, 1mM EDTA, 1xPBS). The staining controls included tumour cells without any antibodies added, cells with just the viability dye, or an isotype control for the intracellular secondary antibody auto-fluorescence. Compensation was performed using UltraComp eBeads (Thermo Fisher Scientific). Flow cytometry was performed on the BD LSRFortessa™ cytometer with a plate adapter. Analysis was performed using FlowJo (BD Biosciences) and gates were drawn based on cell staining controls. Parametric unpaired t-Tests were performed between all groups.

Fecal DNA isolation and 16s rRNA DNA sequencing

Fecal samples were lysed using 750μl of lysis buffer (200mM NaCl, 100mM Tris pH 8.0, 20mM EDTA, 20mg/ml lysozyme (sigma)) at 37˚C for 30 minutes. A blank tube was isolated to serve as a kit contamination control. Samples were resuspended in 85μl 10% SDS in 30ul of Proteinase K (20mg/ml) (NEB) and incubated at 60˚C for 30 min. Samples were added to screwcap tubes with 300mg of 1mm beads and 500μl phenol:chloroform:isoamyl alcohol (25:24:1) (Thermo Fisher Scientific) and beaten in a bead beater on high for 2 minutes, then spun at 10,000xg for 5 minutes. The aqueous layer was added to 500μl of

phenol:chloroform:isoamyl alcohol (25:24:1), vortexed, then spun at 14,000xg for 5 minutes and this step was repeated two more times before the final aqueous phase was precipitated with ethanol and 60μl of 3M sodium acetate (pH 5.2) at -20˚C for ≥1 hour. Samples were spun for 10min at 14,000xg, and the pellets were dried and resuspended in Tris buffer (10mM, pH8.0). The DNA was then isolated using the GeneJET genomic DNA purification kit (Thermo Fisher Scientific) according to the manufacturer's directions, except that DNA was eluted in 40μl of elution buffer. The concentration of each sample was determined using the QuantIT™ PicoGreen™ dsDNA Assay Kit (Thermo Fisher Scientific) according to the manufacturer's directions. The V3-V4 variable regions of the 16s ribosomal RNA (rRNA) gene was PCR amplified using primers 341 Forward and 806 Reverse (Table 1) possessing barcodes along with the Phusion® High-Fidelity PCR Master Mix (New England Biolabs). The preparation of the library was done with the Ion Xpress™ Plus Fragment Library Kit (Thermo Fisher Scientific) and then the samples were sequenced on an Illumina MiSeq platform by Jinghong Kang from the Ben Willing group at the University of Alberta. The data was analyzed in QIIME (Quantitative Insights Into Microbial Ecology) for microbial abundance by Tingting Ju from the Ben Willing group. The average OTU abundance of the *Mlh1*$^{-/-}$ and Empty tumour groups both before injection and at the time of tumour resection were graphed in Prism (GraphPad). Significant changes in the abundance of operational taxonomic units (OTUs) induced by tumor growth were evaluated by conducting a two-way ANOVA (CI>95%) with Sidak's multiple comparisons test between the OTU abundance in feces taken from the mice before tumor injection and at the time of tumour resection within each tumour group. To evaluate how the growth of different tumor types affected microbial composition, the final OTU abundances in mice

bearing *Mlh1*$^{-/-}$ and Empty tumours were normalized to the baseline OTU abundances by subtracting the pre-injection abundances from the abundances at the time of tumor resection in each mouse. A two-way ANOVA (CI>95%) with Sidak's multiple comparisons test was used to determine the OTUs that were significantly different between the Empty and *Mlh1*$^{-/-}$ tumour groups.

Tables

Table 1. Primers		
Primer Name	**Primer Sequence (5'→3')**	**Purpose**
Mlh1 A gRNA Forward	caccgGACGGTAGTGAACCGCATAGCGG	CRISPR
Mlh1 A gRNA Reverse	aaacCCGCTATGCGGTTCACTACCGTCc	CRISPR
Mlh1 B gRNA Forward	caccgGGTAGTGAACCGCATAGCGGCGG	CRISPR
Mlh1 B gRNA Reverse	aaacCCGCCGCTATGCGGTTCACTACCc	CRISPR
Pole gRNA Forward	caccgGGCTTGGGCCTATCCGAGAGGGG	CRISPR
Pole gRNA Reverse	aaacCCCCTCTCGGATAGGCCCAAGCCc	CRISPR
M13/pUC Forward	CCCAGTCACGACGTTGTAAAACG	Sequencing
M13/pUC Reverse	AGCGGATAACAATTTCACACAGG	Sequencing
Mlh1 Seq Forward	GCGCGCGAATTCCCAAATCAAATGTCCGAGGGC	Sequencing
Mlh1 Seq Reverse	GCGCGCGGATCCGTAGCAGGAGTTATTCGGCGT	Sequencing
16s Forward	CCTAYGGGRBGCASCAG	16s Illumina Sequencing
16s Reverse	GGACTACNNGGGTATCTAAT	16s Illumina Sequencing
IL1b Forward	TTCAGGCAGGCAGTATCACTC	qPCR
IL1b Reverse	GAAGGTCCACGGGAAAGACAC	qPCR
IFNg Forward	GGCAAAAGGATGGTGACATGA	qPCR
IFNg Reverse	ACCTGTGGGTTGTTGACCTC	qPCR
Sting Forward	CTACATTGGGTACTTGCGGTT	qPCR
Sting Reverse	GCACCACTGAGCATGTTGTTATG	qPCR
Nlrp3 Forward	ATTACCCGCCCGAGAAAGG	qPCR
Nlrp3 Reverse	TCGCAGCAAAGATCCACACAG	qPCR
Ccr5 Forward	TTTTCAAGGGTCAGTTCCGAC	qPCR
Ccr5 Reverse	GGAAGACCATCATGTTACCCAC	qPCR
Ccl5 Forward	GCTGCTTTGCCTACCTCTCC	qPCR
Ccl5 Reverse	TCGAGTGACAAACACGACTGC	qPCR
CD8a Forward	AAGAAAATGGACGCCGAACTT	qPCR
CD8a Reverse	AAGCCATATAGACAACGAAGGTG	qPCR
Gapdh Forward	CATGTTCCAGTATGACTCCA	qPCR
Gapdh Reverse	TGAAGACACCAGTAGACTCC	qPCR

Table 2. Antibodies			
Target	**Fluorophore or Secondary**	**Purpose**	**Source**
β–Actin	Anti-rabbit IgG HRP	Western Blot	Cell Signaling (8457S)
Mlh1	Anti-rabbit IgG HRP	Western Blot	Abcam (ab92312)
Polε	Anti-mouse IgG HRP	Western Blot	InVitrogen (MA5-13616)
Nlrp3	Anti-rabbit IgG HRP or Alexa 488	Western Blot, Flow Cytometry	Cell Signaling (15101S)
phospho-Sting (Ser365)	Anti-rabbit IgG HRP or Alexa 488	Western Blot, Flow Cytometry	Cell Signaling (72971S)
Sting	Anti-rabbit IgG HRP	Western Blot, IHC	Cell Signaling (13647S)
phospho-Stat3 (Tyr705)	Anti-rabbit IgG HRP	Western Blot	Cell Signaling (9131S)
Stat3	Anti-rabbit IgG HRP	Western Blot	Cell Signaling (12640S)
phospho-NFκBp65 (Ser536)	Anti-rabbit IgG HRP	Western Blot	Cell Signaling (3033S)
phospho-Tbk1 (Ser172)	Anti-rabbit IgG HRP or Alexa 488	Western Blot, Flow Cytometry	Cell Signaling (5483S)
Tbk1	Anti-rabbit IgG HRP	Western Blot	Cell Signaling (3504S)
Gsdmd	Anti-rat IgG HRP	Western Blot	Genentech (10026)
CD8	Anti-mouse IgG HRP	IHC	eBioscience (14-0808-82)
CD3	APCcy7	Flow Cytometry	Biolegend (100222)
CD8	APC	Flow Cytometry	Biolegend (100712)
CD4	PerCPCy5.5	Flow Cytometry	Biolegend (116012)
CD45	PE	Flow Cytometry	Biolegend (103106)
CD69	PeCy7	Flow Cytometry	Biolegend (104512)
Rabbit IgG	Alexa 488	Flow Cytometry	Jackson ImmunoResearch (#111-545-144)
Rabbit IgG	HRP	Western Blot	Cell Signaling (7074S)
Rat IgG	HRP	Western Blot	Cell Signaling (7077S)

CHAPTER 3: RESULTS

Aim 1. Genetic instability from the ablation of *Mlh1* or *Pole* increases the immunogenicity of CRC

CIN is the most common subtype of CRC and is initiated by driver mutations in the *APC* gene.[120] This is reflected in the high frequency of *APC* mutations seen in CRC samples in the TCGA database (Figure 1-3A), many of which would result in a defective or absent APC protein (Figure 1-5A). Comparatively, MSI CRC is driven by the inactivation of the *MLH1* gene resulting in defective DNA MMR.[3] Although there are mutations that occur within the *MLH1* gene in human CRCs (Figure 1-3B), these are typically only seen in the small fraction of patients with Lynch Syndrome.[121] Most sporadic MSI CRC are driven by the epigenetic silencing of *MLH1* via methylation of CpG islands in the gene's promoter region (Figure 1-4).[16] This phenocopies the silencing effect of the documented *MLH1* mutations that would cause the MLH1 protein to be dysfunctional or absent (Figure 1-5B). We thus chose to use mutation in our model MC38 mouse CRC lines to knock out, rather than epigenetically silence, *Mlh1* to render them MSI. A small subtype of CRCs possess mutations in the *POLE* gene (Figure 1-3C, Figure 1-5C). Some of these mutations either delete the gene or alter the exonuclease activity of the polymerase epsilon enzyme during DNA synthesis, resulting in the development of point mutations throughout the genome.[28]

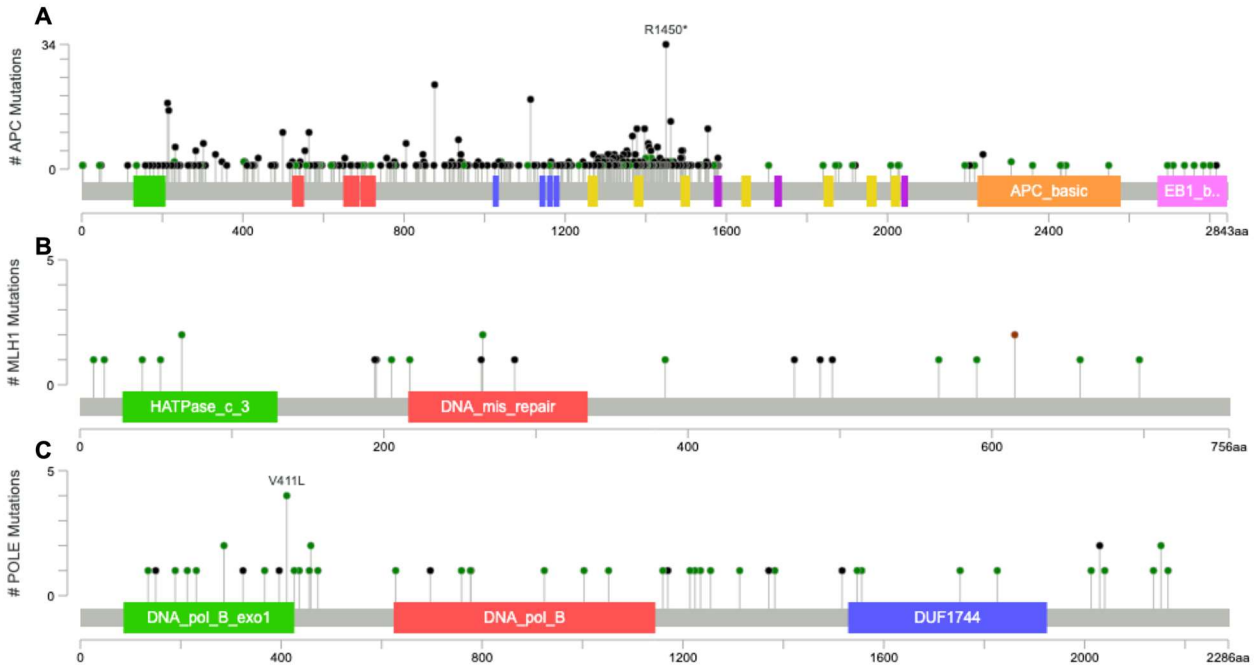

Figure 1-3. Locations of mutations in *APC*, *MLH1*, and *POLE* in human CRCs. Each lollipop marker represents a human CRC that has a mutation at that location in the **(A)** *APC*, **(B)** *MLH1*, or **(C)** *POLE* gene. Green lollipop markers indicate a missense mutation, red markers indicate an in-frame mutation, and black markers indicate a truncating mutation. The height of the marker reflects the number of patient samples that share that mutation (y-axis). These graphics were created by the cBioPortal for Cancer Genomics using data from the TCGA PanCancer Atlas dataset of colorectal adenocarcinomas.

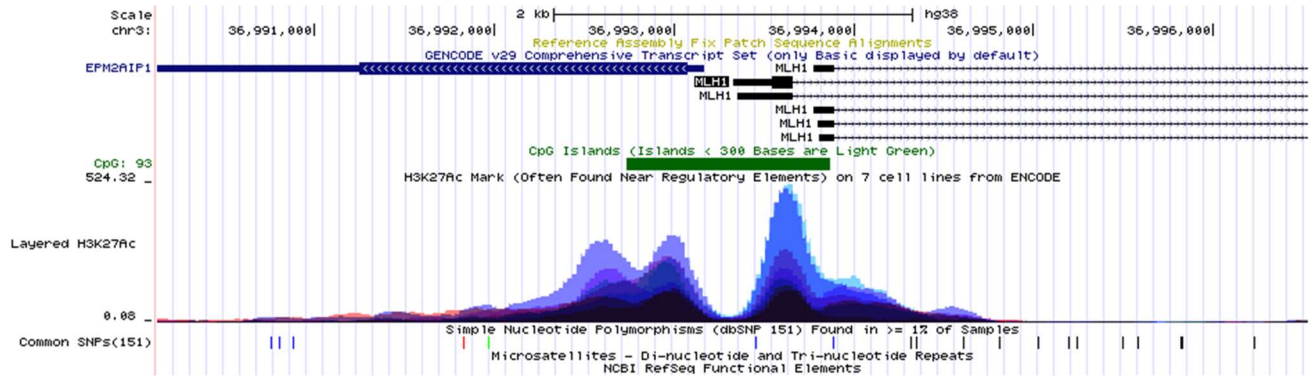

Figure 1-4. The *MLH1* gene can be silenced by hypermethylation of the CpG islands in its promoter region. The location of CpG islands overlapping with the promoter of human *MLH1* is shown in green above the location of H3K27Ac methylation marks shown by the layered blue density curves. This image is extracted from the ENCODE data in the UCSC Genome Browser.

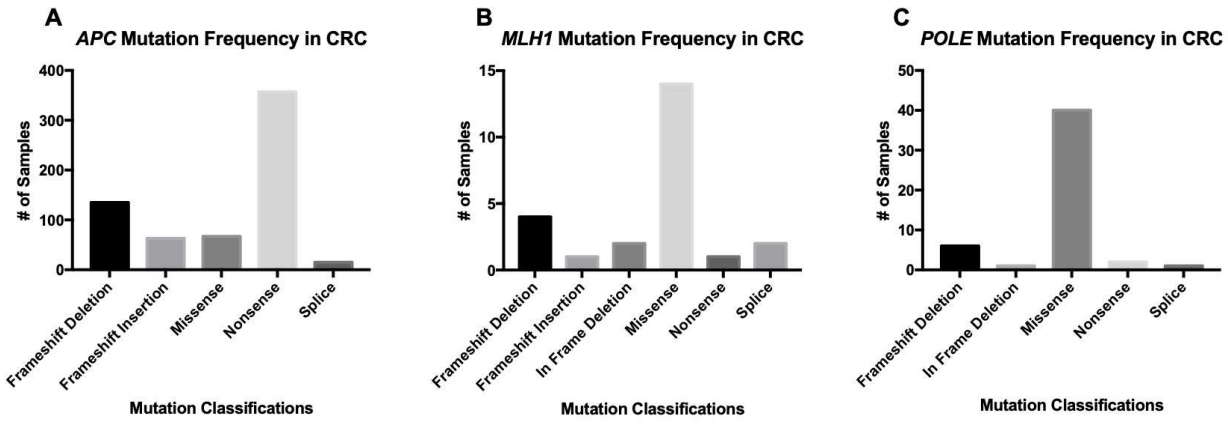

Figure 1-5. Frequency of mutations in *APC*, *MLH1*, and *POLE* in human CRCs. Each graph quantifies the number of human CRC samples on the y-axis that have a mutation resulting in a frameshift deletion, frameshift insertion, in-frame deletion, missense mutation, nonsense mutation, or splicing change in either the **(A)** *APC*, **(B)** *MLH1*, or **(C)** *POLE* gene. The data for these graphs were downloaded from the cBioPortal for Cancer Genomics analysis of the TCGA PanCancer Atlas data on colorectal adenocarcinoma.

To study the immunological differences between MSI and CIN CRCs, we first created a suitable model that would have our mutations of interest on an isogenic background. The MC38

cell line is a murine CIN colorectal carcinoma cell line derived from a C57BL/6 mouse that possesses an inactive *Apc* gene.[122] Ideally, we would have used a non-cancerous immortalized murine colon cell line but, unfortunately, none are available, and other less de-differentiated cell lines (MODE-K and CMT93) that we genetically manipulated failed to grow *in vivo*. In order to determine if the phenotype of MSI CRC results specifically from loss of MLH1 or simply due to increased hypermutability from failed DNA repair, we also sought to target the *Pole* gene in the MC38 cell line to serve as a non-MSI hypermutable model for comparison. *POLE* was specifically chosen because human CRCs possessing *POLE* mutations have discrete and somewhat intermediate clinical attributes compared to either CIN or MSI CRCs,[28] making a *Pole* mutant MC38 cell line a good point of comparison.

To develop ablating mutations in *Mlh1* and *Pole* in the MC38 cell line, we used the CRISPR/Cas9 single gRNA system. Because MC38 is a CIN cell line, we also transfected MC38 with an empty CRISPR plasmid lacking a gRNA to serves as our CIN CRC cell line control. As a CIN cell line, MC38 possesses multiples of many chromosomes; therefore, there is a chance that a gene of interest would have greater than two alleles that need to be ablated, making successful disruption of gene function difficult compared to other cell lines. CRISPR SpCas9 gRNAs were designed to target early exons in our target genes to increase the likelihood of inactivating frameshift mutations. We designed two gRNAs to target the first exon of the *Mlh1* gene (Table 1), resulting in the development of two independent *Mlh1*$^{-/-}$ MC38 cell lines, denoted as A and B, confirmed by both Sanger sequencing (Figure 1-6A), and by Western blot (Figure 1-6B). The

predicted Mlh1 protein from the mutated sequences of either *Mlh1*$^{-/-}$A or B is non-functional. To mutate *Pole*, we also designed multiple gRNAs, but only one resulted in a successful mutant cell line (Table 1). Unfortunately, our efforts to sequence this MC38 *Pole*$^{-/-}$ cell line were unsuccessful, despite the sequencing primers we designed being able to successfully sequence the CRISPR gRNA target region of *Pole* in our parental MC38 cell line, and *Pole*$^{-/-}$ mutants we created in other cell line backgrounds We postulate that there may have been excessive removal of the exposed DNA strands following the Cas9 induced cleavage of the DNA resulting in the ablation of the site our sequencing primers should be binding to in our MC38 *Pole*$^{-/-}$ mutant. Thus, to evaluate successful disruption of gene function, we relied on Western blot visualization alone. Polε is a very large protein (262 KDa) and the antibodies available do not result in a strong Western blot signal. Therefore, we performed a pulldown to concentrate the signal for a reliable comparison between our *Pole*$^{-/-}$ and Empty Vector (hereafter referred to as "Empty") MC38 cell line. We isolated lysates from 10cm plates and normalized the protein input using a BCA assay. We then used anti-Polε (Table 2) bound sepharose-Protein G beads to capture all the Polε protein available in our Empty and *Pole*$^{-/-}$ cell lines. After eluting, we loaded the isolate onto an 8% SDS PAGE gel for western blot analysis with that same antibody. This demonstrated that our MC38 *Pole*$^{-/-}$ cell line appears to lack the Polε protein (Figure 1-6B).

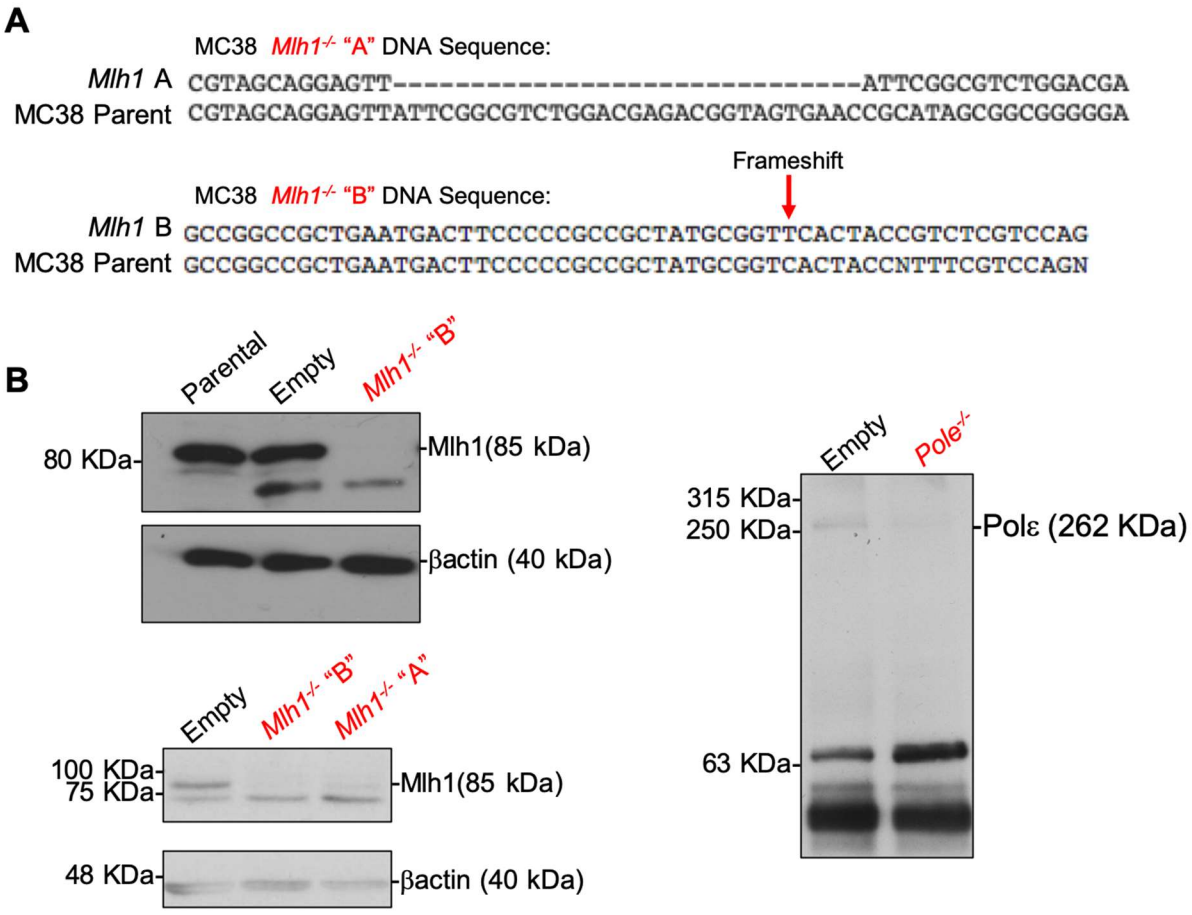

Figure 1-6. Confirmation of *Mlh1* and *Pole* knock-outs in MC38 cells. (A) Sanger sequences of the region containing the *Mlh1* CRISPR target site in two independently derived clones of the MC38 *Mlh1*$^{-/-}$ cell lines aligned to the parental MC38 sequence for *Mlh1*. Sequence alignments were performed using the ApE v2.0.53c software. **(B)** Left: Western blot confirmation of protein level knock-outs of lysates from the two independently derived MC38 *Mlh1*$^{-/-}$ clones compared to the Mlh1 protein expression of either the parental MC38 cell line or the "Empty" control MC38 cell line. Right: Immunoprecipitation of the Polε protein from the lysates of the "Empty" control MC38 cell line and the mutant *Pole*$^{-/-}$ cell line to evaluate presence of the Polε protein by Western blot.

Since the clinical attributes of MSI and *POLE* mutant human CRCs result from the development of mutations downstream of the initiating driver mutations, we decided to continuously passage our CRISPR mutated MC38 cell lines for 6 months to allow the inactivation of *Mlh1* and *Pole* to generate ample downstream mutations and accurately model the hypermutability phenotype. When we performed flow cytometry on subcutaneous tumours derived from the injection of 6-month-old MC38 Empty, *Mlh1*$^{-/-}$A, *Mlh1*$^{-/-}$B, and *Pole*$^{-/-}$ cells in immune competent C57BL/6 mice, we observed that the immune phenotypes of these tumours match the clinical attributes in human CRCs lacking MLH1 and POLε (Figure 1-7). We first noticed that there is a high rejection rate of the *Mlh1*$^{-/-}$ B tumours (Figure 1-7A), and lower size for both *Mlh1*$^{-/-}$ A and B tumours (Figure 1-7B), which we have evidence is attributable to their ability to stimulate an anti-tumour immune response. We consistently saw differences in the growth viability of the two *Mlh1*$^{-/-}$ cell lines *in vivo*, which was not unexpected given the heterogeneity that results from inducing genetic instability and then allowing the cells to be passaged for 6 months. Flow cytometry analysis indicates that *Mlh1*$^{-/-}$ tumours have a significantly higher percent of infiltrating CD8+ T cells compared to the Empty tumours and, of these, a greater percentage of these CD8+ T cells express the CD69 T cell activation marker (Figure 1-7C). The *Pole*$^{-/-}$ and Empty tumours grew equally well (Figure 1-7A) and, although it was not significant, the *Pole*$^{-/-}$ tumours have a higher percent of CD8+ tumour infiltrating lymphocytes compared to the Empty tumours, although a lower percent than the *Mlh1*$^{-/-}$ tumours. There was no significant difference in the percent of CD4+ tumour infiltrating lymphocytes between the tumour subtypes, but of these CD4+ T cells, there were more active

(CD69+) cells in the *Mlh1*$^{-/-}$ and *Pole*$^{-/-}$ tumours compared to the Empty tumours (Figure 1-7D). Consistent with CRC patient data, both the *Mlh1*$^{-/-}$ and *Pole*$^{-/-}$ tumours have higher immunogenicity (higher %CD8+ T cells and %CD4+CD69+ T cells) compared to the Empty CIN tumours, but there is a stronger immune infiltration in the *Mlh1*$^{-/-}$ tumours compared to either the Empty or *Pole*$^{-/-}$ MC38 tumours. This is the first time it has been shown that knocking out a single DNA repair gene on the same CRC cell background can replicate key clinically important features of the immune phenotype of human CRCs.

A

CRISPR MC38 Cell Line	# Mice Injected	# Tumours/# Mice Injected
Empty	4	4/4
Mlh1$^{-/-}$ A	6	6/6
Mlh1$^{-/-}$ B	6	1/6
Pole$^{-/-}$	4	4/4

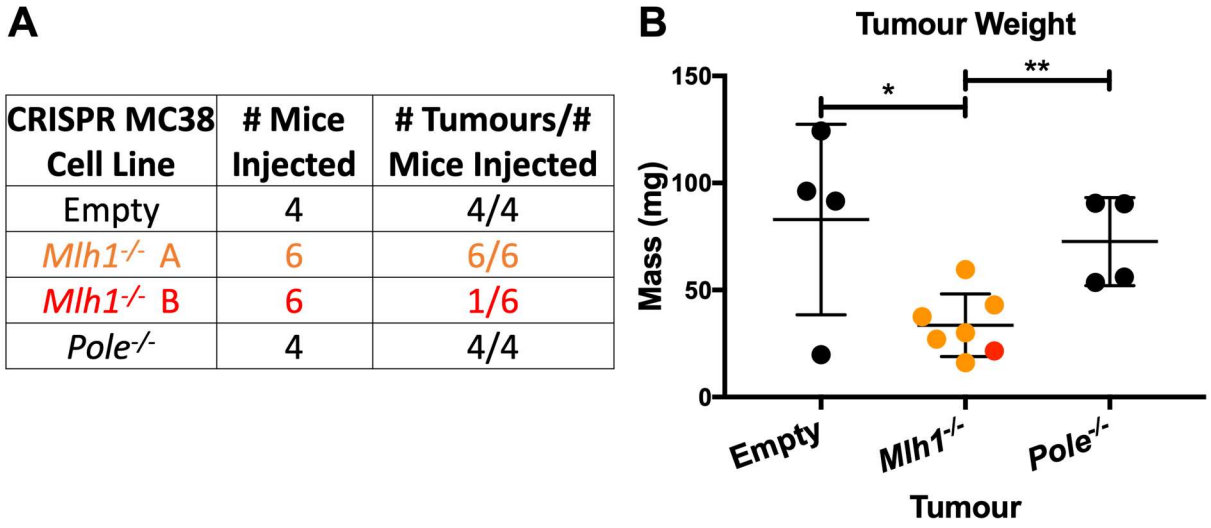

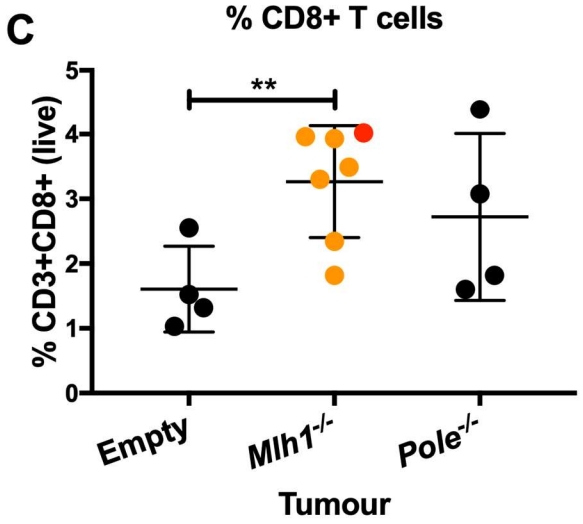

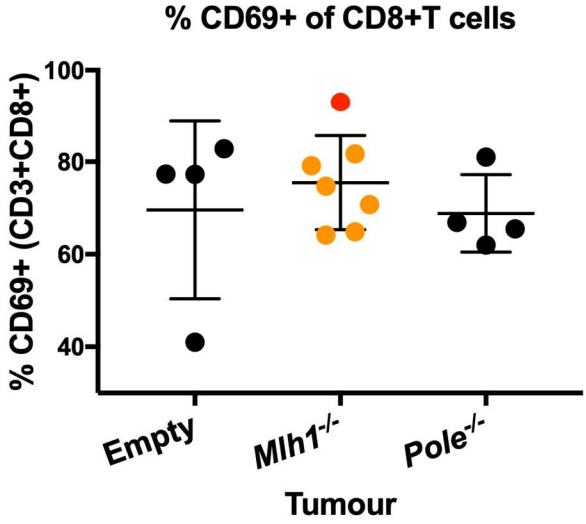

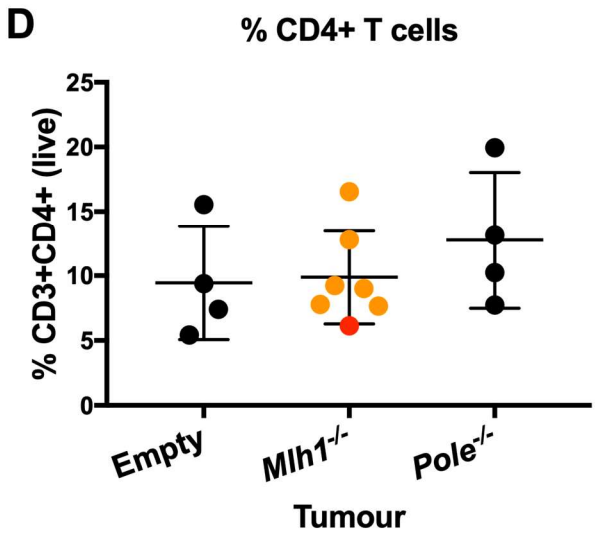

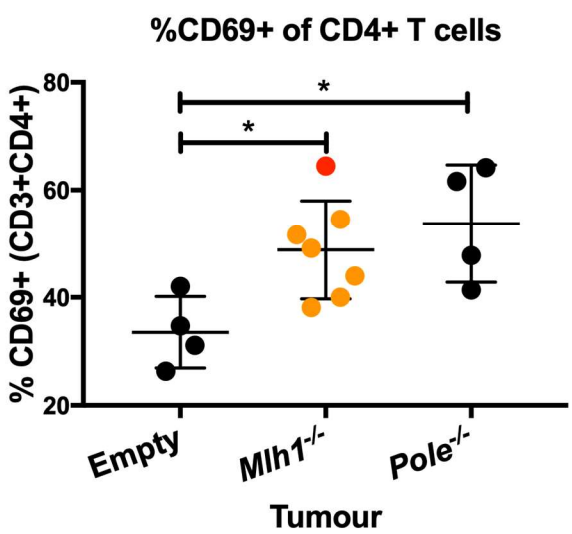

Figure 1-7. Subcutaneous murine MSI CRCs have a higher tumour rejection rate and significantly higher infiltrating CD8+ T cells. (A) Quantification of tumour frequency and **(B)** Tumour mass in C57BL/6 mice subcutaneously injected with each MC38 cell line. **(C)** Flow cytometry analysis showing percent of CD8+ T cells (left) and CD69 activation marker positive CD8+ T cells (right) in the MC38 tumour types listed on the x-axis. **(D)** Flow cytometry analysis showing percent of CD4+ T cells (left) and CD69 activation marker positive CD4+ T cells (right) in the MC38 tumour types listed on the x-axis. The two independently derived *Mlh1*$^{-/-}$ MC38 cell lines are colour coded orange and red for clone A and B respectively. Parametric unpaired t-Test: p-value <0.05*, <0.01**.

Aim 2. MSI colorectal cancers have significantly higher expression of *Sting* and *Nlrp3*

The enhanced number of tumour infiltrating CD8+ T cells observed in MSI compared to CIN CRC has long been attributed to the large TAA load resulting from impairment of the MMR pathway.[122] However, not all hypermutable cancers have better anti-tumour immunity. For instance *POLE* mutated CRCs, although hypermutable, have a worse prognosis compared to even CIN CRCs.[28] This observation indicates that an additional arm of the immune system may be altered in MSI compared to either CIN or other forms of hypermutable CRCs.

When thinking about tumoural immunity, we often focus on the immune cells within the tumour microenvironment. However, epithelial cells must have immune signaling capacity to

prevent the translocation and invasion of foreign pathogens. CRCs originate from the transformation of IECs and, since very few cells in the tumour microenvironment are immune cells, the immune capacity of the cancer cells themselves cannot be overlooked as a contributor to anti-tumour immunity. IECs deal with viral and bacterial insult through the activation of PRRs that initiate signaling cascades that have been well studied in immune cells.[85] Through mining the TCGA database, we observed that MSI CRCs have significantly higher mRNA expression of the PRRs *STING* and *NLRP3* (Figure 2-1A-B). Additionally, there was a significant positive correlation between the transcript expression of *STING* and *NLRP3* (Figure 2-2A), as well as between either *STING* and *NLRP3* expression and the cytotoxic T cell marker *CD8A* in CRCs (Figure 2-2B).

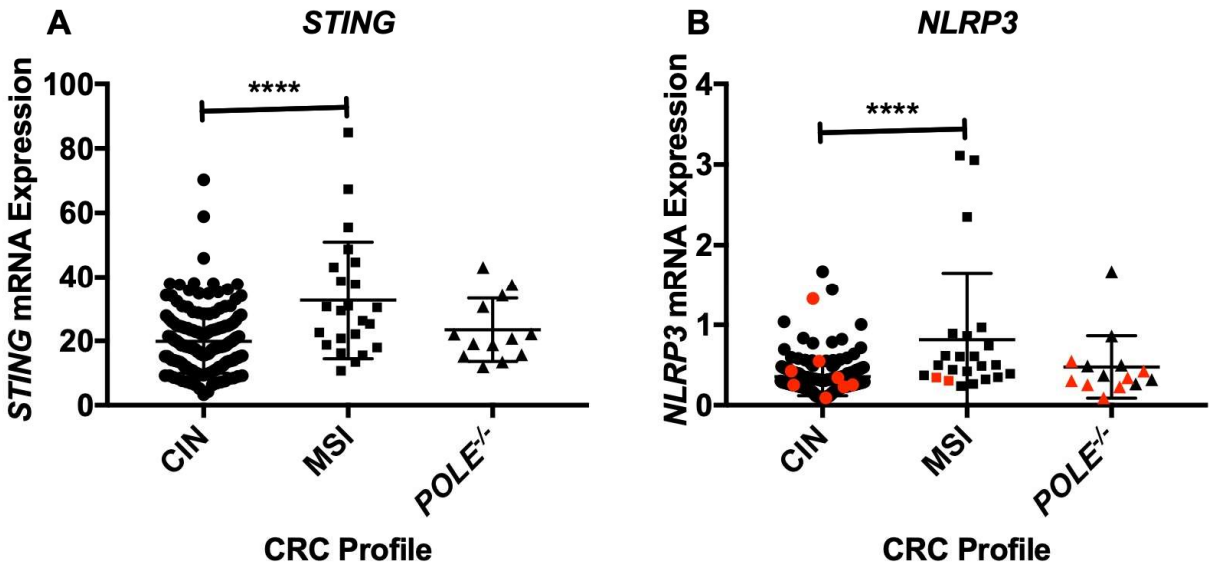

Figure 2-1. Human MSI CRCs have significantly higher expression of NLRP3 and STING compared to CIN or *POLE* mutated CRCs. RNA sequencing for the expression of **(A)** *STING* and

(B) *NLRP3* in human CIN, MSI, and *POLE* mutant colorectal cancers. Y-axis RNAseq units are in Reads Per Kilobase Million (RPKM). Data were downloaded from the cBioPortal for Cancer Genomics analysis of the TCGA (Nature, 2012) data on colorectal adenocarcinoma. Tumours possessing a mutation in the *STING* or *NLRP3* gene are coloured red. Parametric unpaired t-Test between all groups: p-value <0.0001****.

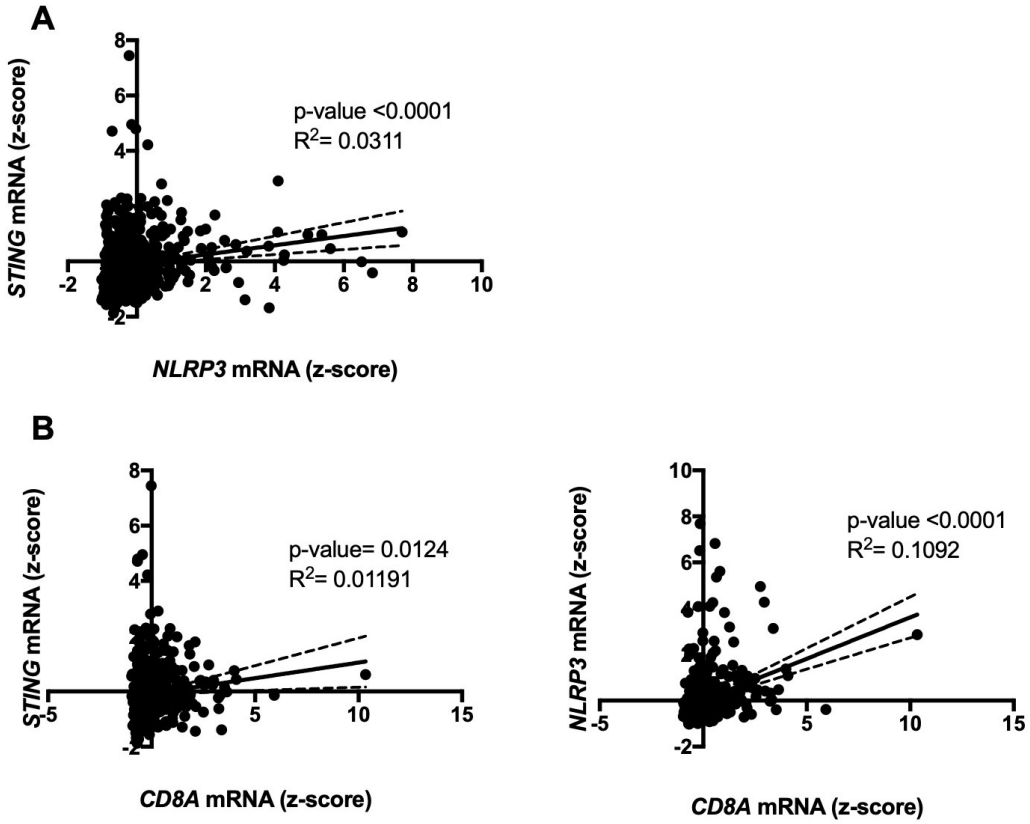

Figure 2-2. *NLRP3* and *STING* are co-expressed and associated with *CD8A* expression in human CRCs. (A) The correlation of *NLRP3* and *STING* mRNA expression in human CRCs. **(B)** The correlation of *STING* (left) and *NLRP3* mRNA expression (right) with *CD8A* mRNA expression (x-axis) in human CRCs. Y-axis RNAseq units are presented as z-scores. Data were downloaded from the cBioPortal for Cancer Genomics analysis of the TCGA PanCancer Atlas data on

Colorectal Adenocarcinoma. Data was analyzed in Prism (Graph Pad) by linear regression (C.I.=95%) with the Pearson correlation R^2 and P-values reported on each graph.

Since the samples analyzed by TCGA are whole tumour tissue, we do not know the relative contribution of *STING* or *NLRP3* expression in the tumour cells compared to that in the immune cells within the tumour. This is important because of the higher numbers of immune cells that infiltrate MSI CRCs. If the tumour cells are driving the expression of Nlrp3 and Sting in the MSI CRCs, then our MC38 *Mlh1*$^{-/-}$A, *Mlh1*$^{-/-}$B cells should have higher expression of these PRRs. Looking at the baseline expression of *Sting* and *Nlrp3* in unstimulated 6-month-old MC38 Empty*, Mlh1*$^{-/-}$A, *Mlh1*$^{-/-}$B, and *Pole*$^{-/-}$ cells *in vitro*, there was no significant difference in the expression of *Nlrp3* or *Sting* mRNA between the cell lines (Figure 2-3A). The protein expression of Sting appeared slightly higher in the hypermutable cell lines compared to the Empty CIN cell line, but the expression of the Nlrp3 protein was negligible at baseline for all cells, with some expression in the *Mlh1*$^{-/-}$A cell line (Figure 2-3B). This observation prompted us to postulate 3 possibilities: 1) The immune cells in MSI CRCs of Sting and Nlrp3, 2) The tumour microenvironment is needed for the MSI tumour cells to express Sting and Nlrp3, or 3) our mouse cell lines are not recapitulating the clinical phenotypes of the CRCs they are intended to model.

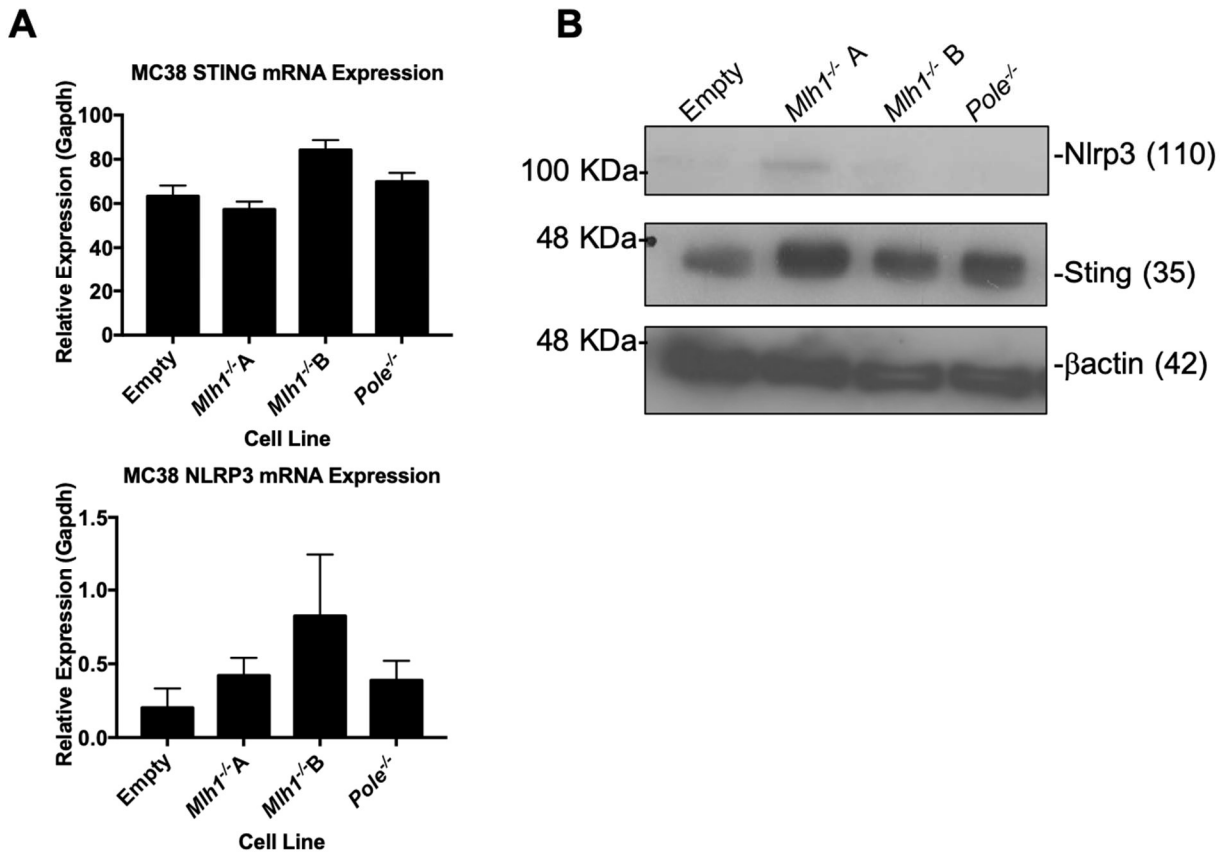

Figure 2-3. MSI cells in vitro do not have higher expression of *Sting* or *Nlrp3* mRNA, and only the *Mlh1*$^{-/-}$ A MSI cell line has higher expression of Sting and Nlrp3 protein at baseline. (A) Baseline expression of *Sting* (top) and *Nlrp3* (bottom) mRNA by qPCR in the murine MC38 Empty, *Mlh1*$^{-/-}$A, *Mlh1*$^{-/-}$B, and *Pole*$^{-/-}$ cells that were passaged for 6 months. Y-axis is the expression of each transcript in the unit $(2^{(-\Delta Ct)})$x10,000. Each sample had 4 technical replicates for *Nlrp3*, *Sting*, and *Gapdh* on the same qPCR plate. Primers used are in table 1. **B)** Western blot of Nlrp3 and Sting in the murine MC38 Empty, *Mlh1*$^{-/-}$A, *Mlh1*$^{-/-}$B, and *Pole*$^{-/-}$ cells that were passaged for 6 months. Expected size (KDa) of each protein is in parentheses on the right. Size markers (KDa) are shown on the left. Antibodies used are in table 2.

To explore these possibilities, we separated the tumour (epithelial) and immune cells (lymphocytes) when isolating subcutaneous tumours derived from 6-month-old MC38 Empty, *Mlh1*$^{-/-}$A, *Mlh1*$^{-/-}$B, and *Pole*$^{-/-}$ cells and looked at the transcript profiles between the epithelial and immune cell populations of each tumour. The *Mlh1*$^{-/-}$ and *Pole*$^{-/-}$ tumours had significantly higher expression of *Cd8a* mRNA in their immune cells compared to that of the Empty CIN CRCs (Figure 2-4A), corroborating our previous flow cytometry data showing more CD8 T-cells in these tumour types (Figure 1-5C). The enhanced *Cd8a* mRNA expression in the immune cells negatively correlated with tumour volume, as would be expected if the CD8+ T cells are restraining CRC growth (Figure 2-4B). Interestingly, we found that the expression of *Sting* and *Nlrp3* in the tumour cells had a significant positive correlation with Cd8a expression in the immune cells, and this was most evident in the MSI CRCs (shown in orange and red) (Figure 2-4C). Comparatively, the expression of *Sting* and *Nlrp3* in the immune cell population had no significant association with their expression of *Cd8a* (Figure 2-4D). When we separated the *Mlh1*$^{-/-}$ tumours from the Empty vector tumours it was evident that the *Mlh1*$^{-/-}$ tumour epithelial cells had a strong positive correlation between *Sting* and *Cd8a* as well as between *Nlrp3* and *Cd8a* expression (Figure 2-4E), while the Empty tumours did not (Figure 2-4F). This indicates that the loss of *Mlh1* in MSI tumour cells could increase recruitment of CD8+ T cells by increasing expression of *Sting* and *Nlrp3*.

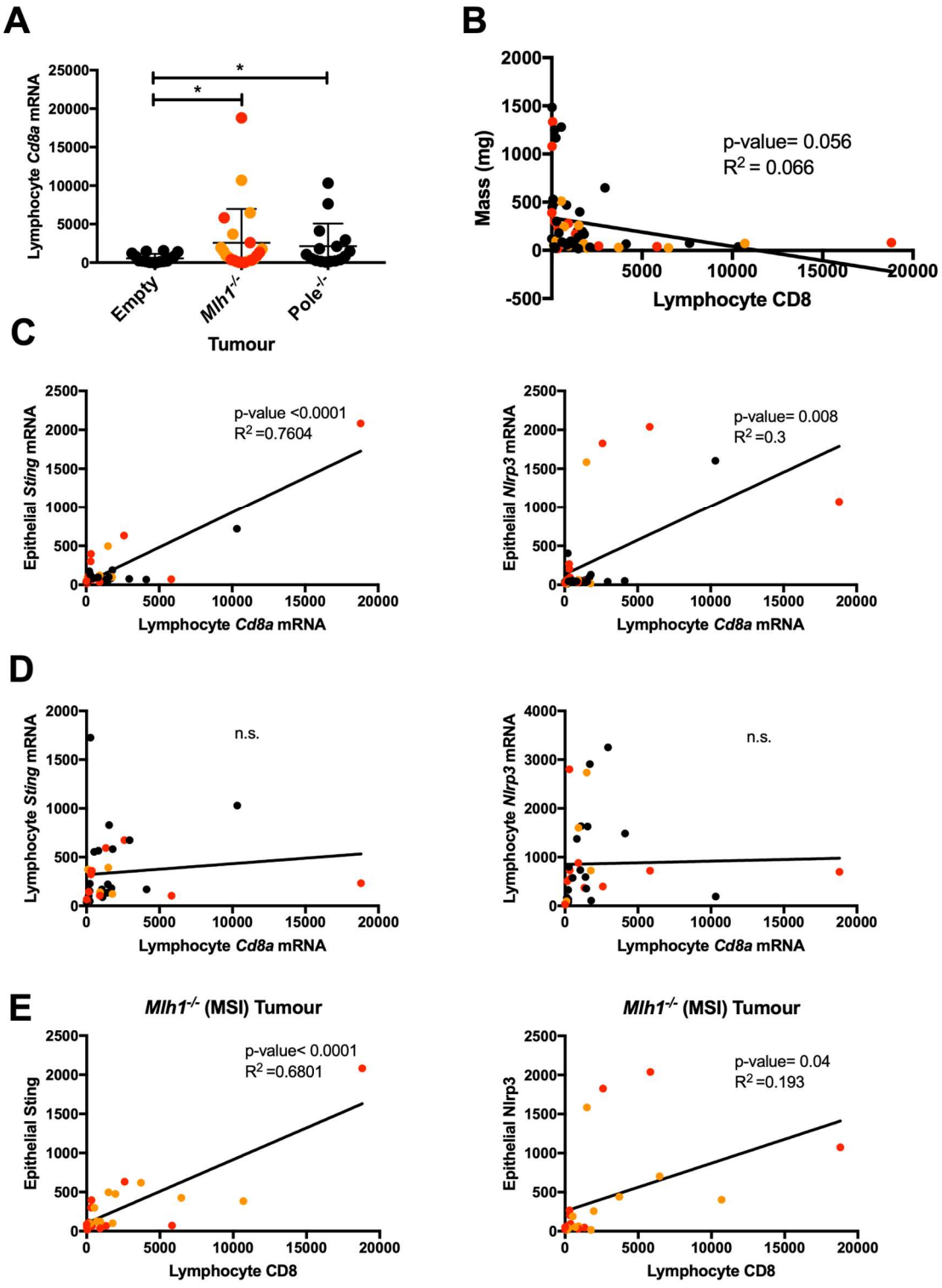
A
Lymphocyte Cd8a mRNA
25000
20000
15000
10000
5000
0
*
*
Empty
Mlh1-/-
Pole-/-
Tumour
B
Mass (mg)
2000
1500
1000
500
0
-500
p-value= 0.056
R2 = 0.066
5000
10000
15000
20000
Lymphocyte CD8
C
Epithelial Sting mRNA
p-value <0.0001
R2 =0.7604
Lymphocyte Cd8a mRNA
Epithelial Nlrp3 mRNA
p-value= 0.008
R2 =0.3
Lymphocyte Cd8a mRNA
D
Lymphocyte Sting mRNA
n.s.
Lymphocyte Cd8a mRNA
Lymphocyte Nlrp3 mRNA
4000
3000
2000
1000
n.s.
Lymphocyte Cd8a mRNA
E
Mlh1-/- (MSI) Tumour
Epithelial Sting
p-value< 0.0001
R2 =0.6801
Lymphocyte CD8
Mlh1-/- (MSI) Tumour
Epithelial Nlrp3
p-value= 0.04
R2 =0.193
Lymphocyte CD8

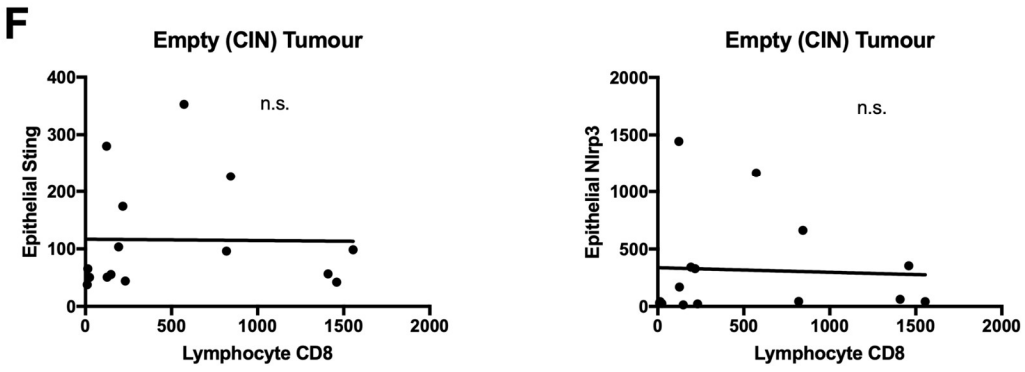

Figure 2-4. Tumour epithelial cell mRNA expression of *Sting* and *Nlrp3* is associated with higher expression of *Cd8a* mRNA in tumoural lymphocyte cells. qPCR of subcutaneous tumours from injection of murine MC38 Empty, *Mlh1*$^{-/-}$A, *Mlh1*$^{-/-}$B, and *Pole*$^{-/-}$ cells into C57BL/6 mice. **(A)** Transcript expression of *Cd8a* in the tumour immune cell population between the Empty, *Mlh1*$^{-/-}$, and *Pole*$^{-/-}$ tumours where *Mlh1*$^{-/-}$A and *Mlh1*$^{-/-}$B are pooled together. Parametric unpaired t-Test: p-value <0.05*. **(B)** Regression plot of the mass of each tumour in mg (y-axis) compared to the transcript expression of *Cd8a* in the tumour immune cell population (x-axis). **(C)** Regression plot of the tumour epithelial cell transcript expression of *Sting* (left) and *Nlrp3* (right) compared to the transcript expression of *Cd8a* in the immune cell population (x-axis). **(D)** Regression plot of the tumour immune cell transcript expression of *Sting* (left) and *Nlrp3* (right) compared to the transcript expression of *Cd8a* in the immune cell population (x-axis). **(E)** Regression plot of *Mlh1*$^{-/-}$ tumour epithelial cell transcript expression of *Sting* (left) and *Nlrp3* (right) compared to the transcript expression of *Cd8a* in the immune cell population (x-axis). **(F)** Regression plot of Empty tumour epithelial cell transcript expression of *Sting* (left) and *Nlrp3* (right) compared to the transcript expression of *Cd8a* in the immune cell population (x-axis). The units of mRNA expression are $(2^{(-\Delta Ct)})$x10,000, where ΔCt is calculated using *Gapdh* expression. The *Mlh1*$^{-/-}$A and *Mlh1*$^{-/-}$B derived tumours are represented as orange and red dots respectively. N=16 Empty, 11 *Mlh1*$^{-/-}$A, 12 *Mlh1*$^{-/-}$B, and 16 *Pole*$^{-/-}$. Data analyzed in Prism (Graph Pad) by linear regression (C.I.=95%) with the Pearson correlation R^2 and P-values reported on each graph.

To elucidate the functional significance of high *Nlrp3* and *Sting* transcript expression in these tumours, we evaluated the expression of molecules that are regulated by signaling downstream of Nlrp3 and Sting. The mRNA expression of both *Sting* and *Nlrp3* in the tumour epithelial cells were significantly positively correlated with the mRNA expression of *Il1b*, *Ifng*, *Ccr5*, and *Ccl5* in the tumour cells (Figure 2-5A&B). Additionally, the expression of these downstream signaling molecules was higher in the *Mlh1*$^{-/-}$, and *Pole*$^{-/-}$ tumours compared to the empty control (Figure 2-5C). The activation and secretion of Il1β is directly downstream of Nlrp3 inflammasome activation,[105] while the expression of Ifnγ is both activated by the cleavage of Il18 by the Nlrp3 inflammasome,[78] and transcriptionally regulated by pNFκBp65, a transcription factor activated in the Sting pathway.[90] Sting activity initiates a type I IFN signaling pathway that has been shown to regulate the expression of Ccr5 and its ligand, Ccl5.[123,124] In CRCs, the expression of CCR5 and CCL5 has been shown to enhance the infiltration of CD8+ T cells, and serve as markers of a good prognosis.[125]

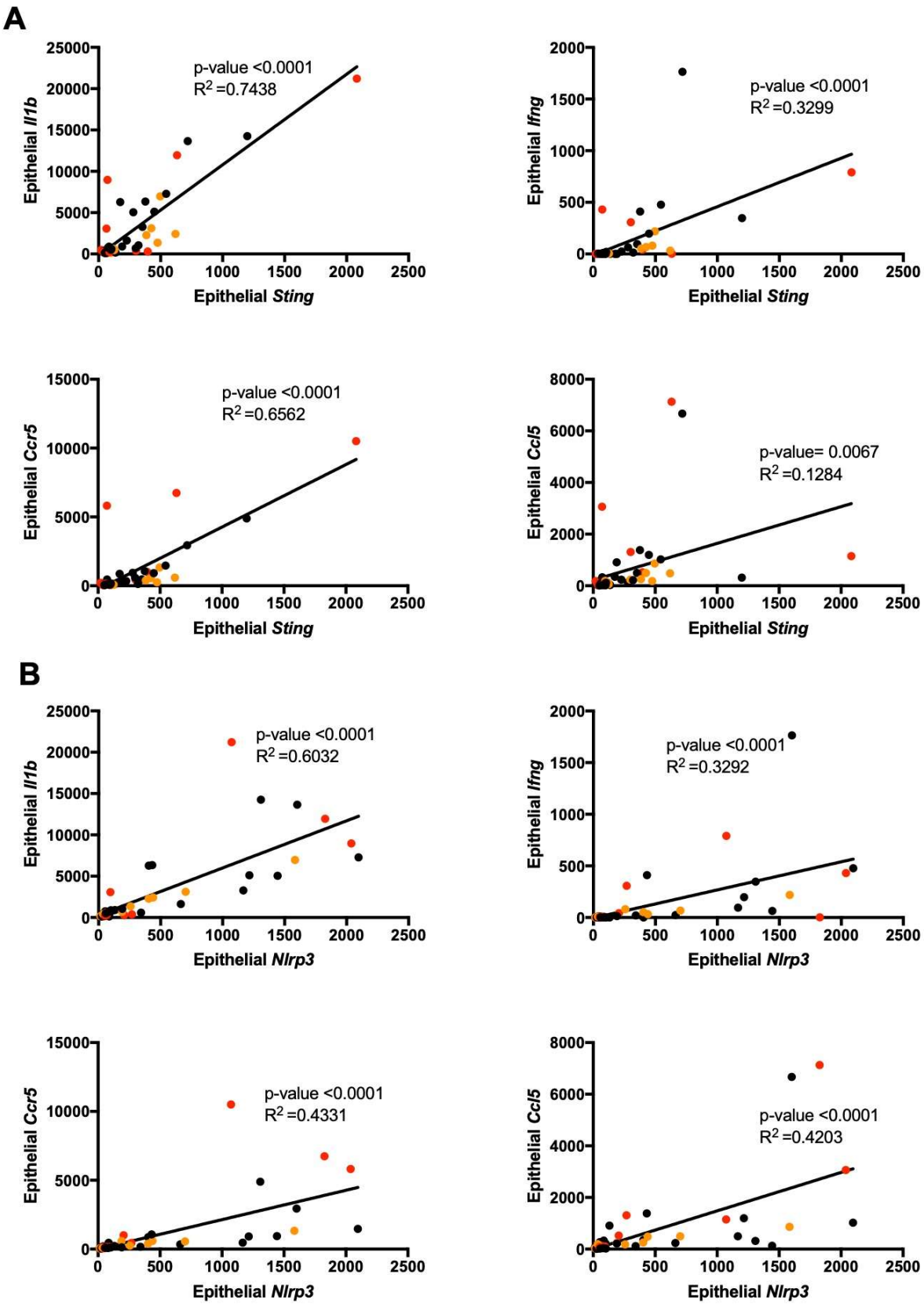
A
p-value <0.0001
R2 =0.7438
Epithelial Il1b
Epithelial Sting
p-value <0.0001
R2 =0.3299
Epithelial Ifng
Epithelial Sting
p-value <0.0001
R2 =0.6562
Epithelial Ccr5
Epithelial Sting
p-value= 0.0067
R2 =0.1284
Epithelial Ccl5
Epithelial Sting
B
p-value <0.0001
R2 =0.6032
Epithelial Il1b
Epithelial Nlrp3
p-value <0.0001
R2 =0.3292
Epithelial Ifng
Epithelial Nlrp3
p-value <0.0001
R2 =0.4331
Epithelial Ccr5
Epithelial Nlrp3
p-value <0.0001
R2 =0.4203
Epithelial Ccl5
Epithelial Nlrp3

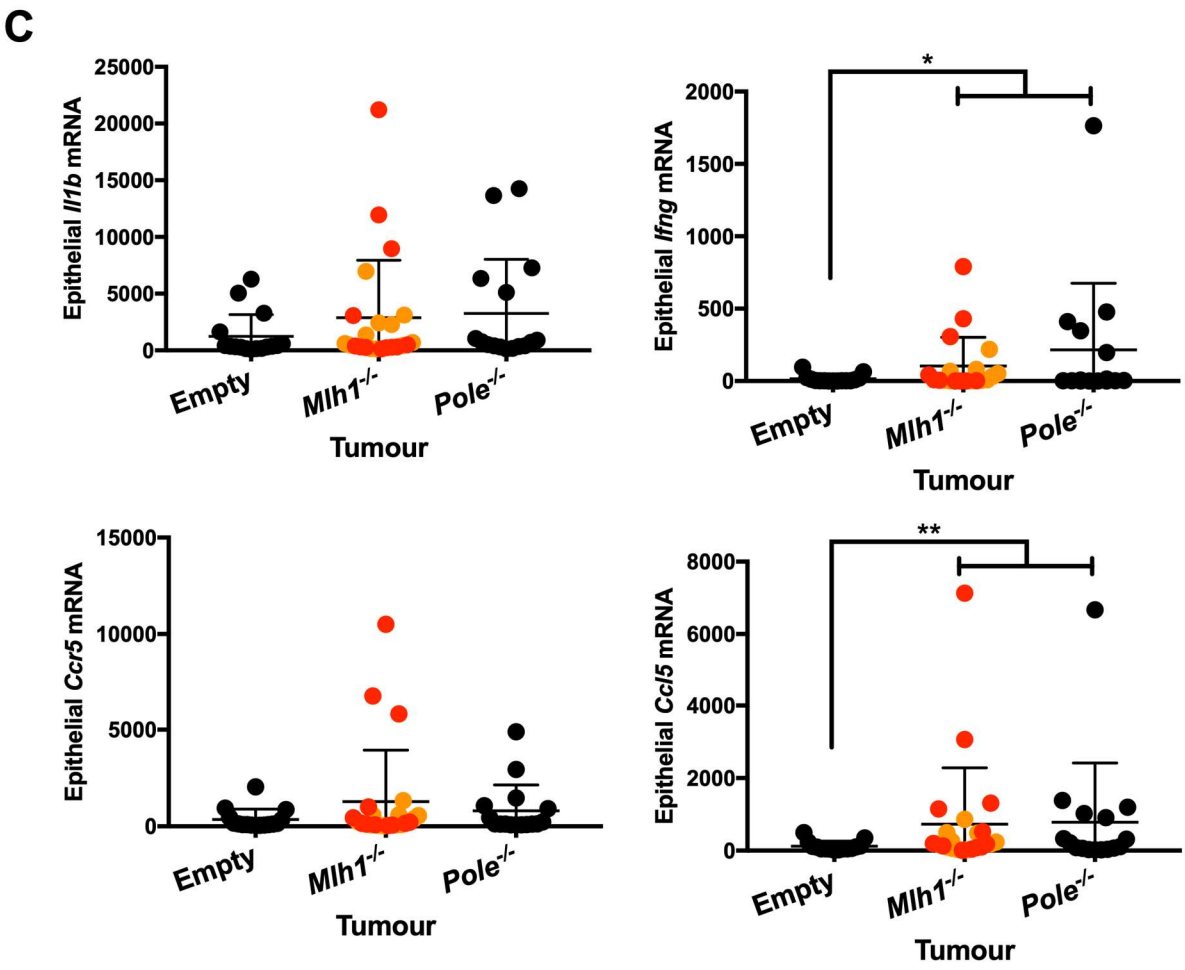

Figure 2-5. Tumour epithelial cell *Sting* and *Nlrp3* mRNA expression is associated with the expression of *Il1b*, *Ifng*, *Ccr5*, and *Ccl5*. qPCR of subcutaneous tumours from injection of murine MC38 Empty, *Mlh1*$^{-/-}$A, *Mlh1*$^{-/-}$B, and *Pole*$^{-/-}$ cells into C57BL/6 mice. **(A)** Regression plot of the tumour epithelial cell transcript expression of *Sting* (x-axis) compared to the transcript expression of *Il1b, Ifng, Ccr5,* and *Ccl5* in the tumour epithelial cells (y-axis). **(B)** Regression plot of the tumour epithelial cell transcript expression of *Nlrp3* (x-axis) compared to the transcript expression of *Il1b, Ifng, Ccr5,* and *Ccl5* in the tumour epithelial cells (y-axis). Data analyzed in Prism (Graph Pad) by linear regression (C.I.=95%) with the Pearson correlation R^2 and P-values reported on each graph. **(C)** Transcript expression of *Il1b, Ifng, Ccr5* and *Ccl5* in the tumour epithelial cell population between the Empty, *Mlh1*$^{-/-}$, and *Pole*$^{-/-}$ tumours where *Mlh1*$^{-/-}$A and *Mlh1*$^{-/-}$B are pooled together. Parametric unpaired t-Test with Welch's correction between

empty and the combination of *Mlh1*$^{-/-}$ and *Pole*$^{-/-}$ tumours: p-value <0.05*, <0.01**. The units of mRNA expression are $(2^{(-\Delta Ct)})$x10,000, where ΔCt is calculated using *Gapdh* expression. The *Mlh1*$^{-/-}$A and *Mlh1*$^{-/-}$B derived tumours are represented as orange and red dots respectively. N=16 Empty, 11 *Mlh1*$^{-/-}$A, 12 *Mlh1*$^{-/-}$B, and 16 *Pole*$^{-/-}$.

The expression of mRNA does not always correlate with the expression of protein.[126] We thus performed immunohistochemistry (IHC) for the expression of Sting and Cd8a in these tumours. Unfortunately, we were unable to locate an anti-Nlrp3 antibody that was successful for IHC, and some of the smaller tumours could not be collected for IHC because we wanted to ensure there was enough material for RNA isolation after the percoll separation of the immune and epithelial cells. Nonetheless, we performed IHC for Sting expression on a subset of tumours and noted that the *Mlh1*$^{-/-}$A and *Mlh1*$^{-/-}$B (and to a lesser extent, the *Pole*$^{-/-}$) subcutaneous tumours had significantly higher expression of Sting compared to the Empty CIN tumours (Figure 2-6A&B). Additionally, IHC indicated that these same *Mlh1*$^{-/-}$A and *Mlh1*$^{-/-}$B tumours had significantly higher numbers of infiltrating Cd8a expressing immune cells (Figure 2-6A&C). Taken together, our data supports a mechanism by which the expression of Sting and Nlrp3, along with their downstream products in MSI CRCs, may be driving the infiltration of CD8+ T cells and, therefore, a reduced tumour burden in patients with these CRCs.

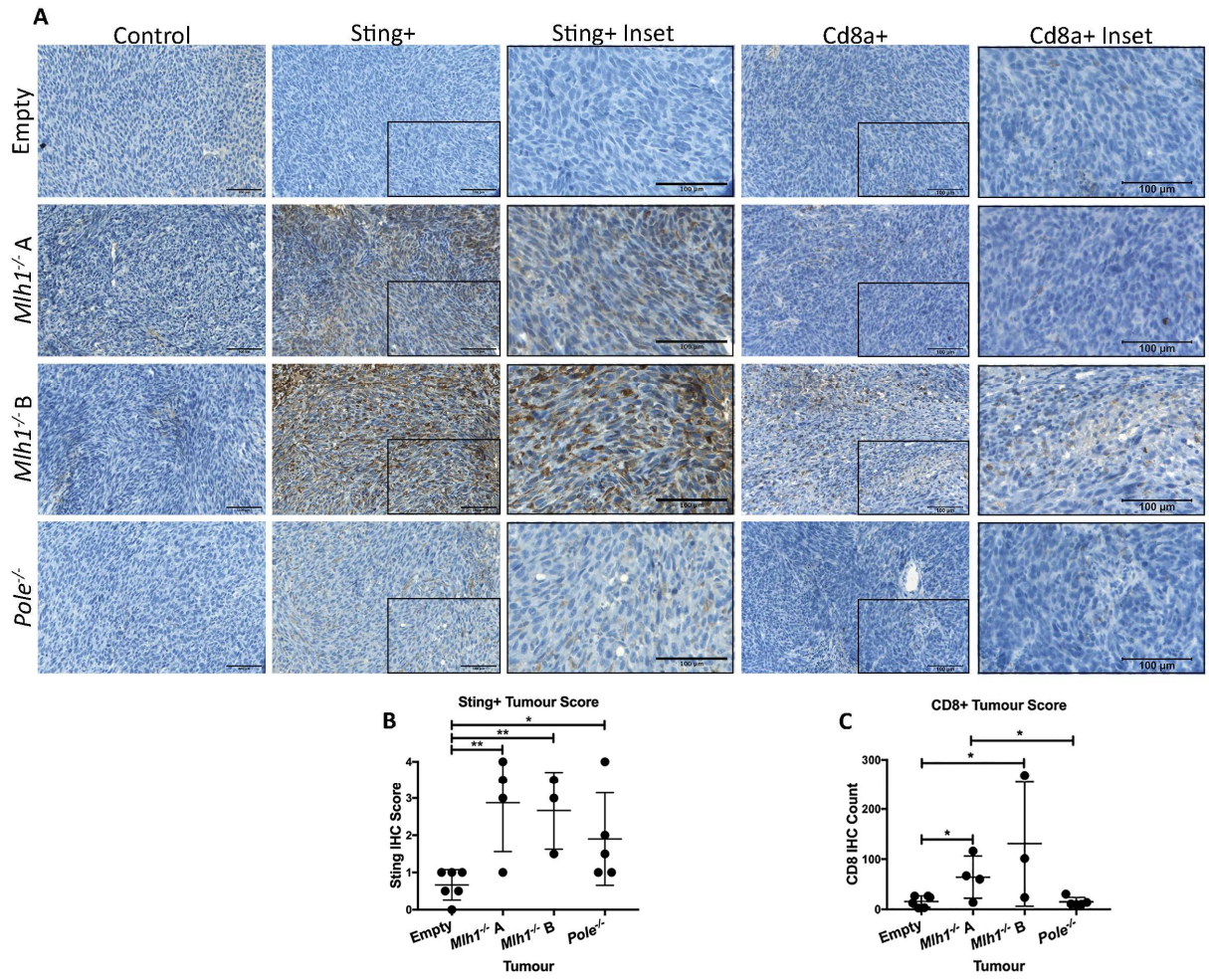

Figure 2-6. Protein expression of Sting and Cd8a is significantly higher in the *Mlh1*$^{-/-}$ MSI subcutaneous tumours compared to the Empty CIN tumours. (A) Representative images of immunohistochemistry with antibodies against Sting and Cd8a (Table 2) of subcutaneous tumours from injection of murine MC38 Empty, *Mlh1*$^{-/-}$A, *Mlh1*$^{-/-}$B, and *Pole*$^{-/-}$ cells. Scale bar=100um. **(B)** Immunohistochemistry score of Sting expression intensity from 0-4 of all tumours. **(C)** Counts of Cd8a+ cells on two 10x images of each tumour. Blinded scores were averaged from two independent scorers. N=6 Empty, 4 *Mlh1*$^{-/-}$A, 3 *Mlh1*$^{-/-}$B, and 5 *Pole*$^{-/-}$. Parametric unpaired t-Test: p-value <0.05*, <0.01**.

The subcutaneous tumour model allowed us to perform an initial evaluation of the immune consequences of *Mlh1* loss because it is simple, fast, and yields a sizeable amount of material. However, this model is lacking some essential parameters for us to accurately answer our scientific question. The immune response to a subcutaneous CRC is very different compared to the response to a CRC grown in the microenvironment of the colon.[65] The subcutaneous model lacks the immune suppressive environment of the mucosal immune system,[127] and it obviously lacks the exposure to microbes that the intestine provides.[128] Accordingly, we found it necessary to validate our results using an orthotopic model where we inject the 6-month-old MC38 Empty, *Mlh1*$^{-/-}$A, *Mlh1*$^{-/-}$B, and *Pole*$^{-/-}$ cells into the descending colon of C57BL/6 mice using an endoscopy machine. Due to humane endpoints, orthotopic murine CRCs are much smaller than subcutaneous ones and therefore do not provide enough material to perform the percoll and qRTPCR readout used previously. Instead, we measured protein expression of these tumours via flow cytometry on the dissociated tumours. Unfortunately, we found that the MC38 cell line has downregulated the expression of several epithelial markers due to being a dedifferentiated cancer cell line. Therefore, we used the lack of a universal immune cell marker (CD45) as a surrogate for identifying the tumour cells. Since we specifically dissected out the tumours, which are predominantly the expanded MC38 tumour cells, we are confident that the bulk of CD45- cells in our populations are in fact tumour cells. Analysis of the tumours revealed that the *Mlh1*$^{-/-}$A and *Mlh1*$^{-/-}$B tumours had a significantly higher percentage of Nlrp3 expressing cells in both the CD4+ T cells and the tumour cells themselves (Figure 2-7A&D), while there was no significant difference in the expression of Nlrp3 in the CD8+ T cells or the immune population as a whole (Figure 2-7B&C). This same trend was seen for Sting

phosphorylation (Figure 2-8A-D), and its downstream signaling kinase, pTbk1 (Figure 2-9A-D). Collectively, these results indicate that the phenomenon we observed in the subcutaneous CRCs holds true, where the *Mlh1*$^{-/-}$ CRCs have significantly higher expression and activation of Nlrp3 and pSting. Additionally, this *in vivo* data supports our second hypothesis outlined previously, that the tumour microenvironment appears to be necessary for MSI tumour cells to express Sting and Nlrp3, since these cells did not show differential expression of these receptors *in vitro* compared to either the Empty or *Pole*$^{-/-}$ cells (Figure 2-3).

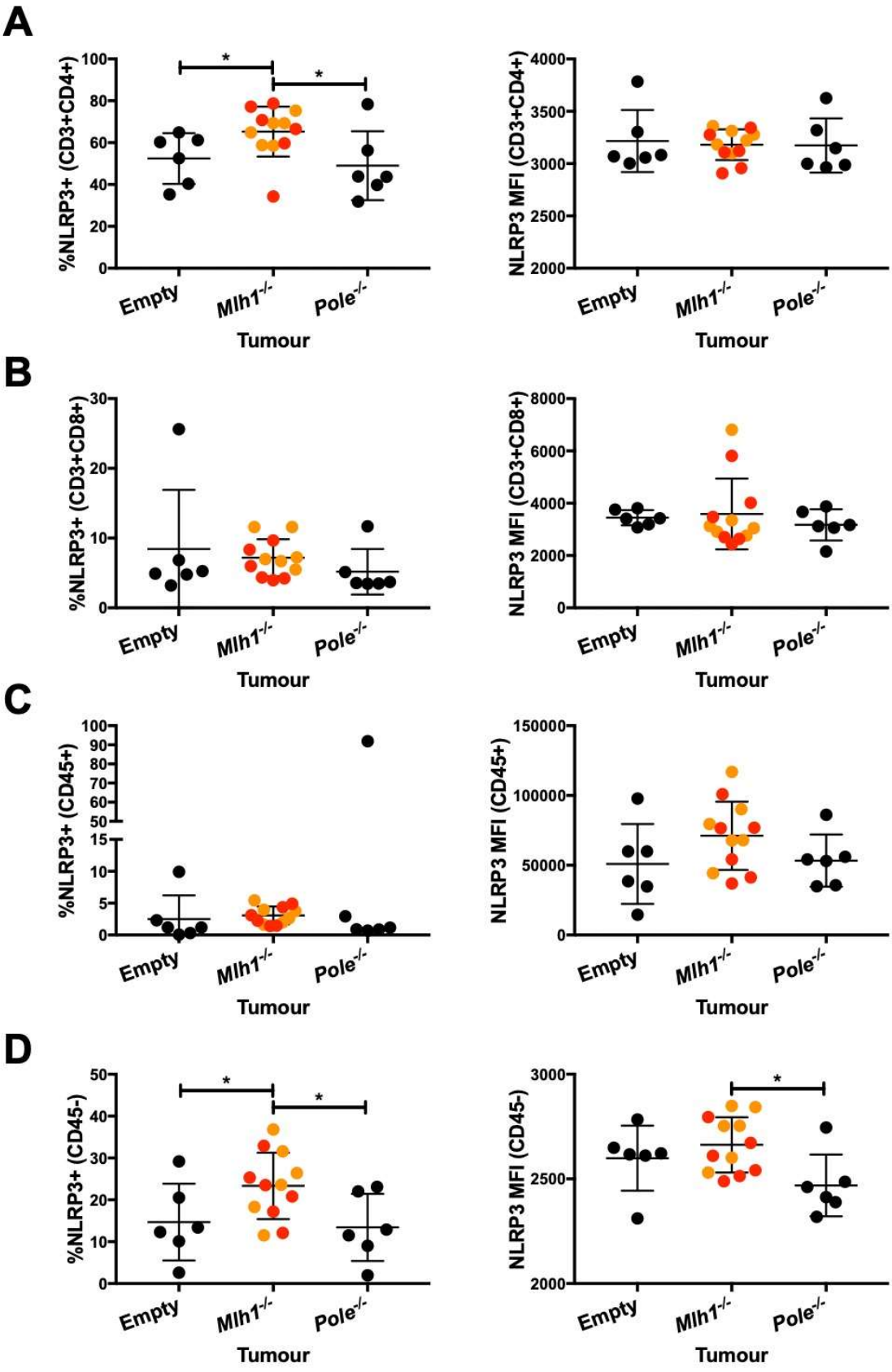
A
%NLRP3+ (CD3+CD4+)
NLRP3 MFI (CD3+CD4+)
B
%NLRP3+ (CD3+CD8+)
NLRP3 MFI (CD3+CD8+)
C
%NLRP3+ (CD45+)
NLRP3 MFI (CD45+)
D
%NLRP3+ (CD45-)
NLRP3 MFI (CD45-)
Empty
Mlh1-/-
Pole-/-
Tumour

Figure 2-7. *Mlh1*$^{-/-}$ MSI orthotopic tumours have significantly higher expression of Nlrp3 in the tumour epithelial cells and CD4+ T cells compared to the *Pole*$^{-/-}$ or Empty CIN CRCs. Flow cytometry analysis of orthotopic tumours in the descending colon of C57BL/6 mice. **(A)** Percent of CD4+ T cells that express Nlrp3 (left) and the mean fluorescent intensity of Nlrp3 expression in CD4+ T cells in each tumour (right). **(B)** Percent of CD8+ T cells that express Nlrp3 (left) and the mean fluorescent intensity of Nlrp3 expression in CD8+ T cells in each tumour (right). **(C)** Percent of CD45+ (immune cells) that express Nlrp3 (left) and the mean fluorescent intensity of Nlrp3 expression in CD45+ cells in each tumour (right). **(C)** Percent of CD45- (tumour cells) that express Nlrp3 (left) and the mean fluorescent intensity of Nlrp3 expression in CD45- cells in each tumour (right). N=6 for all tumour groups. *Mlh1*$^{-/-}$A (orange) and *Mlh1*$^{-/-}$B (red) tumours are pooled together. Parametric unpaired t-Test: p-value <0.05*.

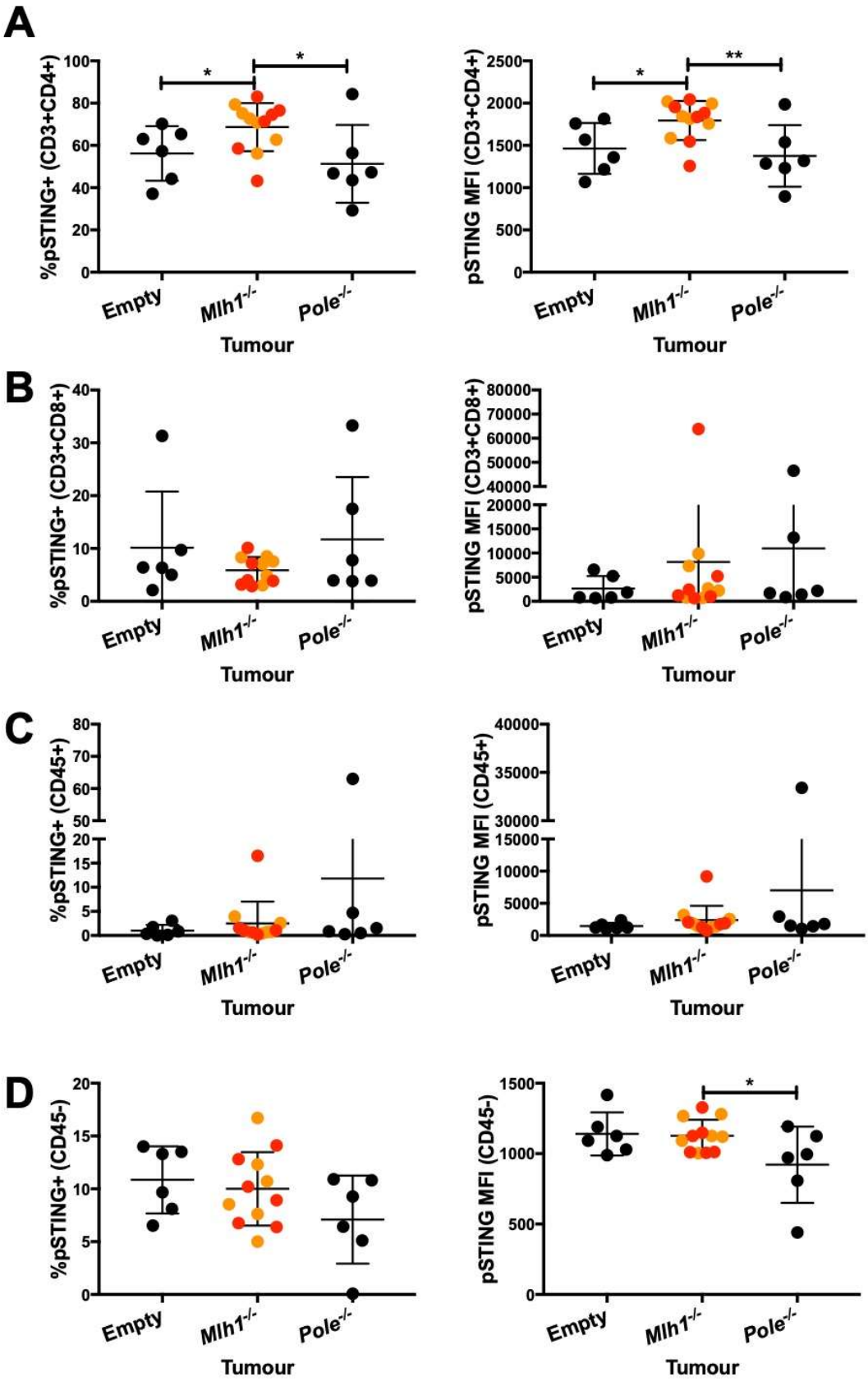
A
%pSTING+ (CD3+CD4+)
pSTING MFI (CD3+CD4+)
B
%pSTING+ (CD3+CD8+)
pSTING MFI (CD3+CD8+)
C
%pSTING+ (CD45+)
pSTING MFI (CD45+)
D
%pSTING+ (CD45-)
pSTING MFI (CD45-)
Empty
Mlh1-/-
Pole-/-
Tumour

Figure 2-8. *Mlh1*$^{-/-}$ MSI orthotopic tumours have significantly higher expression of phospho-Sting in the tumour epithelial cells compared to the *Pole*$^{-/-}$ CRCs and in the CD4+ T cells compared to either the *Pole*$^{-/-}$ or Empty CIN CRCs. Flow cytometry analysis of orthotopic tumours in the descending colon of C57BL/6 mice. **(A)** Percent of CD4+ T cells that express p-Sting (left) and the mean fluorescent intensity of p-Sting expression in CD4+ T cells in each tumour (right). **(B)** Percent of CD8+ T cells that express p-Sting (left) and the mean fluorescent intensity of p-Sting expression in CD8+ T cells in each tumour (right). **(C)** Percent of CD45+ (immune cells) that express p-Sting (left) and the mean fluorescent intensity of p-Sting expression in CD45+ cells in each tumour (right). **(C)** Percent of CD45- (tumour cells) that express p-Sting (left) and the mean fluorescent intensity of p-Sting expression in CD45- cells in each tumour (right). N=6 for all tumour groups. *Mlh1*$^{-/-}$A (orange) and *Mlh1*$^{-/-}$B (red) tumours are pooled together. Parametric unpaired t-Test: p-value <0.05*.

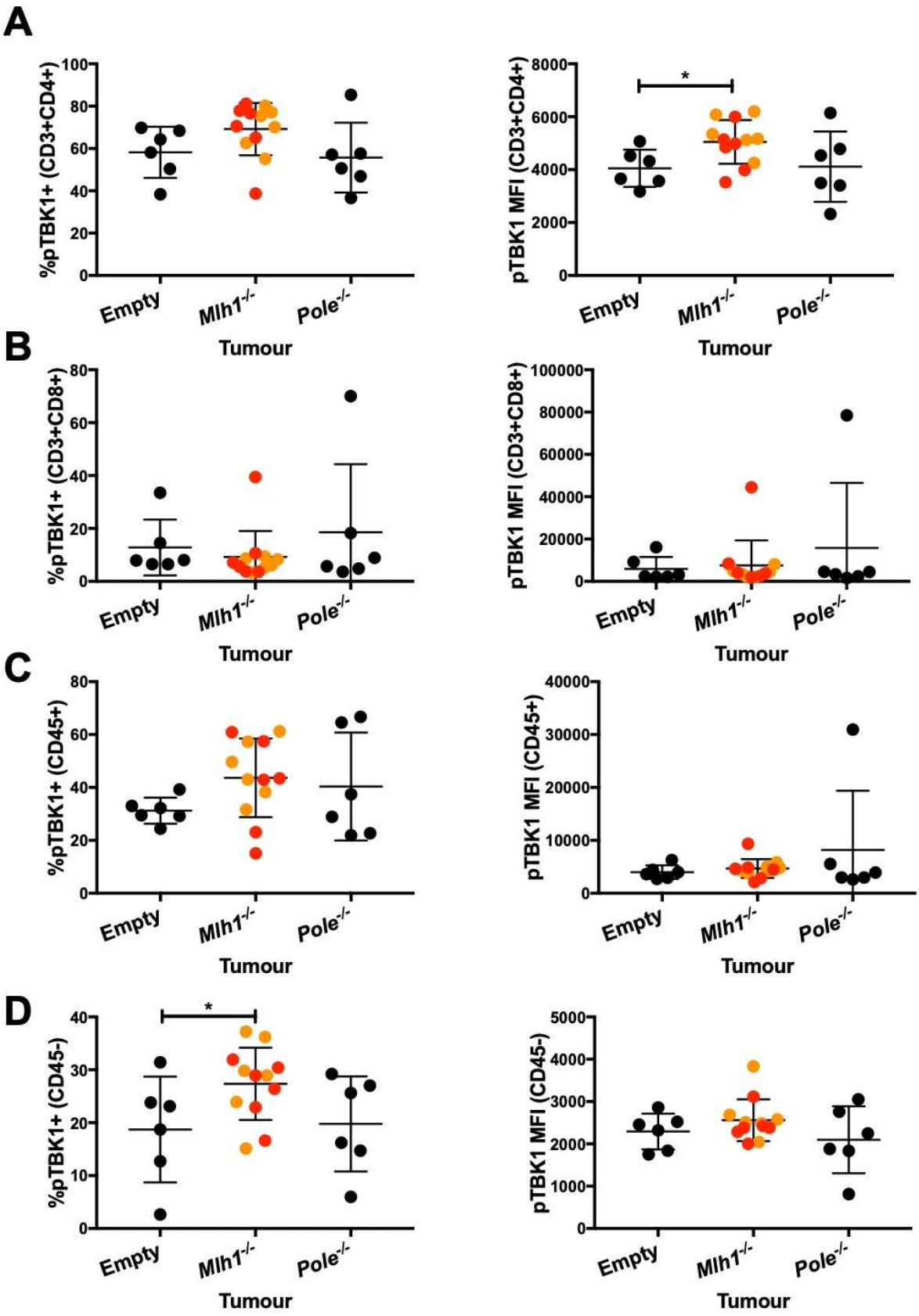
A
%pTBK1+ (CD3+CD4+)
pTBK1 MFI (CD3+CD4+)
B
%pTBK1+ (CD3+CD8+)
pTBK1 MFI (CD3+CD8+)
C
%pTBK1+ (CD45+)
pTBK1 MFI (CD45+)
D
%pTBK1+ (CD45-)
pTBK1 MFI (CD45-)
Empty
Mlh1-/-
Pole-/-
Tumour
*

Figure 2-9. *Mlh1*$^{-/-}$ MSI orthotopic tumours have significantly higher expression of phospho-Tbk1 in the tumour epithelial cells and the CD4+ T cells compared to the Empty CIN CRCs. Flow cytometry analysis of orthotopic tumours in the descending colon of C57BL/6 mice. **(A)** Percent of CD4+ T cells that express p-Tbk1 (left) and the mean fluorescent intensity of p-Tbk1 expression in CD4+ T cells in each tumour (right). **(B)** Percent of CD8+ T cells that express p-Tbk1 (left) and the mean fluorescent intensity of p-Tbk1 expression in CD8+ T cells in each tumour (right). **(C)** Percent of CD45+ (immune cells) that express p-Tbk1 (left) and the mean fluorescent intensity of p-Tbk1 expression in CD45+ cells in each tumour (right). **(C)** Percent of CD45- (tumour cells) that express p-Tbk1 (left) and the mean fluorescent intensity of p-Tbk1 expression in CD45- cells in each tumour (right). N=6 for all tumour groups. *Mlh1*$^{-/-}$A (orange) and *Mlh1*$^{-/-}$B (red) tumours are pooled together. Parametric unpaired t-Test: p-value <0.05*.

Aim 3. Sting and Nlrp3 can be activated in both MSI and CIN CRC cells *in vitro*, and it appears their effects are additive

Observing that Sting and Nlrp3 expression in the tumour cells of MSI CRCs were associated with enhanced CD8 T-cell infiltration and lowered tumour volume was exciting and we sought to determine the mechanism by which this was occurring and whether Sting and Nlrp3 were working to activate one another or acting independently. Extrapolating from the known functions of Sting and Nlrp3, we proposed two non-mutually exclusive mechanisms by which Sting and Nlrp3 could be working together.

Our first possible mechanism is outlined in Figure 3-1, where there is an accumulation of DNA damage in the MSI CRCs, triggering the release of DNA from the nucleus into the cytoplasm. The cytoplasmic DNA is then recognized by the cGAS receptor, which produces cyclic-di-nucleotides that bind to STING,[91] resulting in the translocation of STING from the endoplasmic reticulum to the Golgi apparatus.[92] When STING reaches the Golgi apparatus it interacts with the TBK1 kinase, which phosphorylates STING and itself, resulting in the recruitment of interferon regulatory factors (IRF3, IRF7), as well as NFκBp65, which are phosphorylated by active pTBK1.[94] The phosphorylation of IRFs and NFκBp65 results in their translocation from the cytoplasm to the nucleus, where they transcribe pro-inflammatory genes necessary for NLRP3 assembly, including pro-IL1β, pro-IL18, and NLRP3 itself. The activation of the NLRP3 inflammasome is initiated by several ligands, including extracellular ATP, which could be provided by dying tumour cells in the environment.[80] If ASC and NLRP3 assemble the inflammasome with caspase-1, then pro-IL1β and pro-IL18 are cleaved into their mature forms, resulting in the recruitment of DCs to the tumour in response to their secretion of IL1β. DCs in the gut arise from immature cells and, upon recruitment to the tumour site, the epithelial cells can prime and therefore mature the DCs.[84] DCs are antigen presenting cells that can then form the bridge between the innate and adaptive immune response by migrating to the mesenteric lymph nodes to prime T cells with the TAAs they encounter at the tumour site. When these CD8+ T cells home to the tumour, their activity is enhanced by the production of IFNγ downstream of IL18, creating an even more robust anti-tumour immunity.[114]

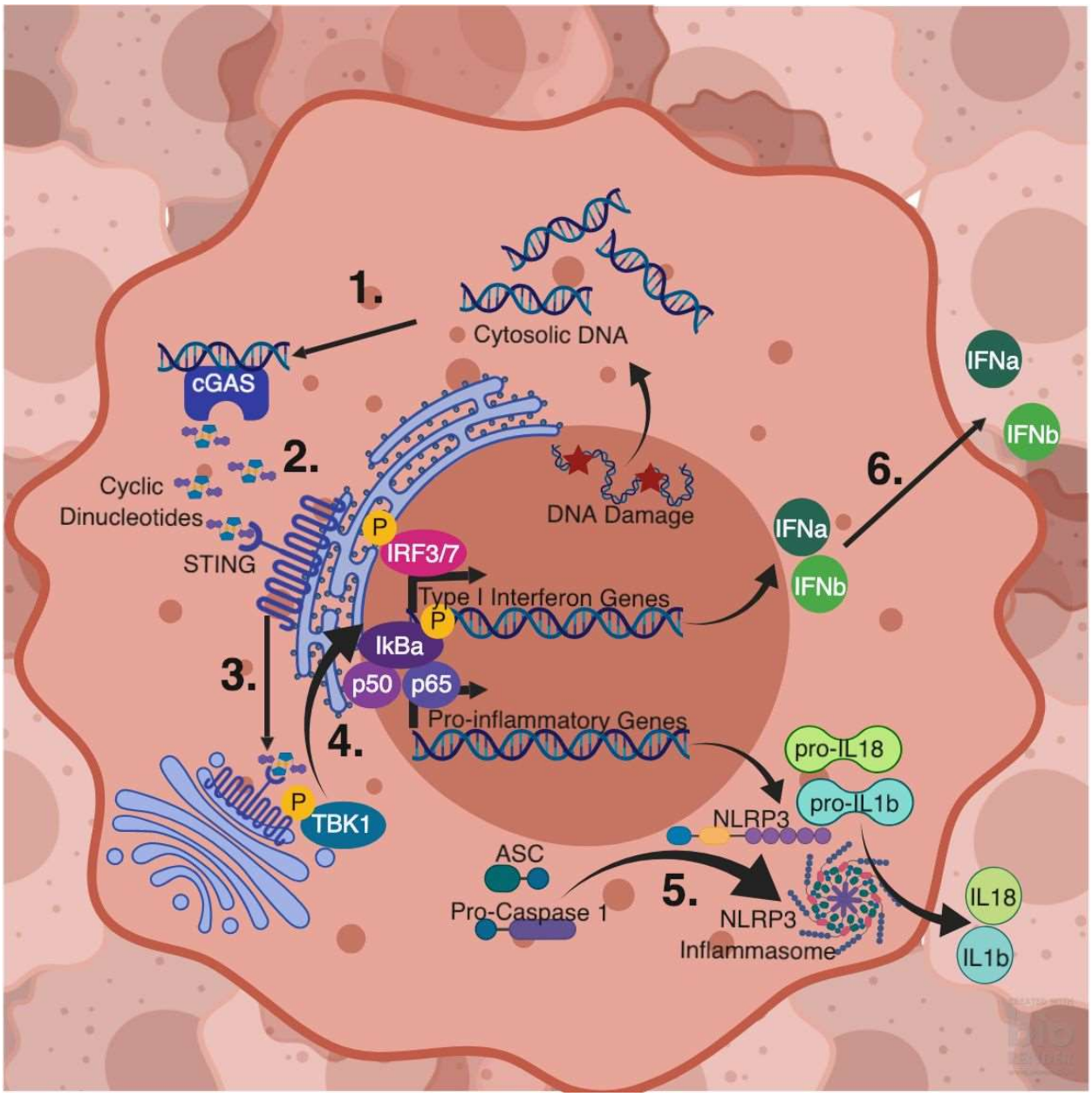

Figure 3-1. Induction of adaptive immunity by microsatellite instable colorectal cancer STING and NLRP3 activity. The accumulation of DNA damage triggers the release of DNA from the nucleus into the cytoplasm that is then recognized by the cGAS receptor **(1)**. cGAS produces cyclic-di-nucleotides that bind to STING **(2)** resulting in the translocation of STING from the endoplasmic reticulum to the Golgi apparatus **(3)**. Sting is phosphorylated by TBK1, resulting in the recruitment of interferon regulatory factors (IRF3, IRF7), as well as NFκB. These are phosphorylated by TBK1 and translocate to the nucleus to transcribe pro-IL1β, pro-IL18, and

NLRP3, along with Type I IFNs **(4)**. ASC and NLRP3 assemble the inflammasome with caspase-1. This activates caspase-1, leading it to cleave pro-IL1β and pro-IL18 into their mature forms **(5)** and resulting in the recruitment of adaptive immune cells. The release of type I IFNs **(6)** aids in the antigen presentation by the recruited DCs to CD8+ T cells. Figure made in ©BioRender - biorender.com.

Our second possible mechanism was that STING and NLRP3 are initiating programmed cell death within MSI CRCs, as depicted in Figure 3-2. This mechanisms begins as above by the release of DNA into the cytoplasm but diverges when the production of IFNs by STING could upregulate caspase-11.[106] If NLRP3 and ASC simultaneously form an inflammasome with caspase-11, pyroptosis is initiated via the cleavage of GSDMD and the cytosolic portion of PANX1.[109] The N-terminal domain of GSDMD creates pores in the cell membrane while the cleaved PANX1 causes ATP to be released from the cell, which can then bind the P2X7 receptor and open the P2X7 pores, resulting in pyroptosis.[109] When cancer cells undergo immunogenic programmed cell death, they release TAAs that can be presented by DCs to naïve T cells in the local lymph nodes. Furthermore, the DCs could pick up the tumoural DNA released by the dying cells, initiating a STING-induced type I IFN response in the DCs, aiding in spontaneous CD8+ T cell priming.[95]

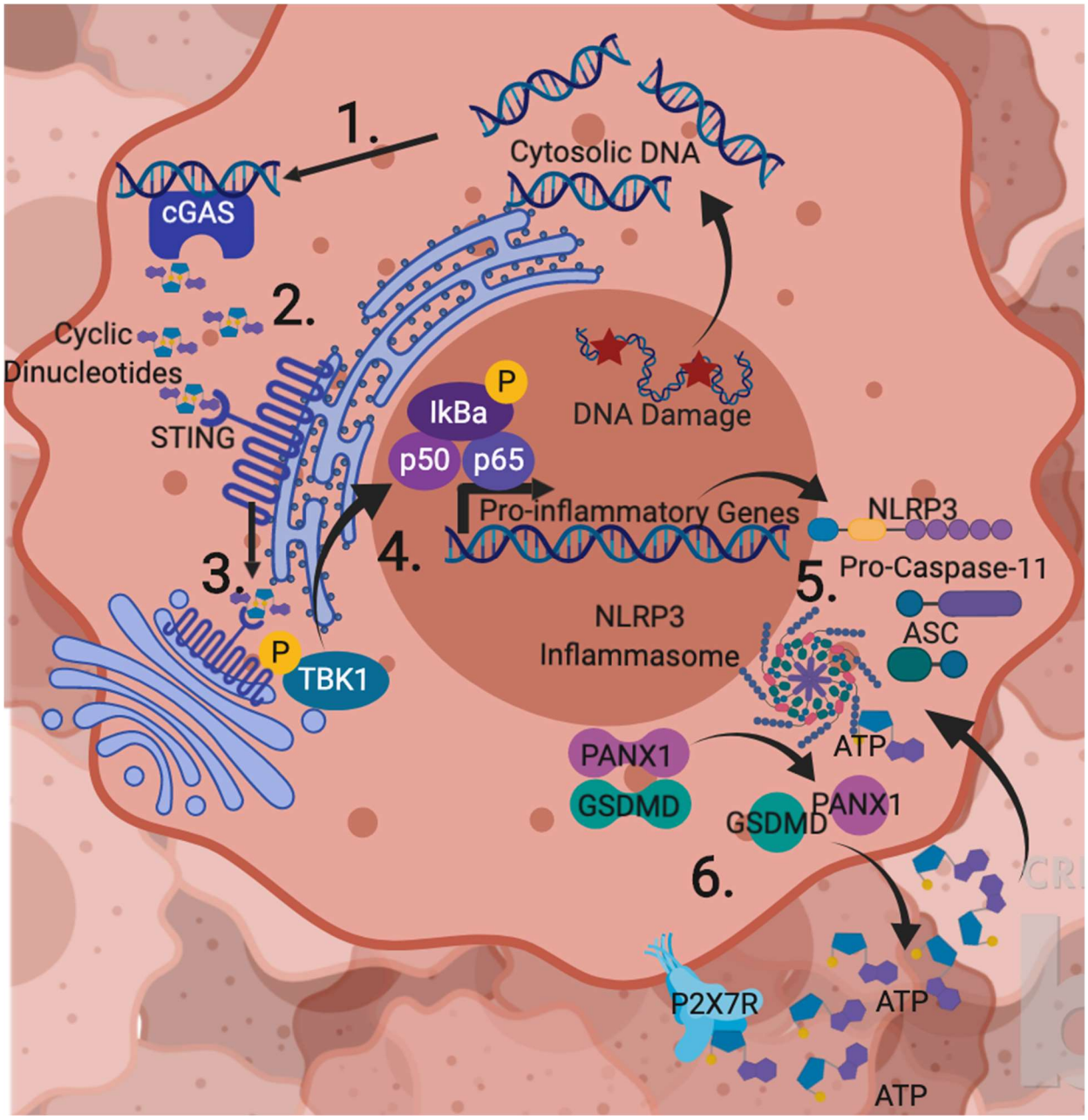

Figure 3-2. Induction of programmed cell death from STING and NLRP3 activity in microsatellite instable colorectal cancer. The accumulation of DNA damage triggers the release of DNA from the nucleus into the cytoplasm that is then recognized by the cGAS receptor **(1)**. cGAS produces cyclic-di-nucleotides that bind to Sting **(2)** resulting in the translocation of STING from the endoplasmic reticulum to the Golgi apparatus **(3)**. Sting is phosphorylated by TBK1, resulting in the phosphorylation of NFκBp65 driving the transcription of NLRP3 **(4)**. The production of IFNs by STING can drive the production of caspase-11, which can form an

inflammasome with NLRP3 and ASC **(5)**. This could initiate pyroptosis via the cleavage of gasdermin D (GSDMD) and the cytosolic portion of pannexin 1 (PANX1). The N-terminal domain of GSDMD creates pores in the cell membrane while the cleaved PANX1 causes ATP to be released from the cell, which can then bind the P2X7 receptor and open the P2X7 pores, resulting in pyroptosis **(6)**. Figure made in ©BioRender.

To test our proposed mechanisms for the interaction of Sting and Nlrp3, we stimulated the 6-month-old MC38 Empty, *Mlh1*$^{-/-}$A, *Mlh1*$^{-/-}$B, and *Pole*$^{-/-}$ cells with cGAMP and/or ATP respectively (Figure 3-3A). The addition of cGAMP indeed activated the Sting pathway, evident from the phosphorylation of Sting and Tbk1, seen in both the single and co-stimulation conditions. Interestingly, the co-stimulation did appear to be additive in that the addition of ATP increased the amount of phosphorylated Sting induced by cGAMP. ATP alone, however, did not appear to induce Sting phosphorylation. Co-stimulation also increased the amount of active phosphorylated NFκBp65 compared to either ATP or cGAMP alone. Unlike what we proposed in our two models, the resulting increase in NFκBp65 activity downstream of Sting activation did not appear to increase the expression of Nlrp3. In fact, none of the stimuli resulted in increased Nlrp3 expression and there did not seem to be enhanced pyroptosis, as measured by cleaved Gsdmd, in any of the conditions when compared to the control condition. Additionally, when we inhibited Sting activity, the expression of Nlrp3 was not decreased as proposed by our two models (Figure 3-3B). We did observe that stimulation of the Nlrp3 inflammasome by ATP resulted in increased phosphorylation of Stat3, most likely from the activation of Il1β by the

inflammasome. Contrary to the mechanisms we proposed, from these data it appears that Sting and Nlrp3 activation work together to enhance Sting activity, rather than Sting increasing Nlrp3 expression. It is noteworthy, however, that while Sting and Nlrp3 synergistically activate Tbk1 and Stat3 signaling, the interaction appeared strongest in *Mlh1* deficient CRCs since only in the *Mlh1*$^{-/-}$ clones did addition of a Sting inhibitor to the co-stimulation fully return activation of Tbk1 and Stat3 to baseline levels (Figure 3-3B). This may be driven by a recently described mechanism where the active Il1β released by cells with active Nlrp3 results in activation of the Il1 receptor pathway in nearby cells, causing the release of mtDNA into the cytoplasm for cGas processing upstream of Sting (Figure 3-4).[124] Confirmation that this is the mechanism through which Sting and Nlrp3 interact will require further testing, along with optimization of the Nlrp3 inhibitor.

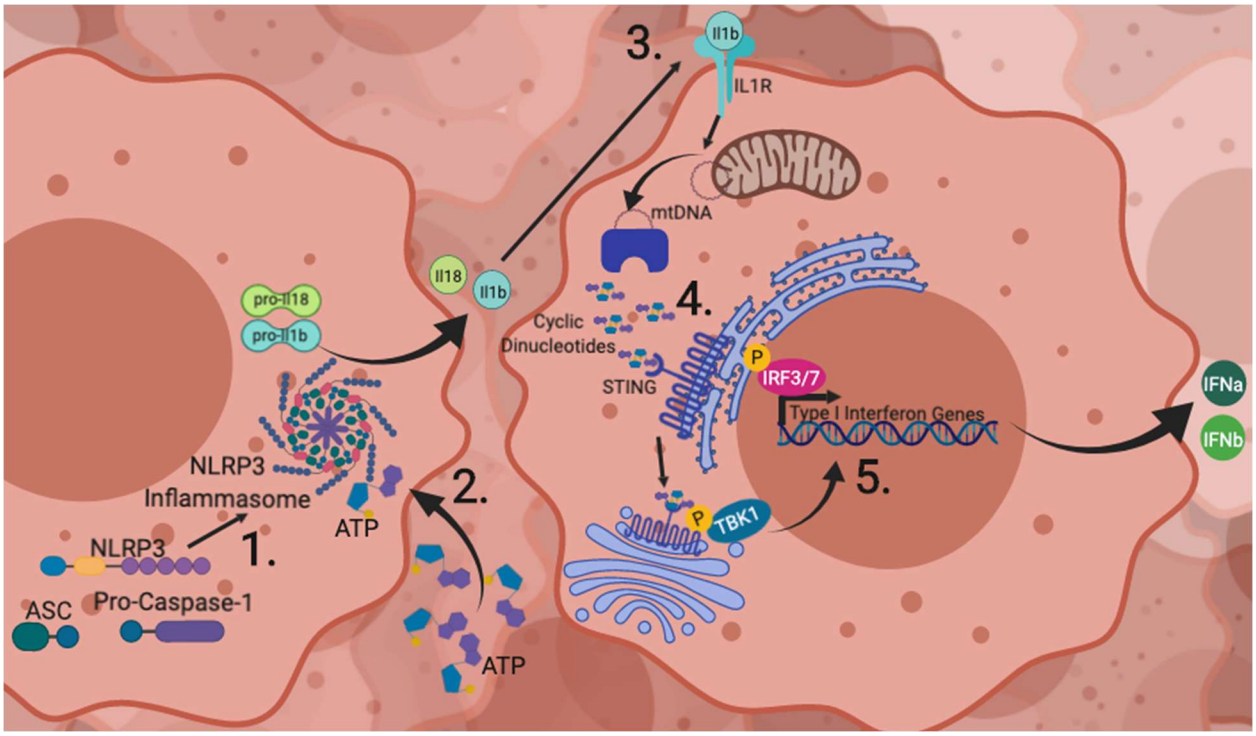

Figure 3-4. Possibility for NLRP3 activation of Sting in anti-CRC immunity. ASC and NLRP3 assemble the inflammasome with caspase-1 **(1)**. ATP from surrounding tumour cells activates caspase-1 in the NLRP3 inflammasome to cleave pro-IL1β and pro-IL18 into their mature forms **(2).** The secreted Il1β binds the IL1 receptor (IL1R) on neighbouring tumour cells, triggering the release of mtDNA into the cytosol to be processed by cGAS into cyclic di-nucleotides **(3)**. These nucleotides bind to STING, resulting in the translocation of Sting from the endoplasmic reticulum to the Golgi apparatus **(4)**, where Sting is phosphorylated by TBK1, recruiting interferon regulatory factors (IRF3/IRF7). These are phosphorylated by TBK1 and translocate to the nucleus to transcribe Type I IFNs **(5)** that aid in the antigen presentation by recruited DCs to CD8+ T cells. Figure made in ©BioRender.

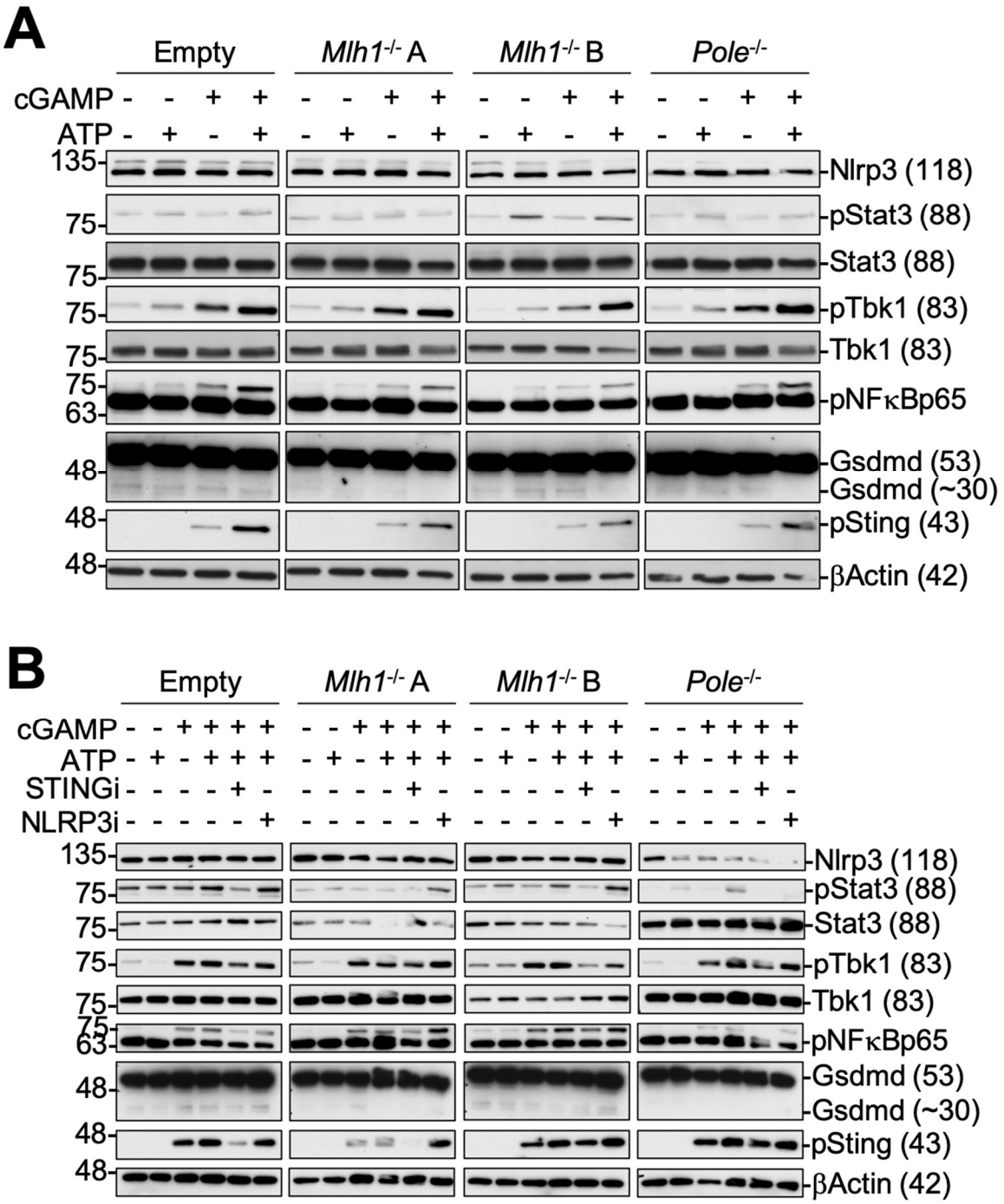

Figure 3-3. ***In vitro*** **co-stimulation of Sting and Nlrp3 exacerbates the Sting signaling pathway expression in all CRC cells.** Western blot of murine MC38 Empty, *Mlh1*$^{-/-}$A, *Mlh1*$^{-/-}$B, and *Pole*$^{-/-}$ cells. Cells were plated at a density of 2.8x10^5 cells/well. **(A)** Cells were stimulated with the ligand for Sting (9ug/ml 2',3'-cGAMP), and/or the ligand for Nlrp3 (2mM ATP) for two hours. **(B)**

Sting and Nlrp3 stimulated cells were inhibited with a Sting inhibitor i.e. STINGi (25 uM CCCP), and/or Nlrp3 inhibitor i.e. NLRP3i (10 uM Isoliquiritigenin) for two hours. Lysates were collected and used for Western blot analysis. Expected protein sizes are shown on the right, size markers (KDa) are shown on the left.

Although we have yet to fully elucidate the mechanism, from these data it is apparent that the activity of Sting and Nlrp3 are additive rather than mutually exclusive in the CRC cells. Of even greater importance, we have found that we are able to stimulate Sting and Nlrp3 in all of our cancer cell lines, regardless of their form of genetic instability. This indicates that the lower expression of these receptors in the Empty CIN or *Pole*$^{-/-}$ tumours *in vivo* is not due to an inherent inability to express or activate these receptors. Therefore, the activation of Sting and Nlrp3 in tumours with CIN or *Pole*$^{-/-}$ genetic instability should be a viable therapeutic option to induce anti-tumour immunity and needs to be further explored. Correspondingly, MSI CRCs must be creating a microenvironment that is endogenously inducing Sting and Nlrp3 receptor activity. We thus next investigated whether differences in the microbiome may contribute to this.

Aim 4. Orthotopic MSI CRCs have a microbial profile that is disparate from CIN CRC

PRRs respond to both endogenous and microbial ligands, meaning that altered expression or activation of PRRs in cancer is likely to change how the intestinal barrier interacts with the resident microbiota. This in turn could alter the microbial populations existing in the colon during tumourigenesis and induce a feedback loop that changes PRR activation. The fecal microbiome of *Nlrp3*$^{-/-}$ and WT mice differ from each other,[129] likely because inflammasome-induced IL18 is needed for a healthy gut flora.[129] Differences in the microbiota of *Sting*$^{-/-}$ mice are also seen.[130] Thus, if STING and NLRP3 work synergistically, as our data suggests, the activity of these receptors could work together to maintain an anti-tumourigenic microbial population during the development of cancer that may also aid in the therapeutic response to immunotherapy. This would be consistent with the observation of differences in the microbiome of MSI compared to CIN human CRCs.[131] Therefore, we hypothesize that NLRP3 and STING could be contributing to the differences observed in the microbiome between these CRC subtypes.

To test whether we see differences in the microbiome of mice with our Empty and *Mlh1*$^{-/-}$ tumours, we isolated feces for 16s ribosomal RNA (rRNA) DNA sequencing from C57BL/6 mice orthotopically injected with 6-month-old MC38 Empty and *Mlh1*$^{-/-}$B cells. Feces was collected both one day prior to tumour cell injection to provide a baseline control for each animal and on the day of tumour resection. The two-way ANOVA comparing the OTUs of the *Mlh1*$^{-/-}$ tumour mice to their baseline revealed significant global OTU differences ($p<0.0001$), while there was no overall significance observed when comparing the Empty tumour mice to their baseline

(Figure 4-1). This indicates that the introduction of MSI CRCs causes significant global OTU abundance changes, while CIN does not. Additionally, using the Sidak's multiple comparisons test we found that the *Mlh1*$^{-/-}$ tumours resulted in a significant expansion of the *Clostridiales* OTU, and reduction of the *Bacteroidales* OTU compared to baseline, while the Empty tumours reduced the *Clostridiales* OTU (Figure 4-1A&B). When the final OTU abundance was normalized to the initial abundance in each mouse and then compared between the Empty, and *Mlh1*$^{-/-}$ groups using a two-way ANOVA, there were significant overall differences in OTU abundances ($p<0.0001$). Additionally, from the Sidak's multiple comparisons test, the *Mlh1*$^{-/-}$ tumours had a significantly higher abundance of the *Clostridiales* OTU compared to the Empty tumours that had significantly higher abundance of the *Bacteroidales* OTU (Figure 4-1A&C). Beyond telling us differences between the microbiome of Empty and *Mlh1*$^{-/-}$ CRCs, these data also illustrate the importance of normalizing 16s rRNA DNA sequencing to a baseline control since, although not statistically significant, there do appear to be qualitative differences in the baseline OTUs of the Empty and *Mlh1*$^{-/-}$ mice. This experiment was intended as a proof-of-concept to test whether the introduction of tumour growth in the mouse intestine for only a short time (2 weeks) would change the microbiome to a degree that reached statistical and biological significance. In future experiments, we will simultaneously examine Nlrp3 and Sting activation as well as 16S microbiota composition in mice bearing orthotopically injected Empty or *Mlh1*$^{-/-}$ tumours. This will allow us to determine if there is an association between Sting and Nlrp3 expression in CRC cells and a specific microbial signature, particularly *Clostridiales*.

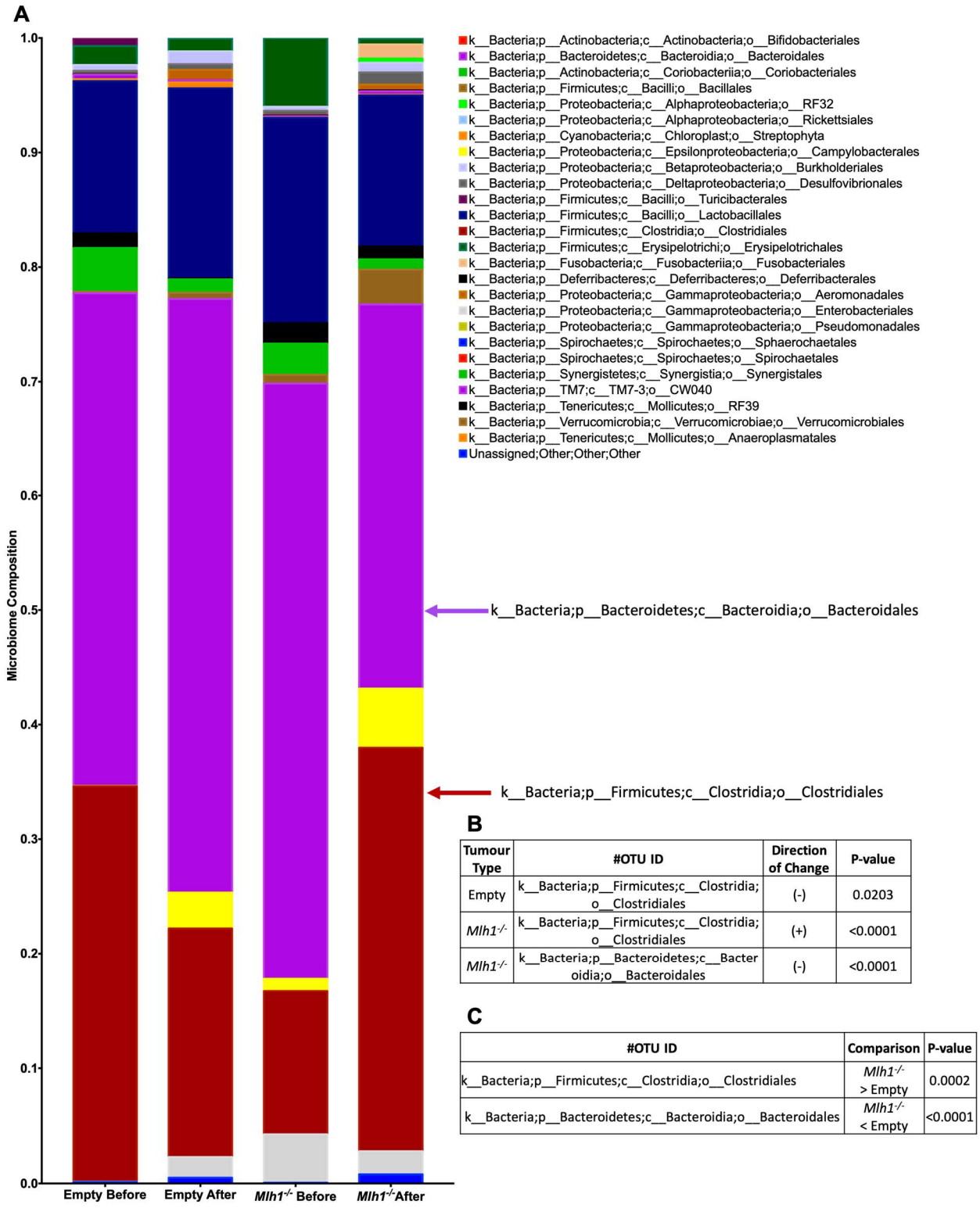

B

Tumour Type	#OTU ID	Direction of Change	P-value
Empty	k__Bacteria;p__Firmicutes;c__Clostridia;o__Clostridiales	(-)	0.0203
Mlh1$^{-/-}$	k__Bacteria;p__Firmicutes;c__Clostridia;o__Clostridiales	(+)	<0.0001
Mlh1$^{-/-}$	k__Bacteria;p__Bacteroidetes;c__Bacteroidia;o__Bacteroidales	(-)	<0.0001

C

#OTU ID	Comparison	P-value
k__Bacteria;p__Firmicutes;c__Clostridia;o__Clostridiales	*Mlh1*$^{-/-}$ > Empty	0.0002
k__Bacteria;p__Bacteroidetes;c__Bacteroidia;o__Bacteroidales	*Mlh1*$^{-/-}$ < Empty	<0.0001

Figure 4-1. Only *Mlh1*$^{-/-}$ CRCs selectively expand the *Clostridiales* OTU in an orthotopic CRC model. 16s rRNA DNA sequencing of feces from mice orthotopically implanted with 1x10^5

MC38 Empty or *Mlh1*$^{-/-}$B CRC cells. **(A)** Average abundance of OTUs in mouse fecal samples evaluated before and after the injection of Empty and *Mlh1*$^{-/-}$B orthotopic tumours. **(B)** Statistical changes in OTUs from before injection to after tumour resection within each tumour group using a two-way ANOVA with Sidak's multiple comparisons test, CI>95%. The (+) direction of change indicates the OTU is of higher abundance in the after group compared to the before group for the specified tumour type. **(C)** OTUs that were significantly different between the *Mlh1*$^{-/-}$B and Empty orthotopic tumours after normalizing each mouse to their baseline OTU abundance using a two-way ANOVA with Sidak's multiple comparisons test, CI>95%. N=3 Empty, and 3 *Mlh1*$^{-/-}$B tumours.

We aim to ascertain whether MSI CRCs have a microbial population that encourages anti-tumour immunity, and if this stems from activation of the STING/NLRP3 axis. If we find the activation of STING and NLRP3 is resulting in an anti-tumourigeneic microbiome, or comparatively, if a specific microbiome results in the activation and subsequent anti-tumour immune effects of STING and NLRP3, then we could aim to manipulate this relationship to help treat CIN CRCs. We could create fecal transplants from healthy donors displaying a fecal 16s signature found to activate STING and NLRP3 driven anti-tumour immunity. Or, if we determine a select few microbes are sufficient for activating STING and NLRP3, the administration of these microbes as probiotics could be a viable option. We are far from therapeutics but understanding what is driving the differences observed between the microbiomes of MSI and CIN CRC is an important endeavour with clear clinical implications.

CHAPTER 4: DISCUSSION

It has long been understood that MSI CRCs result in a better prognosis compared to CIN CRCs. Although this is agreed to be partially due to their genetic instability driving the accumulation of TAAs from mutated genes,[24] other contributing factors have yet to be well established. We hypothesized that innate immune receptors adapted to recognizing foreign pathogens may be activated by the microenvironment that MSI CRCs create. To date, my data from human cancer patients and mouse models have established a correlation between the activity of two PRRs, STING and NLRP3, and anti-tumour immunity in MSI CRCs. My work has allowed us to develop a working model to mechanistically explain this.

Collectively, from our data and understanding of the known properties of STING and NLRP3 in other cell types, we have formulated a model for how these receptors may facilitate anti-tumour immunity in MSI CRCs (Figure 5). We hypothesize that the microbiome of MSI CRCs could activate NLRP3 and STING in MSI CRCs, leading to release of cytokines that recruit the adaptive immune system. The cytokines can then drive the maturation of resident DCs to take up TAAs from surrounding dying cancer cells. The DCs can then process and present these antigens to naïve CD8+ T cells in the local lymph nodes, resulting in their subsequent clonal expansion. These T cells can then seek tumour cells expressing TAAs on MHC class I and induce tumour cell cytolysis. Although there is much work needed to test the validity of this model, the works of this thesis provide preliminary support for its role in anti-CRC immunity.

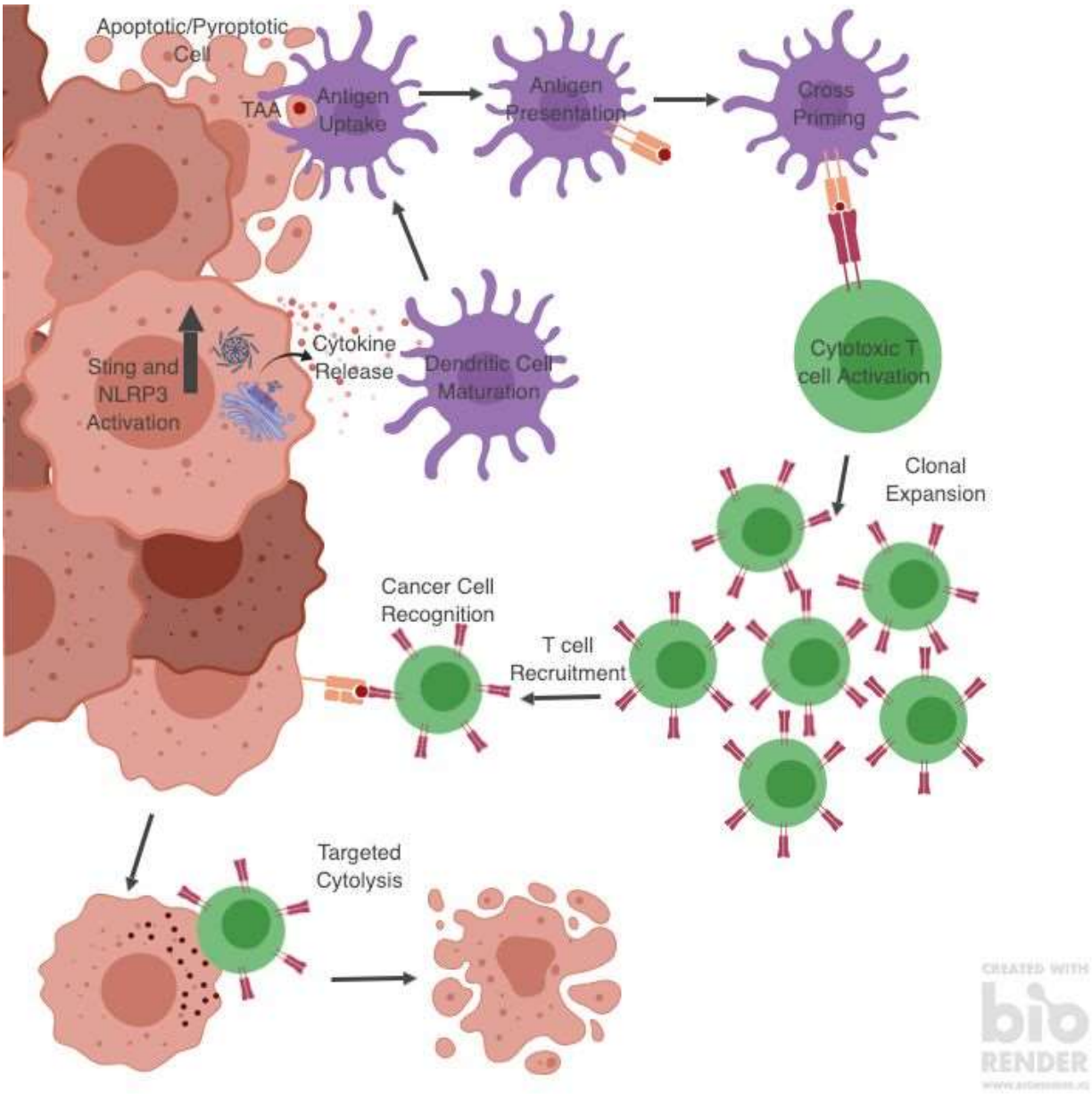

Figure 5. The activity of NLRP3 and STING aid in cytotoxic T cell mediated killing of tumour cells. When STING and NLRP3 are active in tumour cells they release cytokines that mature DCs into a form that can uptake TAAs released from tumour cells undergoing either apoptosis or pyroptosis. These DCs then process these antigens and present them to naïve CD8+ T cells in the local lymph nodes, which can then expand and seek tumour cells expressing these TAAs, inducing tumour cell cytolysis. Figure made in ©BioRender.

MSI CRC can be effectively modeled in mice

In the first aim of this thesis, we determined that we could recapitulate notable characteristics of human MSI CRCs in mice. Specifically, when we ablated the expression of *Mlh1* in the murine MC38 adenocarcinoma cell line and subcutaneously injected these cells into syngeneic mice, we observed a lower growth rate of the *Mlh1*$^{-/-}$ tumours (Figure 1-7). Of those tumours that did become established, they were of a significantly smaller size and had more effector T cells present compared to either the Empty or *Pole*$^{-/-}$ tumours. Ideally, we would have used a non-cancerous immortalized murine colon cell line to conduct this work since we could then have examined the *de novo* process of carcinogenesis after knocking out *Mlh1*. Since no normal colonic mouse cell lines are available, we chose to work with the MC38 CRC cell line despite the fact that this presented us with several limitations. This is because the MC38 cell line has a mutation in *Apc* giving all of our CRISPR mutated cell lines a CIN background.[122] While this mimics what is seen in hereditary *MLH1*$^{-/-}$ CRCs,[132,133] it could be masking important features of the phenotype of sporadic human MSI or *POLE*$^{-/-}$ CRCs. Additionally, the CIN phenotype of the MC38 cell line made it difficult to ablate gene function because the chromosomal instability of this cell line could result in greater than two copies of each gene. This may have contributed to our inability to establish more than one *Pole*$^{-/-}$ cell line clone, when ideally, we would work with two. Multiple clones are ideal because if the same phenotype arises after 6 months of genetic drift in two independently evolving clones, then we can be more confident the effect we see is not due to a stochastic event, but rather the mutation we introduced.

To address the limitation of our model and ensure that our data did not result from artifacts in a single cell line, we also engineered similar mutations into a second murine adenocarcinoma cell line, CMT-93,[134] and a duodenal normal murine IEC line, MODE-K.[135] Although the CMT-93 cell line is also of the CIN type,[136] it is less dedifferentiated and proved much easier to ablate gene function in using CRISPR/Cas9. We were able to make two or more loss-of-function mutant CMT-93 cell line clones for the genes *Pole, Mlh1* and *Msh2* of the DNA MMR pathway, and *Rad51* of the double strand break repair pathway. In the MODE-K cell line, we established one inactivating *Apc* mutant clone, and two or more mutant clones for the genes *Mlh1*, *Msh2*, *Rad51*, *Pole*, and the methyltransferase gene, *Mgmt.* We aimed to complete all *in vivo* work in cells derived from each of the MC38, CMT-93, and MODE-K cells to confirm that the phenotype we observed was not due to artifacts of one cell line or mouse strain. However, despite trying many different injection routes and conditions, all of the MODE-K and CMT-93 derived cell clones failed to grow *in vivo*.

Since starting this project, we have developed the use of GFP labelled CRISPR plasmids to transfect and genetically ablate genes in organoids derived from the normal intestinal crypt cells of mice. Using this technique, we can create *Apc*, *Mlh1*, and *Pole* mutated mouse colon organoids that can be orthotopically injected into syngeneic mice. It is both difficult and expensive to continuously culture intestinal organoids for 6 months as we did with the cell lines. As such, we would have to confirm that the CRISPR mutated organoid systems do indeed model the form of genetic instability that their mutations are intended to create within a

relatively short window for genetic drift. To evaluate the CIN phenotype we will perform a simple metaphase spread with Giemsa banding to assess chromosome abnormalities.[137] Comparatively, MSI and *Pole*$^{-/-}$ hypermutability will be assessed using a reporter plasmid system whereby the introduction of a deletion or insertion in the repeat region is required to bring a beta-galactosidase reporter gene in-frame.[138] Establishing organoid models for MSI, CIN, and *Pole* mutant CRC will address the issue of background lineage we have with our cell lines, allowing us to study the different forms of genetic instability in isolation. Despite the MC38 cell line possessing a background *Apc* mutation, the *Mlh1*$^{-/-}$ and *Pole*$^{-/-}$ MC38 tumours display a disparate immune phenotype compared to the Empty tumours that we have confirmed recapitulates the anti-tumour immunity seen in patients with these forms of hypermutability. As such, we believe the MC38 tumour model is sufficient to address the research questions in this thesis despite its inherent limitations.

The expression of STING and NLRP3 contribute to anti-tumour immunity

The second aim of this thesis was to investigate the role for STING and NLRP3 PRR activity in driving anti-tumour immunity in CRCs. Analyzing publicly available human data revealed that *STING* and *NLRP3* expression is higher in MSI compared to either CIN or *POLE* mutated CRCs (Figure 2-1). We further found a significant positive correlation between the expression of *STING* and *NLRP3* themselves, as well as between expression of the cytotoxic T cell marker, *CD8A*, and either *STING* or *NLRP3* (Figure 2-2). TCGA data was derived from sequencing RNA from whole heterogenous tumours, therefore it cannot identify what cell type within the

tumour is contributing to the differential expression of *STING* and *NLRP3*. If high expression of *STING* and *NLRP3* by infiltrating immune cells account for the differential tissue expression, then these would not be viable targets for therapy because CIN CRCs lack immune cell infiltration. Comparatively, if high expression of *STING* and *NLRP3* by the MSI tumour cells themselves accounts for the differential tissue expression and this leads to the recruitment of CD8+ T cells into the tumour, then *STING* and *NLRP3* make for excellent targets for adjuvant immunotherapy.

Studying this relationship in our mouse models after separating tumour epithelium from infiltrating immune cells, we observed that the expression of *Sting* and *Nlrp3* in the tumour cells themselves, rather than in immune cells within the tumour, is associated with increased *Cd8a* expression in the immune cell population (Figure 2-4). *CD8a* expression also correlated with a smaller tumour size. This is consistent with our finding that protein expression of Sting and Cd8a in the *Mlh1*$^{-/-}$ tumours was higher than in either the *Pole*$^{-/-}$ or Empty tumours (Figure 2-6). Furthermore, the downstream signaling molecules of these pathways were upregulated, and are known to recruit and aid in the activation of adaptive immune cells (Figure 2-5).[80,95,114] This alludes to a potential mechanism where tumour cell expression of *Sting* and *Nlrp3* facilitates the recruiting of CD8+ T cells to the tumour site to initiate anti-tumour immunity. Since the *Mlh1*$^{-/-}$ MC38 cells did not express significantly higher amounts of Sting or Nlrp3 *in vitro*, this indicates that there must be a dialog occurring between the tumour cells and the immune

microenvironment of MSI tumours that is critical in driving Sting and Nlrp3 activation in the tumor cells.

The STING pathway results in the production of type I IFNs as well as pro-IL1β which is the cleavage product of the NLRP3 inflammasome. Type I IFNs are required for the maturation of DCs and therefore antigen presentation to CD8+ T cells[33,81] and have also been shown to induce pSTAT3 expression in CD8+ T cells resulting in the transcription of *GZMB* (Granzyme B).[41] The cleavage of pro-IL1β by the NLRP3 inflammasome results in the secretion of IL1β into the tumour microenvironment where it can aid in the migration and activation of DCs.[139] Additionally, both STING and NLRP3 result in the production of IFNγ, a potent activator of CD8+ T cells.[18] NFκBp50 and NFκBp65 transcription factors downstream of STING transcribe IFNγ,[90] whereas the activation of IL18 by the NLRP3 inflammasome drives the production of IFNγ in surrounding epithelial and lymphocyte cells.[114] Taken together, our data is indicating that the effector molecules downstream of both STING and NLRP3 activation in the cancer cells could be driving the infiltration of CD8+ T cells in MSI CRCs, thereby resulting in a better response to anti-PD-1 therapy[140] as well as better overall survival compared to CIN CRCs.[31]

When we evaluated this phenomenon in the context of the colon microenvironment in our orthotopic model, we observed similar effects. The tumour cells in the *Mlh1*$^{-/-}$ CRCs had both a higher percentage of cells expressing pSting, Nlrp3, and pTbk1, as well as higher expression of

these proteins per cell (Figure 2-7, 2-8, 2-9). In our subcutaneous model, we were not able to evaluate specific immune cell populations due to the isolation protocol we had chosen. However, subsequent flow cytometric analysis of tumor cells from our orthotopic model revealed a signature for heightened pSting, Nlrp3, and pTbk1 expression in the CD4+ T cell population of the *Mlh1*$^{-/-}$ CRCs, but not in other immune populations. Since this result was unexpected, we had not included antibodies to distinguish the CD4 lineage of these cells as either Tregs (Foxp3+) or active helper T cells. Now that we have seen the interesting signature in the CD4+ T cells, we will rearrange our flow cytometry panel to include an anti-Foxp3 stain. I would expect the pSting, Nlrp3, and pTbk1 expressing CD4+ T cells in the *Mlh1*$^{-/-}$ CRCs to be active helper T cells. Helper T cells are known to aid in the recruitment of CD8+ T cells,[141] which we have already established are increased in *Mlh1*$^{-/-}$ CRCs. Comparatively, regulatory T cells perform their function by secreting cytokines to turn off an active immune response,[21] and since the activation of Sting and Nlrp3 result in the production of cytokines that aid in the induction of an active anti-tumour immune response,[80,94] it is logical that the CD4+ T cells expressing pSting, Nlrp3, and pTbk1 are not of a suppressive phenotype. Regardless, it will be interesting to characterize the CD4+ T cells expressing Sting and Nlrp3 in MSI CRCs, and to determine how they may be contributing to anti-tumour immunity.

Our orthotopic mouse model has many strengths compared to more common methods for modeling CRC. Most orthotopic CRC studies are done by injecting the cancer cell suspension into the cecal wall of syngeneic mice.[142] This requires open surgery for the injection of the cells

that can possibly drive local inflammation that could impact tumour growth. Furthermore, since the cecum is between the large and small intestine, this model requires the use of cells with bioluminescent or fluorescent markers to monitor growth using an *in vivo* imaging system. Moreover, the cecum is not a representative location for the development of the large majority of human CRCs. In humans, the cecum is relatively small while in mice it is a comparatively large organ and is a reservoir of *Lactobacillus*, serving as an essential site of fermentation in the gut.[143] Not only does gene expression vary greatly along the intestine,[144] but so does the expression of PRRs,[82] and therefore, it is essential for us to study CRC in the descending colon where most tumours originate.[9] Comparatively, our use of an endoscope with a flexible needle to inject cancer cells into the descending colon is much less invasive, requires less time for the mouse to be under anesthesia, and results in controlled seeding of the primary tumour into the colon. Since we can monitor tumour growth with the endoscope, there is no requirement for using bioluminescent or fluorescent cells, reducing the number of manipulations needed in our CRISPR mutated cells. A drawback of our system is that the scope is rigid, so we cannot seed any cells into the proximal colon, the location where human MSI CRCs are most prevalent. Therefore, our model may be missing the exact specialized niche of that section of the intestine. However, currently no method is available to target the growth of cells into the proximal colon, making our orthotopic model one of the best options available. Collectively, our subcutaneous and orthotopic CRC experiments demonstrate that the consequences of Sting and Nlrp3 activation in the tumour cells may be resulting in the inadvertent recruitment and activation of an anti-tumour immune response in MSI CRCs.

Sting and Nlrp3 can be activated in both MSI and CIN CRC cells

To determine whether Nlrp3 and Sting are suitable therapeutic targets, and if they are working independently or in concert, we stimulated the receptors either alone or simultaneously in our MSI and CIN CRC cells *in vitro*. We observed that the co-stimulation was enhancing expression of the Sting signaling pathway and its downstream mediators compared to stimulating either Sting or Nlrp3 alone (Figure 3-3). Although the MSI CRCs showed higher expression of Nlrp3 and Sting *in vivo*, when the cells were stimulated *in vitro* the pathways were activated in all the cell lines. This is promising, because if we pursue Sting and Nlrp3 as therapeutic targets, we need to be confident there is not an inherent block to their activation in the CIN CRCs as these are the cancers proving difficult to treat with immunotherapy.

Our data suggest that the hypotheses we initially proposed for how STING and NLRP3 may be working together are either incorrect or incomplete. Our current understanding of how NLRP3 and STING work is mostly derived from immune cells, therefore it is uncertain how translatable the functions of these pathways are to epithelial cells. Based off the literature for the known function of STING and NLRP3, we hypothesize that if these receptors are working together it is most likely initiated by STING activating NLRP3. This is because the STING pathway results in the activation of a number of transcription factors that could result in the production of inflammasome components.[90] Subsequent to this, activated NLRP3 can then increase STING signaling activity by increasing cytoplasmic DNA from either the mitochondria or cell nucleus. This hypothesis is consistent with our observation that when we inhibit Sting, there is no

observed depletion of the Nlrp3 protein but a complete abrogation of the synergistic signaling between the two pathways. Our *in vivo* work also provides corroborating circumstantial evidence that Sting and Nlrp3 are working together. Nlrp3 should not activate the expression of interferon-stimulated genes, but there is a significant positive correlation between *Nlrp3* expression and the expression of *Ccr5* and *Ccl5* in the subcutaneous tumour cells. These genes are regulated by transcription factors downstream of the Sting pathway, therefore the interaction of Sting and Nlrp3 may explain the correlation.

Although we were able to stimulate Sting in all of our cell lines regardless of their form of genetic instability, we have yet to evaluate whether this would result in the activation of immune cells to an equal extent. To evaluate TAA-independent effects, we could stimulate Sting in the CRC cells, remove the stimulus, and then perform a co-culture of the CRC cells with C57BL/6 T cells derived from the lamina propria, mesenteric lymph node, or spleen. We would then measure T cell expression of Gzmb and Ifnγ via flow cytometry to assess their activation.[41] Additionally, we could perform an in vitro co-culture of C57BL/6 BMDCs with Sting-stimulated CRCs and evaluate the expression of MHC class I on both the DCs and the tumour cells as a surrogate for antigen presentation.[99] The activation state of the DCs could also be evaluated by measuring the expression of MHC class II, CD80 and CD86 by flow cytometry,[145] or by measuring their production of Il6 and Il12 using Enzyme Linked Immunosorbent Assays (ELISAs).[146] To assess TAA-dependent effects of Sting and Nlrp3, we could also use a model TAA, such as ovalbumin (OVA), to test whether Sting activation of the tumour cells can enhance

antigen specific T cell killing. We have successfully transfected our 6-month-old MC38 Empty, *Mlh1*$^{-/-}$ A, *Mlh1*$^{-/-}$ B, and *Pole*$^{-/-}$ cells with plasmids expressing OVA. T cells isolated from OT-1 C57BL/6 mice bearing an OVA-specific T cell receptor can then be co-cultured with the OVA expressing CRC cell lines post-Sting stimulation to evaluate how Sting activation influences OVA-specific T cell cytolysis of MSI compared to CIN and *Pole*$^{-/-}$ CRC cells. Additionally, once we determine a suitable ligand and readout for Nlrp3 activation, then we could conduct these experiments post-Nlrp3 and post-co-stimulation of Nlrp3 and Sting to get a better understanding of how the activation of these PRRs influences various processes of the adaptive anti-tumour immune response. These experiments should elucidate how important Sting and Nlrp3 activation may be compared to the production of TAAs by the tumour cells for triggering a potent anti-tumour immune response.

We had hoped to elucidate the mechanistic relationship between STING and NLRP3, but unfortunately faced some experimental challenges. There are several described ligands for NLRP3, and since it is a pathway best studied in immune cells, it was difficult to decide what ligand to pursue first since many of the readouts for activation are not sensitive enough to detect the response seen in epithelial cells. The two most commonly used ligands are ATP and nigericin, an antibiotic produced by the microbe *Streptomyces hygroscopicus*.[103] We decided to begin with ATP because nigericin is not as ubiquitous in the tumour microenvironment. Unfortunately, ATP is a molecule that is involved in several different pathways, making it difficult to specifically determine if we were successfully inducing or inhibiting Nlrp3 activation.

We were expecting that ATP would increase expression of Nlrp3 if it activates inflammasome assembly, but we did not see this occur *in vitro*. Therefore, to circumvent this problem, we could perform co-immunoprecipitation with anti-Nlrp3 antibodies to see if it associates with Asc or Nek7 following ATP stimulation, thereby indicating that ATP stimulation of our cells is indeed resulting in inflammasome assembly.[103] This would also allow us to sufficiently evaluate whether the stimulation of Sting alone is directly activating Nlrp3 assembly, which would support the hypothesis we proposed.

We also experienced challenges evaluating the downstream signaling of Nlrp3 because unlike Sting, Nlrp3 has a short signaling cascade and therefore limited readouts. This also makes it difficult to tell whether we are sufficiently inhibiting Nlrp3 with the inhibitor isoliquiritigenin. Although we performed Western blots for cleaved Il1β, caspase-1, and caspase-11 in the supernatant of the stimulated cells, the quality of the blots was poor, making the readout uncertain. To address this, we could instead use an ELISA for activated Il1β and Il18 in the supernatants of stimulated cells. However, this would also be challenging because epithelial cells produce these cytokines at much lower levels than immune cells and we would have to perform a longer stimulation to accumulate enough cytokine for detection. These experiments would hopefully also allow us to detect cleaved caspase-1 and caspase-11, which should also accumulate in the supernatant and be easier to detect by Western Blot. Beyond measuring caspase-1/11 activity, the only other readout for pyroptosis is through measuring Gsdmd cleavage. There are ample antibodies available for human GSDMD, but only one specific for

Gsdmd in mice. Full length Gsdmd is constitutively expressed in cells and remains inactive until it becomes cleaved and can form pores in the membrane.[108] We indeed observed the full length Gsdmd in all our stimulation conditions, but to our surprise the active cleaved form was present at baseline for some cells. Since we did not observe cell death in the unstimulated cells, unlike with the ATP condition, it makes us uncertain as to the reliability of this Gsdmd antibody as a readout of pyroptosis.

The additive activation of the STING pathway by ligands for NLRP3 and STING may be driven by a recently described mechanism in which mature IL1β released by cells with active NLRP3 results in activation of the IL1 receptor (IL1R) pathway in nearby tumour cells.[124] By an unknown mechanism, signaling via the IL1R appears to result in the release of mtDNA into the cytoplasm that is then processed by cGas, upstream of STING, leading to STING activation but not the induction of apoptosis (Figure 3-4). If this mechanism exists in CRC cells, then we would expect the NLRP3 stimulated cells to have more mtDNA in their cytosol compared to unstimulated cells. Similarly, knocking out NLRP3 or using an NLRP3 inhibitor should then abrogate the accumulation of cytosolic mtDNA. We will conduct this experiment using a protocol we have established in our lab for cytosolic DNA isolation[147] along with the quantification of mtDNA using specific qPCR primers. Although the mechanism of how NLRP3 and STING may interact to drive anti-tumour immunity requires considerable investigation, our data provides preliminary evidence that these receptors are interacting in a way that makes them promising therapeutic targets for most CRCs.

MSI CRCs have an expansion of the *Clostridiales* OTU

Sequencing the fecal 16s rRNA DNA of mice with either Empty or *Mlh1*$^{-/-}$ orthotopic CRCs revealed that growing orthotopic tumours for two weeks is sufficient to influence the microbiome and that *Mlh1*$^{-/-}$, but not Empty, tumours result in significant expansion of the *Clostridiales* OTU (Figure 4-1). As of yet, we cannot claim an association between *Clostridiales* and Nlrp3 or Sting activity. We could approach this using several different strategies. First, we could sequence the microbiota in mice bearing orthotopic *Mlh1*$^{-/-}$ and Empty CRCs for which we know the status of Nlrp3 and Sting expression and activation in the tumour cells. We could also use *Nlrp3*$^{-/-}$ or *Sting* $^{-/-}$ *Mlh1*$^{-/-}$ tumour cells since, if the *Clostridiales* expansion in *Mlh1*$^{-/-}$ CRCs is driven by expression of Nlrp3 and Sting, we should no longer see an expansion of *Clostridiales* in the fecal microbiome of mice bearing these tumours. Confirming if the relationship exists in the opposing direction is trickier. If microbes belonging to the *Clostridiales* OTU are indeed activating Sting and Nlrp3 in the orthotopic *Mlh1*$^{-/-}$ CRCs, then a fecal transplant[148] from mice with a *Clostridiales* abundant microbiome into mice bearing MC38 Empty orthotopic CRCs should result in increased Sting and Nlrp3 expression in these tumours and a stronger anti-tumour immune response.

The *Clostridiales* are a large and diverse group of bacteria including both pathogenic and commensal members.[149] As such, to identify the abundance of specific members of *Clostridiales* in the feces of *Mlh1*$^{-/-}$ CRC bearing mice, we would perform qPCR using primers for defined *Clostridiales* species. Additionally, if we consider that the commensal members of the

Clostridiales group are predominantly characterized as producers of the short chain fatty acid, butyrate, it would be logical to specifically quantify *Clostridiales* butyrate producers via qPCR along with measuring the production of butyrate in the colon of *Mlh1*$^{-/-}$ CRC bearing mice.[150] Although *Clostridiales* are difficult to grow due to being strict anaerobes,[149] they are culturable with specialized equipment. If we could identify specific species by qPCR that are commercially available, then we could create axenic orthotopic models by introducing these species into the colon of mice treated with universal antibiotics. With this model, we could assess the impact of these specific species of *Clostridiales* on tumourigenesis in MSI compared to CIN CRCs and determine whether they increase the expression of Sting or Nlrp3 in the tumours resulting in an anti-tumour immune phenotype. Through this process we could identify probiotics that drive anti-tumour immunity through activating Sting and Nlrp3 that could be used as an adjuvant for CRC immunotherapy.

Future Directions

Our results show a correlation between Sting and Nlrp3 activity and the infiltration of CD8+ T cells into CRCs but we have not yet demonstrated a causative mechanism between these. We are currently in the process of stably knocking down *Nlrp3* and *Sting* in the 6-month Empty, *Mlh1*$^{-/-}$A, *Mlh1*$^{-/-}$B, and *Pole*$^{-/-}$ MC38 cell lines. Once we have these knock-downs established in our CRC cells, we can use them to mechanistically test our hypothesis in *in vitro* stimulations. We expect that the cell lines with an *Nlrp3* knockdown stimulated with ATP should no longer

induce the Sting signaling pathway if Nlrp3 is indeed activating Sting, and if Sting is regulating Nlrp3, then we expect the opposite to be true.

The Sting and Nlrp3 knockdown cells will also prove essential for *in vivo* studies to evaluate if the absence of *Nlrp3* and/or *Sting* in CRC cells ablates the infiltration of CD8+ T cells observed in *Mlh1*$^{-/-}$ tumours. We will determine whether Sting activation with the clinical candidate Sting agonist ADU-S100 (S100)[151] enhances infiltration of CD8+ T cells in orthotopic CIN CRC bearing mice and expect that mice with the *Sting* knockdown CIN tumors will not experience enhanced CD8+ T cell infiltration. Finally, we want to test the efficacy of S100 with anti-PD1 therapy (pembrolizumab) in the Empty, *Mlh1*$^{-/-}$, and *Pole*$^{-/-}$ CRCs with or without the *Sting* knockdown to evaluate whether this enhances the response of CIN CRCs to pembrolizumab to the same extent observed in MSI CRC.

The lack of a specific Nlrp3 agonist makes it difficult to initiate *in vivo* stimulations of this receptor, as ATP is too ubiquitous to be used in animal models. While using the Nlrp3 knockdown cell lines orthotopically *in vivo* can provide proof-of-concept and validate the mechanism we are proposing, this will not identify a therapeutically tractable way of using our finding. We thus plan to test various Nlrp3 ligands *in vitro* to identify a molecule that not only potently stimulates Nlrp3 in our cell lines but is safe and effective for *in vivo* work. Once a suitable ligand is determined, we can evaluate whether the Nlrp3 agonist enhances infiltration

of CD8+ T cells in the orthotopic CIN CRCs compared to the *Nlrp3* knockdown tumours, and if the infiltration is to a similar degree as the MSI CRCs. Additionally, we will test the efficacy of the combination of Pembrolizumab, S100, and the Nlrp3 ligand for ablating tumour growth in both CIN and MSI CRCs.

To evaluate the translatability of the combination of pembrolizumab, S100, and the Nlrp3 agonist in human CRCs, we will create an *ex vivo* primary human co-culture. This will be achieved through creating an autologous co-culture between organoids derived from CIN or MSI CRC patients and their isolated immune cells. Using this system, we can evaluate how the combination therapy compares to its individual constituents in the recruitment, activation, and tumour killing capability of the immune cells. This will allow us to determine whether the activation of Sting and Nlrp3 can initiate an anti-tumour immune response following pembrolizumab treatment in the CIN CRCs to a similar degree as the MSI CRCs in humans. Should the corresponding *in vivo* mouse and *ex vivo* human experiments prove successful, then we could seek a collaboration for a phase-I trial for the combination of pembrolizumab, S100, and the Nlrp3 agonist in CRCs.

CLOSING REMARKS

Collectively, our work aims to uncover the driving forces behind the natural anti-tumour immunity observed in MSI CRC to identify global mechanisms that can then be manipulated to

create novel CRC therapies. Since the bulk of CRCs respond poorly to clinical treatments,[152,153] using adjuvant therapies to boost an anti-tumour immune response is a promising avenue for enhancing overall rates of CRC survival. If we can determine that MSI CRC's enhanced prognosis is derived from the upregulation of the STING/NLRP3 axis, then agonists, probiotics, or fecal transplants, could be used to enhance the activity of these receptors to improve the response of CIN CRCs to immunotherapies, thereby increasing overall CRC survival.

REFERENCES

1. Canadian Cancer Statistics Advisory Committee. Canadian Cancer Statistics Special topic: Pancreatic cancer. *Can. Cancer Stat.* 1–114 (2017). doi:0835-2976

2. Canadian Cancer Statistics Advisory Committee. *Canadian Cancer Statistics*. *Canadian Cancer Society* (2018). doi:0835-2976

3. Liu, Y. *et al.* Comparative Molecular Analysis of Gastrointestinal Adenocarcinomas. *Cancer Cell* **33**, 721-735.e8 (2018).

4. Bakhoum, S. F. & Cantley, L. C. The Multifaceted Role of Chromosomal Instability in Cancer and Its Microenvironment. *Cell* **174**, 1347–1360 (2018).

5. Vogelstein, B. *et al.* Genetic Alterations during Colorectal-Tumor Development. *N. Engl. J. Med.* **319**, 525–532 (1988).

6. Fodde, R. *et al. Mutations in the APC tumour suppressor gene cause chromosomal instability*. *communications NATURE CELL BIOLOGY* **3**, (2001).

7. Baldus, S. E. *et al.* Prevalence and heterogeneity of KRAS, BRAF, and PIK3CA mutations in primary colorectal adenocarcinomas and their corresponding metastases. *Clin. Cancer Res.* **16**, 790–9 (2010).

8. Watanabe, T. *et al.* Molecular Predictors of Survival after Adjuvant Chemotherapy for Colon Cancer. *N. Engl. J. Med.* **344**, 1196–1206 (2002).

9. Vilar, E. & Gruber, S. B. Microsatellite instability in colorectal cancer-the stable evidence. doi:10.1038/nrclinonc.2009.237

10. Jover, R. *et al.* Mismatch repair status in the prediction of benefit from adjuvant fluorouracil chemotherapy in colorectal cancer. *Gut* **55**, 848–855 (2006).

11. Dahlin, A. M. *et al.* Colorectal cancer prognosis depends on T-cell infiltration and molecular characteristics of the tumor. *Mod. Pathol.* **24**, 671–682 (2011).

12. Tougeron, D. *et al.* Efficacy of Adjuvant Chemotherapy in Colon Cancer With Microsatellite Instability: A Large Multicenter AGEO Study. *J. Natl. Cancer Inst.* **108**, djv438 (2016).

13. Boland, C. R. & Goel, A. Microsatellite Instability in Colorectal Cancer. doi:10.1053/j.gastro.2009.12.064

14. Zhao, P., Li, L., Jiang, X. & Li, Q. Mismatch repair deficiency/microsatellite instability-high as a predictor for anti-PD-1/PD-L1 immunotherapy efficacy. *J. Hematol. Oncol.* **12**, 54 (2019).

15. Nebot-Bral, L. *et al.* Hypermutated tumours in the era of immunotherapy: The paradigm of personalised medicine. *European Journal of Cancer* **84**, 290–303 (2017).

16. Kawakami, H., Zaanan, A. & Sinicrope, F. A. The role of microsatellite instability testing in management of colorectal cancer. *Clin. Adv. Hematol. Oncol.* **14**, 476–479 (2016).

17. Hooper, L. V. & MacPherson, A. J. Immune adaptations that maintain homeostasis with the intestinal microbiota. *Nature Reviews Immunology* **10**, 159–169 (2010).

18. Lei-Leston, A. C., Murphy, A. G. & Maloy, K. J. Epithelial Cell Inflammasomes in Intestinal Immunity and Inflammation. *Front. Immunol.* **8**, 1168 (2017).

19. McGuckin, M. A., Lindén, S. K., Sutton, P. & Florin, T. H. Mucin dynamics and enteric pathogens. *Nat. Rev. Microbiol.* **9**, 265–278 (2011).

20. Rimoldi, M. *et al.* Intestinal immune homeostasis is regulated by the crosstalk between epithelial cells and dendritic cells. *Nat. Immunol.* **6**, 507–514 (2005).

21. OKUMURA, R. & TAKEDA, K. Maintenance of gut homeostasis by the mucosal immune system. *Proc. Japan Acad. Ser. B* **92**, 423–435 (2016).

22. Zhang, L. *et al.* Immune Landscape of Colorectal Cancer Tumor Microenvironment from Different Primary Tumor Location. *Front. Immunol.* **9**, 1578 (2018).

23. Saeterdal, I. *et al.* Frameshift-mutation-derived peptides as tumor-specific antigens in inherited and spontaneous colorectal cancer. *Proc. Natl. Acad. Sci.* **98**, 13255–13260 (2001).

24. Lal, N., Beggs, A. D., Willcox, B. E. & Middleton, G. W. An immunogenomic stratification of colorectal cancer: Implications for development of targeted immunotherapy. *Oncoimmunology* **4**, 1–9 (2015).

25. McFarland, C. *et al.* The damaging effect of passenger mutations on cancer progression. *Cancer Res.* canres.3283.2015 (2017). doi:10.1158/0008-5472.CAN-15-3283-T

26. Sillo, T. O., Beggs, A. D., Morton, D. G. & Middleton, G. Mechanisms of immunogenicity in colorectal cancer. *Br. J. Surg.* (2019). doi:10.1002/bjs.11204

27. Howitt, B. E. *et al.* Association of Polymerase e–Mutated and Microsatellite-Instable Endometrial Cancers With Neoantigen Load, Number of Tumor-Infiltrating Lymphocytes, and Expression of PD-1 and PD-L1. *JAMA Oncol.* **1**, 1319 (2015).

28. Stenzinger, A. *et al.* Mutations in POLE and survival of colorectal cancer patients – link to disease stage and treatment. *Cancer Med.* **3**, 1527–1538 (2014).

29. Yuan, Y., Jiang, Y. C., Sun, C. K. & Chen, Q. M. Role of the tumor microenvironment in tumor progression and the clinical applications. *Oncol. Rep.* **35**, 2499–2515 (2016).

30. Diaz-Padilla, I. *et al.* Mismatch repair status and clinical outcome in endometrial cancer: A systematic review and meta-analysis. *Crit. Rev. Oncol. Hematol.* **88**, 154–167 (2013).

31. Kim, T.-M., Laird, P. W. & Park, P. J. The Landscape of Microsatellite Instability in Colorectal and Endometrial Cancer Genomes. *Cell* **155**, 858–868 (2013).

32. Baker, K., Rath, T., Pyzik, M. & Blumberg, R. S. Neonatal Fc receptors for IgG drive CD8 $^{+}$ T cell-mediated anti-cancer immunosurveillance at tolerogenic mucosal sites. *Oncoimmunology* **3**, e27844 (2014).

33. Galluzzi, L., Buqué, A., Kepp, O., Zitvogel, L. & Kroemer, G. Immunogenic cell death in cancer and infectious disease. *Nature Reviews Immunology* **17**, 97–111 (2017).

34. Rg, J., Fritz, H., Le Bourhis, L., Magalhaes, J. G. & Philpott, D. J. Innate immune recognition at the epithelial barrier drives adaptive immunity: APCs take the back seat. *Trends Immunol* **29**, (2007).

35. Taube, J. M. *et al.* Colocalization of inflammatory response with B7-H1 expression in human melanocytic lesions supports an adaptive resistance mechanism of immune escape. *Sci. Transl. Med.* **4**, (2012).

36. Hanahan, D. & Weinberg, R. A. Hallmarks of cancer: the next generation. *Cell* **144**, 646–74 (2011).

37. Lanitis, E., Dangaj, D., Irving, M. & Coukos, G. Mechanisms regulating T-cell infiltration and activity in solid tumors. *Ann. Oncol.* **28**, xii18–xii32 (2017).

38. Catherine S. Grasso, Marios Giannakis, Daniel K. Wells, Tsuyoshi Hamada, Xinmeng Jasmine Mu,

Michael Quist, Jonathan A. Nowak, Reiko Nishihara, Zhi Rong Qian, Kentaro Inamura, Teppei Morikawa, Katsuhiko Nosho, Gabriel Abril-Rodriguez, Charles Connolly, He, and U. P. Genetic mechanisms of immune evasion in colorectal cancer. *Cancer Discov.* (2018). doi:10.1158/2159-8290.CD-17-1327

39. Kloor, M. *et al.* Immunoselective pressure and human leukocyte antigen class I antigen machinery defects in microsatellite unstable colorectal cancers. *Cancer Res.* **65**, 6418–6424 (2005).

40. Pauken, K. E. & Wherry, E. J. Overcoming T cell exhaustion in infection and cancer. *Trends Immunol.* **36**, 265–76 (2015).

41. Lu, C. *et al.* Type I interferon suppresses tumor growth through activating the STAT3-granzyme B pathway in tumor-infiltrating cytotoxic T lymphocytes. *J. Immunother. Cancer* **7**, 157 (2019).

42. Griffioen, A. W., Damen, C. A., Martinotti, S., Blijham, G. H. & Groenewegen, G. Endothelial intercellular adhesion molecule-1 expression is suppressed in human malignancies: the role of angiogenic factors. *Cancer Res.* **56**, 1111–17 (1996).

43. Schaaf, M. B., Garg, A. D. & Agostinis, P. Defining the role of the tumor vasculature in antitumor immunity and immunotherapy article. *Cell Death Dis.* **9**, (2018).

44. Nagata, S. & Tanaka, M. Programmed cell death and the immune system. *Nat. Rev. Immunol.* **17**, 333–340 (2017).

45. Ribas, A. & Wolchok, J. D. Cancer immunotherapy using checkpoint blockade. *Science (80-.).* **359**, 1350–1355 (2018).

46. McDermott, D. *et al.* Durable benefit and the potential for long-term survival with

immunotherapy in advanced melanoma. *Cancer Treat. Rev.* **40**, 1056–1064 (2014).

47. Sharma, P., Hu-Lieskovan, S., Wargo, J. A. & Ribas, A. Primary, Adaptive, and Acquired Resistance to Cancer Immunotherapy. *Cell* **168**, 707–723 (2017).

48. Faïs, T., Delmas, J., Cougnoux, A., Dalmasso, G. & Bonnet, R. Targeting colorectal cancer-associated bacteria: A new area of research for personalized treatments. *Gut Microbes* **7**, 329–333 (2016).

49. Conde, J., Oliva, N., Zhang, Y. & Artzi, N. Local triple-combination therapy results in tumour regression and prevents recurrence in a colon cancer model. *Nat. Mater.* **15**, 1128–1138 (2016).

50. Kather, J. N., Halama, N. & Jaeger, D. Genomics and emerging biomarkers for immunotherapy of colorectal cancer. *Semin. Cancer Biol.* (2018). doi:10.1016/j.semcancer.2018.02.010

51. Kaiser, J. Too much of a good thing? *Science* **359**, 1346–1347 (2018).

52. Shimabukuro-Vornhagen, A. *et al.* Cytokine release syndrome. *J. Immunother. Cancer* **6**, 56 (2018).

53. Linsley, P. S. *et al.* Immunosuppression in vivo by a soluble form of the CTLA-4 T cell activation molecule. *Science (80-.).* **257**, 792–795 (1992).

54. Domogalla, M. P., Rostan, P. V., Raker, V. K. & Steinbrink, K. Tolerance through education: How tolerogenic dendritic cells shape immunity. *Frontiers in Immunology* **8**, 1764 (2017).

55. Rudd, C. E., Taylor, A. & Schneider, H. CD28 and CTLA-4 coreceptor expression and signal transduction. (2009). doi:10.1111/j.1600-065X.2009.00770.x

56. Dong, H. *et al.* Tumor-associated B7-H1 promotes T-cell apoptosis: A potential mechanism of

immune evasion. *Nat. Med.* **8**, 793–800 (2002).

57. Keir, M. E., Butte, M. J., Freeman, G. J. & Sharpe, A. H. PD-1 and Its Ligands in Tolerance and Immunity. *Annu. Rev. Immunol.* **26**, 677–704 (2008).

58. Emambux, S., Tachon, G., Junca, A. & Tougeron, D. Results and challenges of immune checkpoint inhibitors in colorectal cancer. *Expert Opin. Biol. Ther.* 1–13 (2018). doi:10.1080/14712598.2018.1445222

59. Sun, C., Mezzadra, R. & Schumacher, T. N. Regulation and Function of the PD-L1 Checkpoint. *Immunity* **48**, (2018).

60. Schwartz, R. *et al.* A cell culture model for T lymphocyte clonal anergy. *Science (80-.).* **248**, 1349–1356 (1990).

61. Diaz, L. A. & Le, D. T. PD-1 blockade in tumours with mismatch-repair deficiency. *N Engl J Med* **372**, 2509–20 (2015).

62. Arora, S. P. A. & Mahalingam, D. Immunotherapy in colorectal cancer: for the select few or all? *J. Gastrointest. Oncol.* **9**, 170–179 (2018).

63. Takamatsu, M. *et al.* Inhibition of indoleamine 2,3-dioxygenase 1 expression alters immune response in colon tumor microenvironment in mice. *Cancer Sci.* **106**, 1008–1015 (2015).

64. Mellman, I., Coukos, G. & Dranoff, G. Cancer immunotherapy comes of age. *Nature* **480**, 480–489 (2011).

65. Zhao, X., Li, L., Starr, T. K. & Subramanian, S. Tumor location impacts immune response in mouse models of colon cancer. *Oncotarget* **8**, 54775–54787 (2017).

66. Ahn, J. *et al.* Human Gut Microbiome and Risk for Colorectal Cancer. *JNCI J. Natl. Cancer Inst.* **105**, 1907–1911 (2013).

67. Iida, N. *et al.* Commensal Bacteria Control Cancer Response to Therapy by Modulating the Tumor Microenvironment. *Science (80-.).* **342**, 967–970 (2013).

68. Yoon, H. *et al.* Comparisons of Gut Microbiota Among Healthy Control, Patients With Conventional Adenoma, Sessile Serrated Adenoma, and Colorectal Cancer. *J. CANCER Prev. Cancer Prev* **2222**, 108–114 (2017).

69. Ahmed, I. & Umar, S. Microbiome and Colorectal Cancer. *Current Colorectal Cancer Reports* **14**, 217–225 (2018).

70. Bullman, S. *et al.* Analysis of Fusobacterium persistence and antibiotic response in colorectal cancer. *Science (80-.).* **358**, 1443–1448 (2017).

71. Bhatt, A. P., Redinbo, M. R. & Bultman, S. J. The role of the microbiome in cancer development and therapy. *CA. Cancer J. Clin.* **67**, 326–344 (2017).

72. Tilg, H., Adolph, T. E., Gerner, R. R. & Moschen, A. R. The Intestinal Microbiota in Colorectal Cancer. *Cancer Cell* **33**, 954–964 (2018).

73. Chen, J., Pitmon, E. & Wang, K. Microbiome, inflammation and colorectal cancer. *Semin. Immunol.* 0–1 (2017). doi:10.1016/j.smim.2017.09.006

74. Faïs, T., Delmas, J., Cougnoux, A., Dalmasso, G. & Bonnet, R. Targeting colorectal cancer-associated bacteria: A new area of research for personalized treatments. *Gut Microbes* **7**, 329–333 (2016).

75. Sivan, A. *et al.* Commensal Bifidobacterium promotes antitumor immunity and facilitates anti–PD-L1 efficacy. (2015). doi:10.1126/science.aad1329

76. Routy, B. *et al.* Gut microbiome influences efficacy of PD-1–based immunotherapy against epithelial tumors.

77. Zitvogel, L., Ayyoub, M., Routy, B. & Kroemer, G. Microbiome and Anticancer Immunosurveillance. *Cell* **165**, 276–287 (2016).

78. Moossavi, M., Parsamanesh, N., Bahrami, A., Atkin, S. L. & Sahebkar, A. Role of the NLRP3 inflammasome in cancer. *Molecular cancer* **17**, 158 (2018).

79. Chen, Q., Sun, L. & Chen, Z. J. Regulation and function of the cGAS-STING pathway of cytosolic DNA sensing. *Nature Immunology* **17**, 1142–1149 (2016).

80. Shekarian, T. *et al.* Pattern recognition receptors: Immune targets to enhance cancer immunotherapy. *Annals of Oncology* **28**, 1756–1766 (2017).

81. He, L. *et al.* Nucleic acid sensing pattern recognition receptors in the development of colorectal cancer and colitis. *Cell. Mol. Life Sci.* **74**, 2395–2411 (2017).

82. Gourbeyre, P. *et al.* Pattern recognition receptors in the gut: Analysis of their expression along the intestinal tract and the crypt/villus axis. *Physiol. Rep.* **3**, (2015).

83. Vandenabeele, P. & M Bertrand, M. J. The role of the IAP E3 ubiquitin ligases in regulating pattern-recognition receptor signalling. *Nat. Publ. Gr.* **12**, (2012).

84. Huang, S. W. *et al.* P2X7 receptor-dependent tuning of gut epithelial responses to infection. *Immunol. Cell Biol.* **95**, 178–188 (2017).

85. Sellin, M. E., Maslowski, K. M., Maloy, K. J. & Hardt, W. D. Inflammasomes of the intestinal epithelium. *Trends Immunol.* **36**, 442–450 (2015).

86. Man, S. M., Karki, R. & Kanneganti, T. D. DNA-sensing inflammasomes: regulation of bacterial host defense and the gut microbiota. *Pathogens and disease* **74**, ftw028 (2016).

87. Li, T. & Chen, Z. J. The cGAS–cGAMP–STING pathway connects DNA damage to inflammation, senescence, and cancer. *J. Exp. Med.* **215**, 1287–1299 (2018).

88. Roers, A., Hiller, B. & Hornung, V. Recognition of Endogenous Nucleic Acids by the Innate Immune System. *Immunity* **44**, 739–754 (2016).

89. Fu, J. *et al.* STING agonist formulated cancer vaccines can cure established tumors resistant to PD-1 blockade. *Sci. Transl. Med.* **7**, (2015).

90. Vanpouille-Box, C., Demaria, S., Formenti, S. C. & Galluzzi, L. Cytosolic DNA Sensing in Organismal Tumor Control. *Cancer Cell* **34**, 361–378 (2018).

91. Ablasser, A. *et al.* cGAS produces a 2'-5'-linked cyclic dinucleotide second messenger that activates STING Europe PMC Funders Group. *Nature* **498**, 380–384 (2013).

92. Ishikawa, H. & Barber, G. N. STING is an endoplasmic reticulum adaptor that facilitates innate immune signalling. *Nature* **455**, 674–8 (2008).

93. Zhang, C. *et al.* Structural basis of STING binding with and phosphorylation by TBK1. *Nature* **567**, 394–398 (2019).

94. Abe, T. & Barber, G. N. Cytosolic-DNA-Mediated, STING-Dependent Proinflammatory Gene Induction Necessitates Canonical NF- B Activation through TBK1. *J. Virol.* **88**, 5328–5341 (2014).

95. Woo, S. R. *et al.* STING-dependent cytosolic DNA sensing mediates innate immune recognition of immunogenic tumors. *Immunity* **41**, 830–842 (2014).

96. Xia, T., Konno, H., Ahn, J. & Barber, G. N. Deregulation of STING Signaling in Colorectal Carcinoma Constrains DNA Damage Responses and Correlates With Tumorigenesis. *Cell Rep.* **14**, 282–297 (2016).

97. Sokolowska, O. & Nowis, D. STING Signaling in Cancer Cells: Important or Not? *Archivum Immunologiae et Therapiae Experimentalis* **66**, 125–132 (2018).

98. Dowling & Luke, J. K. & O'neill, A. J. Biochemical regulation of the inflammasome. *Crit. Rev. Biochem. Mol. Biol.* **47**, 424–443 (2012).

99. Düwell, P., Heidegger, S. & Kobold, S. Innate Immune Stimulation in Cancer Therapy. *Hematol. Oncol. Clin. North Am.* **33**, 215–231 (2019).

100. Yang, Y., Wang, H., Kouadir, M., Song, H. & Shi, F. Recent advances in the mechanisms of NLRP3 inflammasome activation and its inhibitors. *Cell Death and Disease* **10**, 128 (2019).

101. Gaidt, M. M. & Hornung, V. Alternative inflammasome activation enables IL-1β release from living cells. *Current Opinion in Immunology* **44**, 7–13 (2017).

102. Gaidt, M. M. & Hornung, V. The NLRP3 Inflammasome Renders Cell Death Pro-inflammatory. *Journal of Molecular Biology* **430**, 133–141 (2018).

103. Swanson, K. V., Deng, M. & Ting, J. P.-Y. The NLRP3 inflammasome: molecular activation and regulation to therapeutics. *Nature Reviews Immunology* 1 (2019). doi:10.1038/s41577-019-0165-0

104. Chen, G. Y. & Nez, G. Inflammasomes in intestinal inflammation and cancer. *Gastroenterology* **141**, 1986–1999 (2011).

105. He, Y., Hara, H. & Núñez, G. Mechanism and Regulation of NLRP3 Inflammasome Activation. *Trends in Biochemical Sciences* **41**, 1012–1021 (2016).

106. Kayagaki, N. *et al.* Non-canonical inflammasome activation targets caspase-11. *Nature* **479**, 117–121 (2011).

107. Man, S. M. & Kanneganti, T. D. Converging roles of caspases in inflammasome activation, cell death and innate immunity. *Nature Reviews Immunology* **16**, 7–21 (2016).

108. Rogers, C. *et al.* Gasdermin pores permeabilize mitochondria to augment caspase-3 activation during apoptosis and inflammasome activation. *Nat. Commun.* **10**, (2019).

109. Yang, D., He, Y., Muñoz-Planillo, R., Liu, Q. & Núñez, G. Caspase-11 Requires the Pannexin-1 Channel and the Purinergic P2X7 Pore to Mediate Pyroptosis and Endotoxic Shock. *Immunity* **43**, 923–932 (2015).

110. Zaki, M. H., Vogel, P., Body-Malapel, M., Lamkanfi, M. & Kanneganti, T.-D. IL-18 Production Downstream of the Nlrp3 Inflammasome Confers Protection against Colorectal Tumor Formation. *J. Immunol.* **185**, 4912–4920 (2010).

111. Allen, I. C. *et al.* The NLRP3 inflammasome functions as a negative regulator of tumorigenesis during colitis-associated cancer. *J. Exp. Med.* **207**, 1045–1056 (2010).

112. Dupaul-Chicoine, J. *et al.* The Nlrp3 Inflammasome Suppresses Colorectal Cancer Metastatic Growth in the Liver by Promoting Natural Killer Cell Tumoricidal Activity. *Immunity* **43**, 751–763 (2015).

113. Flood, B. *et al.* Caspase-11 regulates the tumour suppressor function of STAT1 in a murine model of colitis-associated carcinogenesis. *Oncogene* 2658–2674 (2018). doi:10.1038/s41388-018-0613-5

114. Novick, D., Kim, S., Kaplanski, G. & Dinarello, C. A. Interleukin-18, more than a Th1 cytokine. *Semin. Immunol.* **25**, 439–448 (2013).

115. Banerjea, A. *et al.* Colorectal cancers with microsatellite instability display mRNA expression signatures characteristic of increased immunogenicity. *Mol. Cancer* **3**, (2004).

116. Cerami, E. *et al.* The cBio cancer genomics portal: an open platform for exploring multidimensional cancer genomics data. *Cancer Discov.* **2**, 401–4 (2012).

117. Jianjiong, G. *et al.* Integrative analysis of complex cancer genomics and clinical profiles using the cBioPortal. *Sci. Signal.* **6**, pl1 (2013).

118. Olszak, T. *et al.* Protective mucosal immunity mediated by epithelial CD1d and IL-10. *Nature* **509**, 497–502 (2014).

119. Chen, L. *et al.* The Short Isoform of the CEACAM1 Receptor in Intestinal T Cells Regulates Mucosal Immunity and Homeostasis via Tfh Cell Induction. *Immunity* **37**, 930–946 (2012).

120. Fletcher, R. *et al.* Colorectal cancer prevention: Immune modulation taking the stage. *Biochimica et Biophysica Acta - Reviews on Cancer* **1869**, 138–148 (2018).

121. Maletzki, C., Beyrich, F., Hühns, M., Klar, E. & Linnebacher, M. The mutational profile and infiltration pattern of murine MLH1$^{-/-}$ tumors: concurrences, disparities and cell line establishment for functional analysis. *Oncotarget* **7**, 53583–53598 (2016).

122. Efremova, M. *et al.* Targeting immune checkpoints potentiates immunoediting and changes the dynamics of tumor evolution. *Nat. Commun.* **9**, (2018).

123. Cremonesi, E. *et al.* Gut microbiota modulate T cell trafficking into human colorectal cancer. *Gut* **67**, 1984–1994 (2018).

124. Aarreberg, L. D. *et al.* Interleukin-1β Induces mtDNA Release to Activate Innate Immune Signaling via cGAS-STING. *Mol. Cell* **74**, 801-815.e6 (2019).

125. Musha, H. *et al.* Selective infiltration of CCR5+CXCR3+ T lymphocytes in human colorectal carcinoma. *Int. J. Cancer* **116**, 949–956 (2005).

126. Liu, Y., Beyer, A. & Aebersold, R. On the Dependency of Cellular Protein Levels on mRNA Abundance. *Cell* **165**, 535–550 (2016).

127. Allaire, J. M. *et al.* The Intestinal Epithelium: Central Coordinator of Mucosal Immunity. (2018). doi:10.1016/j.it.2018.04.002

128. Belkaid, Y. & Harrison, O. J. Homeostatic Immunity and the Microbiota. *Immunity* **46**, 562–576 (2017).

129. Hirota, S. A. *et al.* The NLRP3 inflammasome plays key role in the regulation of intestinal homeostasis. *Inflamm Bowel Dis* **17**, 1359–1372 (2011).

130. Canesso, M. C. C. *et al.* The cytosolic sensor STING is required for intestinal homeostasis and control of inflammation. *Mucosal Immunol.* **11**, 820–834 (2018).

131. Hale, V. L. *et al.* Distinct Microbes, Metabolites, and Ecologies Define the Microbiome in Deficient and Proficient Mismatch Repair Colorectal Cancers. *bioRxiv* 1–13 (2018). doi:10.1101/346510

132. Yurgelun, M. B. *et al.* Identification of a Variety of Mutations in Cancer Predisposition Genes in Patients with Suspected Lynch Syndrome. *Gastroenterology* **149**, 604e20-613.e20 (2015).

133. Sekine, S. *et al.* Mismatch repair deficiency commonly precedes adenoma formation in Lynch Syndrome-Associated colorectal tumorigenesis. *Mod. Pathol.* **30**, 1144–1151 (2017).

134. Franks, L. M. & Hemmings, V. J. A cell line from an induced carcinoma of mouse rectum. *J. Pathol.* **124**, 35–38 (1978).

135. Vidal, K., Grosjean, I., Revillard, J.-P., Gespach, C. & Kaiserlian, D. Immortalization of mouse intestinal epithelial cells by the SV40-large T gene: Phenotypic and immune characterization of the MODE-K cell line. *J. Immunol. Methods* **166**, 63–73 (1993).

136. Suzuki, N., Tsukihara, H., Nakagawa, F., Kobunai, T. & Takechi, T. Synergistic anticancer activity of a novel oral chemotherapeutic agent containing trifluridine and tipiracil in combination with anti-PD-1 blockade in microsatellite stable-type murine colorectal cancer cells. *Am. J. Cancer Res.* **7**, 2032–2040 (2017).

137. Khalid, G., Neumann', H., Flemans, R. J. & Hayhoe, F. G. J. *A comparative study of chromosome G-banding using trypsin, papain, and pretreatment with emulphogene*. *Journal of Clinical Pathology* **32**, (1979).

138. Nicolaides, N. C., Littman, S. J., Modrich, P., Kinzler, K. W. & Vogelstein, B. A Naturally Occurring hPMS2 Mutation Can Confer a Dominant Negative Mutator Phenotype. *Mol. Cell. Biol.* **18**, 1635–1641 (1998).

139. Ghiringhelli, F. *et al.* Activation of the NLRP3 inflammasome in dendritic cells induces IL-1B-dependent adaptive immunity against tumors. *Nat. Med.* **15**, 1170–1178 (2009).

140. Chang, L., Chang, M., Chang, H. M. & Chang, F. Expending Role of Microsatellite Instability in Diagnosis and Treatment of Colorectal Cancers. *Journal of Gastrointestinal Cancer* **48**, 305–313 (2017).

141. Chiang, C., Coukos, G. & Kandalaft, L. Whole Tumor Antigen Vaccines: Where Are We? *Vaccines* **3**, 344–372 (2015).

142. Evans, J. P. *et al.* Development of an orthotopic syngeneic murine model of colorectal cancer for use in translational research. *Lab. Anim.* (2019). doi:10.1177/0023677219826165

143. Hugenholtz, F. & de Vos, W. M. Mouse models for human intestinal microbiota research: a critical evaluation. *Cellular and Molecular Life Sciences* **75**, 149–160 (2018).

144. LaPointe, L. C. *et al.* Map of differential transcript expression in the normal human large intestine. *Physiol. Genomics* **33**, 50–64 (2008).

145. Hou, Y. *et al.* Non-canonical NF-κB Antagonizes STING Sensor-Mediated DNA Sensing in Radiotherapy. *Immunity* **49**, 490-503.e4 (2018).

146. Marielem Carvalho-Costa, T. *et al.* Light-Emitting Diode at 460-20 nm Increases the Production of IL-12 and IL-6 in Murine Dendritic Cells. doi:10.1089/pho.2016.4244

147. West, A. P. *et al.* Mitochondrial DNA stress primes the antiviral innate immune response. *Nature* **520**, 553–557 (2015).

148. Wei, Y. L. *et al.* Fecal microbiota transplantation ameliorates experimentally induced colitis in mice by upregulating AhR. *Front. Microbiol.* **9**, (2018).

149. Lopetuso, L. R., Scaldaferri, F., Petito, V. & Gasbarrini, A. Commensal Clostridia: leading players in

the maintenance of gut homeostasis. *Gut Pathog.* **5**, 23 (2013).

150. Galloway-Peña, J. R. *et al.* Fecal microbiome, metabolites, and stem cell transplant outcomes: A single-center pilot study. *Open Forum Infect. Dis.* **6**, (2019).

151. Sivick, K. E. *et al.* Magnitude of Therapeutic STING Activation Determines CD8 + T Cell-Mediated Anti-tumor Immunity. *Cell Rep.* **25**, 3074–3085 (2018).

152. Singh, P. P., Sharma, P. K., Krishnan, G. & Lockhart, A. C. Immune checkpoints and immunotherapy for colorectal cancer. *Gastroenterol. Rep.* **3**, 289–97 (2015).

153. Viale, G., Trapani, D. & Curigliano, G. Mismatch Repair Deficiency as a Predictive Biomarker for Immunotherapy Efficacy. *BioMed Research International* **2017**, (2017).